Miniaturized single-cell analyses for biomedical applications

THÈSE N^{O} 6960 (2017)

PRÉSENTÉE LE 10 MARS 2017

À LA FACULTÉ DES SCIENCES DE BASE
LABORATOIRE DE CHIMIE PHYSIQUE DES POLYMÈRES ET MEMBRANES
PROGRAMME DOCTORAL EN CHIMIE ET GÉNIE CHIMIQUE

ÉCOLE POLYTECHNIQUE FÉDÉRALE DE LAUSANNE

POUR L'OBTENTION DU GRADE DE DOCTEUR ÈS SCIENCES

PAR

Loïc Arvind Roger ARM

acceptée sur proposition du jury:

Prof. S. Gerber, présidente du jury
Prof. H. Vogel, Prof. K. Johnsson, directeurs de thèse
Prof. M. Winterhalter, rapporteur
Prof. M. Mayer, rapporteur
Prof. H. Altug, rapporteuse

ÉCOLE POLYTECHNIQUE
FÉDÉRALE DE LAUSANNE

Suisse
2017

“Internet is no reliable source of information.”

— Abraham Lincoln

A mes proches, quelle que soit la distance qui nous sépare. . .

List of abbreviations

AFM	Atomic force microscopy
BSA	Bovine serum albumin
BHK	Baby hamster kidney
Chol	Cholesterol
CTC	Circulating tumor cells
DDAB	Dimethyldioctadecylammonium bromide
DGS	1,2-dioleoyl-sn-glycero-3-succinate
Diyne-PC	1,2-bis(10,12-tricosadiynoyl)-sn-glycero-3-phosphatitdylcholine
DMEM	Dulbecco's modified Eagle's medium
DOBAQ	N-(4-carboxybenzyl)-N,N-dimethyl-2,3-bis(oleoyloxy)propan-1-aminium
DODAP	1,2-dioleoyl-3-dimethylammonium-propane
DOPC	1,2-dioleoyl-sn-glycero-3-phosphatidylcholine
DOPE	1,2-dioleoyl-sn-glycero-3-phosphatidylethanolamine
DOPG	1,2-dioleoyl-sn-glycero-3-phosphatidylglycerol
DOTAP	1,2-dioleoyl-3-trimethylammonium-propane chloride
DPPC	1,2-dipalmitoyl-sn-glycero-3-phosphatidylcholine
DPPG	1,2-dipalmitoyl-sn-glycero-3-phosphatidylglycerol
EDTA	Ethylenediamine tetraacetate
eGFP	Enhanced green fluorescent protein
eGFP-His10	Enhanced green fluorescence protein with an N-terminal decahistidine tag
EV	Extracellular vesicle
GUV	Giant unilamellar vesicle
HB	Human brain tumor
HEK	Human embryo kidney
ITO	Indium-doped tin oxide

Liss-Rhod-PE	1,2-dioleoyl-sn-glycero-3-phosphatidylethanolamine-N-lissamine rhodamine B sulfonyl ammonium
LUV	Large unilamellar vesicle
MT	Magnetic tweezers
NBCS	Newborn calf serum
NBD-PE	1,2-dipalmitoyl-sn-glycero-3-phosphatidylethanolamine-N-(7-nitro-2-1,3-benzoxadiazol-4-yl) ammonium
NGC	Neuronal growth cones
Ni-NTA	Nickel 2^+ nitrilotriacetic acid
NK_1R	Neurokinin 1 receptor
PBS	Phosphate buffered saline
PCI	Photochemical internalization
PDMS	Polydimethylsiloxane
PEG	Polyethylene glycol
POPC	1-palmitoyl-2-oleoyl-sn-glycero-3-phosphatidylcholine
POPG	1-palmitoyl-2-oleoyl-sn-glycero-3-phosphatidylglycerol
PTFE	Polytetrafluoroethylene
RBC	Red blood cell
RFP	Red fluorescent protein
SDS	Sodium dodecylsulfate
SM	Sphingomyelin
SOPC	1-stearoyl-2-oleoyl-sn-glycero-3-phosphatidylcholine
SNARE	soluble N-ethylmaleimide–sensitive factor attachment protein receptor
SUV	Small unilamellar vesicle
$TPPS_{2a}$	Meso-tetraphenyl porphyrin disulphonate

Abstract

Numerous diseases affecting living beings have as a cause a modification of gene expression resulting in anomalous expression of proteins in up- or down-regulated fashion, with altered functions or expression of proteins that are not present in the cell in a normal situation. Among the well-known examples is cancer, where a series of DNA damages turn cells out of control of the rest of the body, from which they do not receive or follow control signals. To have a better understanding of the mechanism of these diseases, in particular the genetic diversity existing in a single affected tissue, it is necessary to be able to perform single-cell analyses that unveil the subpopulations of diseased cells leading to adequate medical treatment.

In the course of this thesis, we report on the development of single-cell analysis methods which are of interest for medical applications. The first part focuses on the investigation of the viscoelastic properties of cell membranes by observing the back-relaxation of plasma membrane nanotubes which have been pulled out of a cell by an optical tweezer. Applied to the investigation of the viscoelastic properties of individual tumor cells taken from patients, we could show that this method can distinguish the state of progress of skin melanoma.

In the second part, we used beads comprising a chemically modified surface to capture specifically one or several proteins inside single-cells. After extraction out of the cell, the affinity bead is transferred in a microfluidic stream of a fluorescently labeled antibody to detect and quantify the protein(s) of interest. The extraction and detection procedures occur inside a microfluidic platform to allow future automatization of the process.

The last chapter focuses on the use of cell-derived extracellular vesicles (EVs) as diagnostic and therapeutic agents. With this goal in mind, we explore the potential of EVs as carriers to transfer genetic material into cells. To demonstrate the feasibility of this approach, we encapsulate EVs inside a giant unilamellar vesicle and release their cargo in a time- and space-controlled manner. This method could have therapeutic applications using a patient's self-EVs for gene therapy.

Key words: Single-cell analysis, microfluidics, optical tweezers, functionalized micro-beads,

chemical cytometry, fluorescence microscopy, lipid membranes, plasma membranes, extracellular vesicles, lipid vesicles, nanocontainers

Résumé

Nombres d'affections dont souffrent les êtres vivants ont pour origine une modification de l'expression des gènes résultant en une production anormale de protéines en trop grand ou trop petit nombre, en des protéines avec une fonction altérée, ou l'expression d'un certain type de protéines dans une cellule qui en temps normal n'en a ni besoin, ni usage. Parmi les exemples les plus connus de ce type de maladies, on trouve le cancer, où une série de dégâts causés à l'ADN perturbe les mécanismes biologiques des cellules qui commencent alors à se multiplier sans plus recevoir ou suivre les signaux du reste du corps. Afin d'améliorer notre compréhension des mécanismes de ces maladies, en particulier la diversité génétique présente au sein d'un tissu affecté, il est nécessaire de pouvoir effectuer des analyses cellule-par-cellule permettant de mettre à jour les sous-populations composant le tissu malade, permettant ainsi un traitement médical adéquat.

Dans cette thèse, nous posons les bases de méthodes d'analyses cellule par cellule prometteuses pour des applications biomédicales. La première partie se concentre sur l'analyse des propriétés visco-élastiques de cellules en observant la relaxation de nanotubes de membrane plasmique tirés par la force d'une pince optique. Il est ainsi possible de déterminer l'état d'avancement moléculaire d'un mélanome humain grâce à un petit nombre de cellules examinées individuellement.

Dans la seconde partie nous avons utilisé des billes dont la surface est chimiquement modifiée pour capturer de manière spécifique une ou plusieurs protéines à l'intérieur d'une cellule. Après son extraction hors de la cellule, la bille est mise en suspension dans un flux liquide contenant un anticorps fluorescent qui permet de détecter et quantifier la ou les protéine(s) recherchée(s). L'extraction et la détection ont lieu à l'intérieur d'une plateforme de micofluidique de manière à permettre une future automatisation du procédé.

Le dernier chapitre se concentre sur l'utilisation de vésicules extracellulaires (EVs) comme potentiels agents thérapeutiques et outils de diagnostique. Avec cette idée en tête, nous explorons la possibilité d'utiliser les EVs comme transporteurs de matériel génétique dans des cellules vi-

vantes. Pour démontrer la faisabilité de cette approche, nous choisissons d'encapsuler des EVs dans des vésicules géantes unilamellaires pour pouvoir les relâcher au moment et à l'endroit souhaité. Le développement de cette méthode permettrait d'agir dans un but thérapeutique en utilisant les EVs provenant du patient lui-même à des fins de thérapie génique.

Mots clefs : analyse de cellule unique, microfluidique, pince optique, micro-billes fonctionalisées, cytométrie chimique, microscopie de fluorescence, membranes lipidiques, membranes plasmiques, vésicules extracellulaires, vésicules lipidiques, nanocontainers

Contents

1 Introduction **1**

1.1 Measuring at the single-cell level - Motivation of the thesis 1

1.1.1 Why single-cell experiments 2

1.1.2 Presently used methods for single-cell analysis 4

1.2 Optical tweezers 10

1.3 Microfluidics 13

1.4 Cancer 15

2 Probing plasma membranes with optical tweezers **19**

2.1 Introduction 19

2.1.1 The cell membrane 19

2.1.2 Probing viscoelastic characteristics of cell membranes 21

2.1.3 Optical tweezers/microfluidic microscope 26

2.2 Experimental 29

2.2.1 Requirements for optical trapping 29

2.2.2 Cell culture 29

2.2.3 Microchip fabrication 30

2.2.4 Attaching cells inside microfluidic chip 31

2.2.5 Membrane relaxation experiments 31

2.3 Results and discussions 32

2.3.1 Melanoma tumor cells 32

2.3.2 Pulling membranes with no handles 33

2.3.3 Back-relaxation of pulled nanotubes 35

2.3.4 In-flow immobilizing microchip 40

2.4 Conclusions and outlook 42

3 Single-cell analysis with affinity beads **43**

3.1 Introduction . . . 44

3.2 Experimental . . . 47

3.2.1 Preparation of mixed Ni-NTA-antibody functionalized beads . . . 47

3.2.2 Cell transfection and bead internalization . . . 47

3.2.3 Phagosomal escape . . . 47

3.2.4 Cell trapping . . . 48

3.2.5 Cell analysis . . . 48

3.3 Results and discussion . . . 50

3.3.1 Phagocytosis in multiple cell lines . . . 50

3.3.2 Capture of a single analyte . . . 50

3.3.3 Simultaneous capture of two orthogonal analytes . . . 52

3.3.4 Maximal imidazole concentration in analysis buffer . . . 54

3.3.5 Correlation of eGFP fluorescence on the bead with eGFP concentration in the cell . . . 56

3.3.6 Detection of an analyte on microbeads using a secondary antibody . . . 58

3.4 Conclusion and outlooks . . . 61

4 Exosomes as potential vectors of drugs and DNA for medical treatment **63**

4.1 Introduction . . . 63

4.1.1 Extracellular vesicles . . . 63

4.1.2 Liposomes as carriers of material and information to cells . . . 66

4.2 Experimental . . . 67

4.2.1 Isolation of extracellular vesicles . . . 67

4.2.2 Modification of the lipid composition of extracellular vesicles . . . 67

4.2.3 Insemination of mammalian cells with extracellular vesicles . . . 67

4.2.4 Giant unilamellar vesicle (GUV) fabrication . . . 68

4.2.5 Controlled opening of GUVs . . . 68

4.3 Results and discussion . . . 70

4.3.1 Cell insertion of EVs carrying genetic material . . . 70

4.3.2 Encapsulation of microparticles in GUVs . . . 70

4.3.3 Giant vesicle disruption . . . 72

4.3.4 Towards EV liberation from GUV cargos . . . 77

4.4 Conclusion and outlook . . . 81

5 Overall conclusion **83**

Acknowledgements - Remerciements **117**

1 Introduction

1.1 Measuring at the single-cell level - Motivation of the thesis

This thesis concerns the development of miniaturized analytical methods to characterize biochemical and biophysical properties of single cells in the micrometer and nanometer range for biomedical diagnostics. To demonstrate the applicability of our bioanalytical tools, we will primarily focus on tumor cells, which show deeply modified cellular characteristics, such as mechanical properties, gene expression, or cellular signaling cascades; however, out tools are not limited to cancer, but might be of interest for diagnosis of many other diseases which are modifying cellular characteristics, such as chronic inflammatory diseases or viral infections to mention a few. The first part focusses on the development of methods to probe the viscoelastic properties of cellular plasma membranes and how diseases like cancer can modify the properties of plasma membranes. The second part focusses on the methods to investigate molecular composition of individual cells, especially cytoplasmic proteins; as many diseases affect the production of cellular components, we developed a method to quantify cytoplasmic proteins using micron-sized affinity beads, keeping a single-cell resolution. The third part is dedicated to the use of extracellular vesicles as a carrier for genetic material for potential applications in gene therapy, supplying cells with missing/mistranslated genetic material or silencing undesirable mRNA.

In the context of defining the general objectives of this thesis, we give in the following paragraphs (i) a brief outline why single-cell experiments deliver important novel information on the function of biological cells which cannot be obtained from ensemble measurements and therefore are of utmost interest for fundamental biological research and biomedical applications, and (ii) an overview of presently available single-cell technologies which are of

relevance for the present thesis.

1.1.1 Why single-cell experiments

Discovered at the end of the XVIIth century, the biological cell is considered since the middle of the XIXth century being the constitutive unit of every living being having ever existed on the planet Earth.[1] The very structure of a cell is defined by its plasma membrane isolating the cytoplasm from the outside environment. Major cellular components are DNA, RNA, proteins and lipids. The local concentrations and interactions of these components over time describe the dynamic biochemical network of a cell. The determination of this networks remains a challenge, but it would eventually be essential to understand the function or dysfunction of a living cell in its full complexity.[2] The diverse activities performed by proteins result from millions of years of evolutionary selection to optimize function, efficiency and synergy to make the organism as competitive as possible inside its environmental context. Changes in protein synthesis based on genetic or post-translational modifications lead to substantial changes of protein function and may turn into diseases.[3, 4, 5] Determination of tissue-specific composition (concentration and sequence/modifications) of the proteome delivers utmost important information about the condition of a human being with respect to potential development of diseases.

The characterization of a cell's proteome, the proteins expressed in a cell, is a bioanalytical field that contributes to a better understanding of cellular functions on a molecular basis.[6, 7] The proteome of a diseased cell can be quite different from that of a healthy cell, notably in the case of cancer, viral infections or inflammatory diseases.[8, 9, 10, 11, 12] Many diagnostic methods are focussing on the detection of abnormally expressed proteins, often referred to as pathology markers, to determine if a person is suffering from a specific disease.[13, 14, 15, 16] These methods often rely on a "cell extract" containing components that were constituting particular cells and are able to exhibit the presence of a specific marker after a step of concentration, tagging, confinement or a chemical reaction. Usually many cells are required for analysing the cellular content; the information obtained is consequently an average value over the number of cells constituting the sample under investigation.

As tissues are composed of an assembly of different types of cells, the principle of using an average extract of all these cells as a reference to judge whether the tissue is healthy or not and from which disorders it suffers, appears to be a poorly precise mode of investigation, unless

the illness has grown to remarkable extent. To circumvent the issues of averaging ensemble measurements, single-cell analyses have been developed.[17] Single-cell measurements deliver actual data of an analyte of interest for each and every cell of a given tissue sample. The global, average result stays invariant, but the detailed data provide much more information about the distribution of the different phenotypes. It also provides the possibility to find in a cell population rare cells that could be of a great functional importance, such as stem cells or rare sick cells.[18, 19] Indeed, the averaged signal hides the contribution of the diverse types of signals, which could have a strong biological relevance.[20, 21]

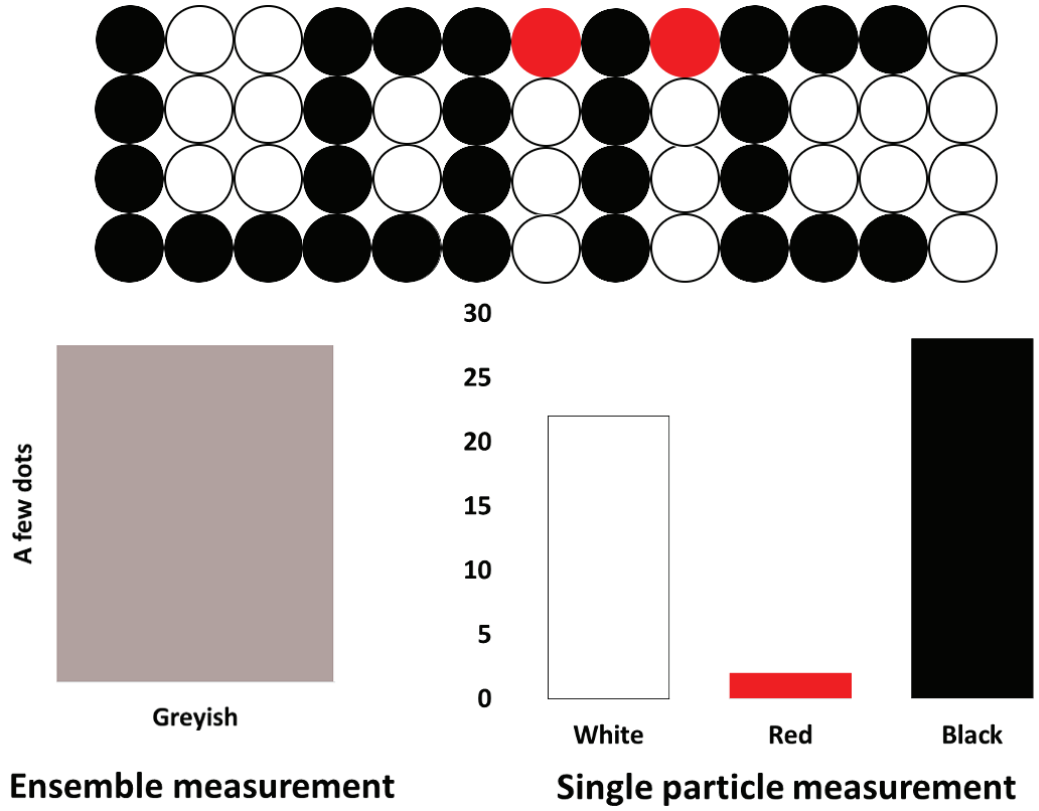

Figure 1.1: Schematic comparison between an ensemble and a single-particle measurement. *Shown is an ensemble of three different sorts of particles distinguished by color. Single-particle analysis would distinguish the three sorts of particles and count them individually. An ensemble measurement on the other hand would detect only the average properties, here the average color, of the ensemble of particles and thus hide the fact that they are actually composed of different sorts.*

Diseases such as cancer strongly rely on single-cell analysis to understand their characteristics. As explained in section 1.4, cancer progresses with sequential DNA mutations that increase progressively the disease's malignancy. A specific mutation occurs in one single cell, which then proliferates to form a new population, eventually overwhelming less malignant

previous populations. Detecting new mutations at an early stage requires the capability of detecting a specific phenotype or genotype in a small subpopulation of cells hidden among a large population. If bulk methods would engulf low frequency signals into measurement noise or misinterpretation, single-cell techniques leave no doubt about their existence. Cells propagating metastases, so-called cancer stem cells, are highly malignant tumor cells that circulate in blood or lymph and, once fixed to a suitable location, seed the initial tumor to another niche in the patient's body. Detection of these cells in a blood or lymph stream may be difficult due to the large number of other cells present in body fluids. Single-cell methods are the most suitable techniques for this operation, as cancer cells differ significantly by their atypical phenotype and mutated genotype.

Prior to analysis itself, samples must be correctly selected. If biopsies remain the most evident way of collecting targeted cells, it remains, in some cases, a challenge, if not simply impossible. Various methods are being developed to render the collection of cells of interest easier for the medical staff as well as for the patients. As an example, we will briefly go through a few of them directed towards circulating tumor cells (CTC) which are cells detached from their tumor of origin and circulating in suspension in blood or lymph. The challenge consists of finding these cells present in a very low concentration in blood, among millions of blood cells, and then to characterize them in order to understand as much as possible the characteristics of the mother tumor.

Cell Search® is a method that allows a reliable detection of the CTC.[22] Ferromagnetic nanoparticles coated with antibodies recognizing epithelial adhesion molecules are used to enrich CTCs and to analyze them. Antibodies conjugated to a red dye and directed to biomarkers of the tumor, in this case cytokeratin proteins, are introduced in the cells of the enriched sample sample, together with a cell nucleus dye and and a blue dye-conjugated antibody against a white blood cell specific protein, after cell permeabilization. After multiple automated washing steps and magnetic separation, cells containing both the red dye and the nuclear stainer are recognized as circulatory tumor cells.

1.1.2 Presently used methods for single-cell analysis

The **"CTC-chip"** captures circulating tumor cells inside a microfluidic chip using multiple PDMS structures coated with anti-epithelial antibodies.[23] At a flow rate up to 2 ml/hr, the cells have an optimal speed to be in close contact with the surface of cylinders to which the antibodies are attached. CTC remain attached to the cylinders whereas all other blood cells

simply flow through the chip. An enrichment surface of 920 mm^2 comprising 78,000 polymer cylinders is optimal for the enrichment of CTCs from blood volumes of several milliliters. CTCs attached to the microstructures are then ready for subsequent analyses, for example, using immunostaining. This isolation procedure has been further enhanced with the implementation of microvortices, using a two-level micro-patterning of the chip polymer, increasing both the interaction sites of the CTC with the antibodies as well as the throughput and specificity.[24] The ultimate version of this isolation and sorting procedure, the **CTC-iChip**, uses a combination of antibody marking, hydrodynamic sorting and magnetophoretic displacement to extract CTC from blood samples.[25] Blood is first incubated with magnetic beads coated with epithelial antibodies. The sample is then injected into the CTC-iChip where small blood cells (erythrocytes and platelets) are removed by hydrodynamic separation of large cells from the rest of the sample.[26] After hydrodynamic inertial refocusing of large cells, CTCs are separated from white blood cells by exposition to a magnetic field that shifts the magnetically tagged cells towards the collection stream.

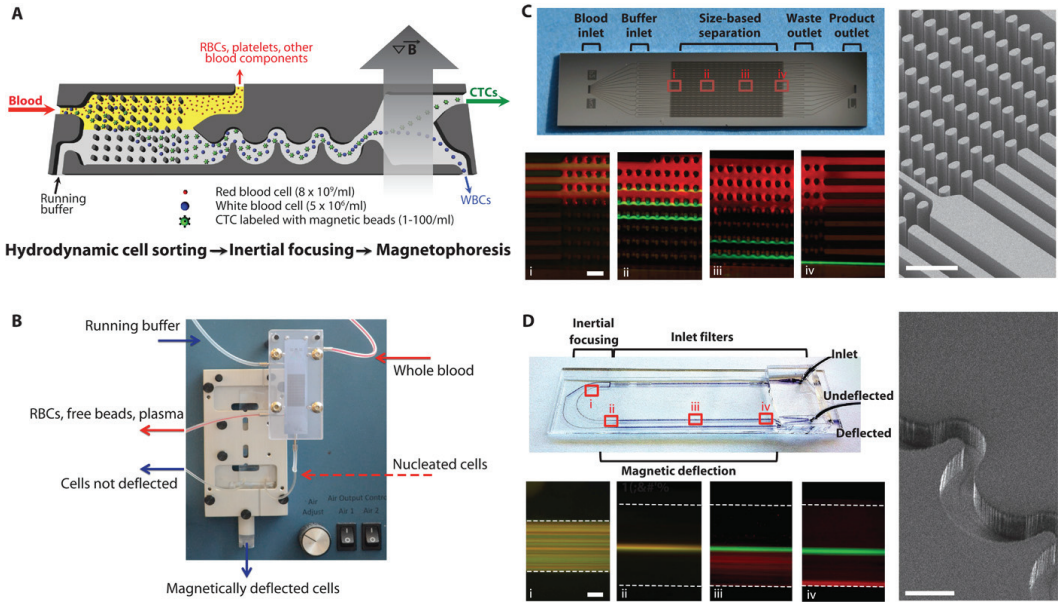

Figure 1.2: CTC-iChip. *Separation and collection of CTC from whole blood sample incubated with immunomagnetic beads. (A) Scheme of the working principles of the CTC-iChip. (B) Picture of the actual chip. To allow multiple work modes, it is divided in two units. (C) Size separation unit of the chip by hydrodynamic sorting. (i, ii, iii, iv) 10 µm sized green fuorescent beadsd are separated from 2 µm sized red fluorescent beads. (D) Inertial cell focusing and magnetophoretic unit. (i) randomly mixed cells enter the focusing unit. (ii) Cells are focused by the passage through 60 asymmetric turns. (iii) Focused cell stream is flowing through a magnetic field that gently separates the magnetically tagged CTCs, creating two separated streams (iv). Image from [25].*

Single-cell analyses can operate mainly on two levels: genotype and phenotype. **Single-cell genotype analyses** investigate DNA, mRNA and other forms of genetic material. The main goal is to find aberrant mutations resulting from DNA lesions or to determine the copy number of a particular mRNA. These analyses are often processed in three steps: firstly a lysis of the cell, secondly an amplification of the genetic material followed by sequencing or identification of the target piece of genetic material.[27] These steps are performed by the **GenomePlex® Single Cell Whole Genome Amplification commercial kit** from Sigma Aldrich. Single-cells are isolated in a small volume where cell lysis together with proteolysis are proceeded. DNA is fragmented at random locations by enzymes to an average fragment size of 400 base pairs. A library of primers is added to the fragmented DNA for massive amplification, resulting in whole genomic DNA that can be sequenced easily by classical methods. Subtle features may be added to increase the amplification fidelity, as for example the multiple annealing and looping-based amplification cycles (MALBAC) method which uses a displacement polymerase[28] in addition to randomized primers with a 27 nucleotide invariant sequence.[29] The invariant sequence makes the second generation replicated strand loop on itself, preventing further random amplification. Self-looped DNA fragments are then used a template for PCR as quasi-linear pre-amplified DNA from the chromosomes of a single-cell of origin. MALBAC confers to the single-cell whole genomic analysis a very high sensitivity capable of detecting single-nucleotide variations on two alleles of a cell.

On the phenotypic side of single-cell analyses, proteins are detected for the characterization of diseases. Proteins can be probed directly, by measuring their presence, quantity or activity, as well as in indirect manner by probing the whole cell properties in a specific way linked to the protein of interest. In difference to genetic material, proteins cannot be amplified to increase the quantity of material to analyse. The average total number of proteins in one single cell is about 10^8, for a total mass of approximately 75 pg of protein per cell.[30] This gives, for a low expression level protein of interest, a total copy number of approximately 10^4 in one single cell available for detection.[31] Detection methods must thus be sensitive enough to capture the information in very low concentration or rely on spatiotemporal confinement of the proteins of interest. The use of optical biosensors is among the most widely used ways for monitoring the number and activity of molecules in cells, in particular fluorescent biosensors. They may be divided into synthetic and genetically encoded biosensors. Synthetic fluorescent sensors are typically small organic molecules that change their fluorescence properties upon sensing a biological property, such as the concentration of a soluble molecule or the pH.[32] Many

different genetically encoded fluorescent reporters have been developed. In this context, the expression of fluorescent fusion proteins has been a major breakthrough, making it possible to directly visualize the proteins of interest.[33] For example, **fluorescence microscopy** allows the observation of single-cell mechanics. Commonly used is the localization of fluorescence species in a cell. Localizing molecular species gives information regarding their role and function; for example proteins located in the nucleus are likely to be related to genetic information, whereas membrane proteins are often involved in signal transduction.[34] Changes in location of a signaling molecule can be observed upon activation of a signaling cascade.[35, 36] Another example concerns **colocalization** of multiple fluorescent molecules to correlate the position and interactions of proteins inside a cell. **FRET** (Förster Resonance Energy Transfer) can resolve visually spatial interactions in the nanometer range, which goes beyond simple colocalization. This technique uses non radiative energy transfer from a fluorescent donor molecule to a spectrally overlapping fluorescent acceptor resulting in photon emission of the acceptor molecule upon photoexcitation of the donor. The efficiency of this energy transfer relies on the spectral overlap of the two fluorescent molecules, the orientation of the respective fluorophores and their distance with subnanometer precision. This method is extensively used to monitor conformational changes of proteins, as the distances involved are typically in the nanometer or subnanometer range.[37] In addition, genetically encoded sensors for measuring concentration of signaling species have been developed using FRET principles.[38, 39]

Limitations of fluorescence microscopy may arise from the fluorescent probe itself, in terms of potential insufficient lifetime, steric hinderance, or changing protein function. Another limiting feature is the spatial resolution of fluorescence/optical microscopy, that is restricted to approximately 200 nm the smallest distance to be distinguished. Novel developments circumvent this limitation of spatial resolution. Examples are **PALM** (Photoactivation Localization Microscopy) [40] and **STORM** (Stochastic Optical Reconstruction Microscopy)[41]. They work by stochastic activation of a small number of fluorescent molecules and determining their spatial location with nanometer precision by calculating the maximum intensity of the point spread function of each fluorescent molecule; the subset of these activated molecules is then shut off and another subset of fluorophores is subsequently activated and the location of these fluorophores is determined again. This process is repeated many times, thus determining the position of all fluorophores with nanometer precision. A superposition of all determined positions finally results in an image of fluorophores with overall nanometer resolution. Another

method of superresolution microscopy is **STED** (Stimulated Emission Depletion). [42] Here the effective area of the fluorescence excitation laser beam is reduced below the diffraction limit by depleting fluorophores in a ring-like shape leaving a nanometer-sized unbleached excitation area. Only the central reduced excitation area is emitting fluorescence photons, thus increasing the localization accuracy of the fluorophores down to the nanometer range.
Flow cytometry allows a rapid, yet less precise and less specific treatment of single-cells labeled with fluorescent molecules. If localization inside the cell remains an unsolved challenge, flow cytometry is able to process thousands of cells per minute with the averaged fluorescence of the whole cell as an outcoming data. Genetic labeling of the protein of interest is commonly used. However, due to their higher brightness, their much smaller size and the capability of labeling other kinds of molecules than proteins, synthetic fluorophores are often preferred via post-translational labeling. Data that are not in relation with exogenous fluorescence can also be obtained, such as size, morphological characteristics or autofluorescence.[43]
The major problems limiting the use of fluorescence in single-cell measurements comes from the necessity of submitting cells to a pre-treatment to introduce the fluorescent molecules inside the cell of interest, whether it is genetically encoded (transfecion) or not (permeation, microinjection).[44, 45] An alternative method is to add the fluorescent component after lysis of the cell, which may cause dilution related loss of signal intensity.[46]

An alternative method takes advantage of the naturally fluorescent amino acid tryptophan to detect and identify proteins.[30, 47, 48] Here cells are manipulated with optical tweezers in a PDMS microfluidic device to be lysed by a strong electric field pulse. The cellular content is then separated by electrophoresis and the proteins are detected by the intrinsic fluorescence of tryptophan residues. Finally, they are expected to be identified by their electrophoretic displacement, although this method suffers from poor precision.
Microfluidic devices have been coupled to capillary electrophoresis and **mass spectrometry** to perform single-cell proteomic analysis.[45] Here cells are injected in a microchip channel to undergo detergent-free lysis mediated by a methanol-containing buffer. The cell content then flows into a channel where proteins are electrophoretically separated before analysis by electrospray ionization mass spectrometry. An alternative method uses MALDI-TOF, where the proteins are immobilized on an antibody-coated surface prior mass spectrometry analysis.[49, 50]

Building up statistical relevant data sets requires the ability to analyze multiple individual cells with sufficiently high throughput. **Parallelization** of analysis on the micrometer scale

is one of the most common ways to achieve it. Parallelization can be realized by different means, such as multiplication of the microfluidic channels[51], multiple single-cell trapping in refractive optical tweezers[52], single-resolved cells immobilized in hydrogels[53] or cells docked in microstructured elements[54]. An alternative is to implement an automated spatial segregation of individual cells by the generation of immiscible microdroplets from the cell suspension in a hydrophobic carrier fluid[55], where the different liquid phases can be easily detected and can be scaled to the sampling frequency of the detector.

The advances in single-cell measurements are on the way to revolutionize medical possibilities towards the development of personalized treatments that are finely tuned to each individual patient, with one's own disease configuration and own reactive pattern towards treating agents.[56, 57, 58] Every step forwards to the achievement of quantitative single-cell analysis is one step further towards personalized medicine.

1.2 Optical tweezers

Among many others, light has been one of the most fascinating tools used to probe cellular processes, using for example optical microscopy [59], spectroscopy [60, 61] or small angle scattering [62], to mention a few. A less intuitive way of using light consists of focusing a laser beam onto a micrometer sized object to act on it as tweezer. Optical tweezers have been first developed by Ashkin in 1970.[63] Thanks to multiple interactions of light with a given small dielectric object, a laser beam with a Gaussian intensity profile can trap the object inside the beam while still pushing it forwards. It has been shown later that focusing the laser beam with a large numerical aperture microscope objective provides the ability to trap a particle in the focus (Figure 1.3).[64] The trapping force is generated by the deflection of the electromagnetic fields as it passes the dielectric object. As the light rays change direction, they change momentum, transferring energy to the particle. In a Gaussian laser intensity profile, the transmission process provides maximal energy in the centre of the beam because the gradient of the electromagnetic intensity reaches its local maximum. The combination of these two effects allows the efficient trapping and manipulation of small objects in the micrometer range in free space.[65] As these effects occur over the volume covered by the laser beam, the forces exerted formally by individual rays have to be integrated over the entire particle volume submitted to light. Forces delivered are in the order of pN, making optical tweezers particularly suitable for the manipulation and investigation of biopolymers.[66, 67]

The ray-optics approximation considers that the whole laser beam is split into single individual rays with each of them having their individual intensity, propagation direction and incident angle on the particle.[65] Forces delivered by optical tweezers are to be decomposed in two distinct components: a force F_Z acting in the direction of light propagation, the scattering force, and a force F_Y acting in the plane perpendicular to the light propagation vector, the gradient force. These forces can be described as follows [65] :

$$F_Z = \frac{n_1 P}{c}\{1 + Rcos(2\theta) - \frac{T^2[cos(2\theta - 2r)] + Rcos(2\theta)}{1 + R^2 + 2cos(2r)}\} \tag{1.1}$$

$$F_Y = \frac{n_1 P}{c}\{Rsin(2\theta) - \frac{T^2[sin(2\theta - 2r)] + Rsin(2\theta)}{1 + R^2 + 2sin(2r)}\} \tag{1.2}$$

where $\frac{n_1 P}{c}$ is the incident momentum per second of a ray of power P in a medium of refractive index n_1. R and T, respectively, are the Fresnel reflection and transmission coefficients[68] of the particle surface at the incident angle θ, and r is the refraction angle. The spatial integral

covering the whole particle hit by the light beam yields the total momentum transmitted and the force exerted to the particle by the trap.

Since optical tweezers do not require invasive interactions, it allows non-contact manipulation of small, high refractive index objects. As the trapping force is proportional to the difference in refractive index between the trapped object and the surrounding medium, it is easier to trap the optically denser organelles such a nuclei or chloroplasts inside the cell than the entire cell itself.[69, 70, 71] Further, it is easier to exert spatial control on certain cellular components with the help of latex or polystyrene micrometer sized beads that can be used as supports or handles for small cellular components which would be difficult to trap directly. Many DNA related optical tweezers applications have been reported using this approach.[72, 73, 74]

As the trapping laser can be directly integrated into the microscope excitation optical path, it does not require any supplementary manipulation device. The only crucial step consists of the correct alignment of the trapping laser to place its focus such that the movement of the trapped object scales to the movement of the field of view of the microscope.

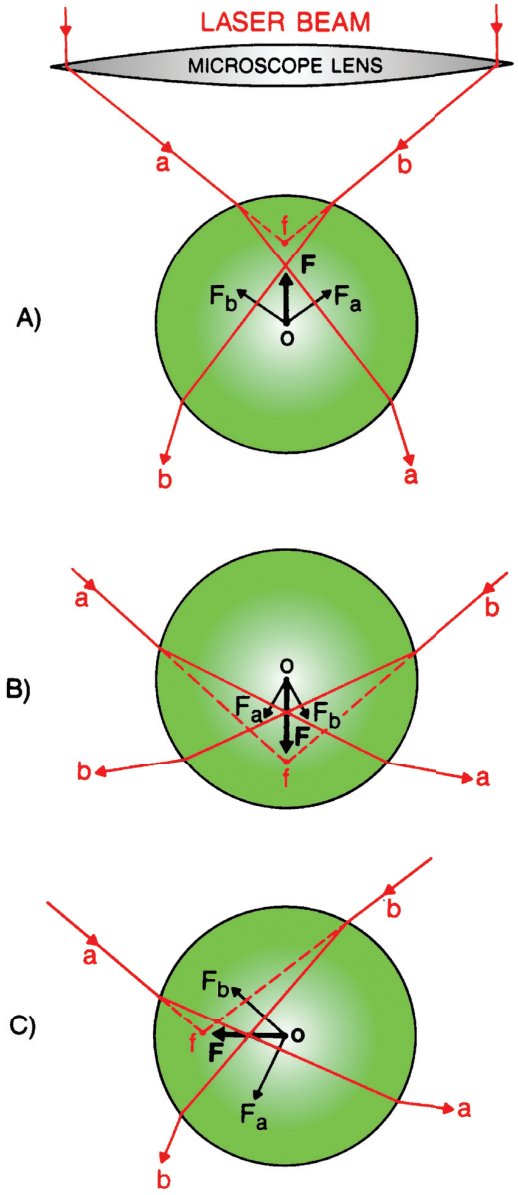

Figure 1.3: Schematic view of a three-dimensional trapping of a spherical dielectric particle in a focused laser beam with a Gaussian intensity profile. *The refraction of a typical pair of rays a and b of a trapping laser beam exerts forces F_a and F_b whose vector sum gives a net force* ***F*** *which points towards the focus of the beam f for any displacement of the sphere from the trap focus. Thereby, the sphere is stably trapped in the trap focus. (A) Optical trapping of a spherical object out of the laser focus in the direction of propagation of the laser beam. The instant net force* ***F*** *resulting from the change in momentum of light drags the particle towards the focus. The same physical phenomenon takes place for a particle positioned closer to the lens (B) or aside of the focus +(C). Figure adapted from [65]*

1.3 Microfluidics

Miniaturization is becoming increasingly important for bioanalytical devices.[75, 76, 77] Microfluidics, the miniaturization of fluidic systems, offer a wide variety of platforms for performing analysis of samples at the micrometer and (sub-)microliter scale. Fluidics reduced down to the diameter at the micrometer scales give rise to specific properties usually not found at macroscopic scale. For example, the dimensions of the flow channels imply a very high surface to volume ratio; in turn unspecific adsorption phenomena to channel walls become of major importance.[78] The micrometer channel dimensions give to the flow a laminar character. Liquids flowing in microsized channels are displaying a low Reynolds number $Re = \frac{\rho UL}{\mu}$, where ρ is the fluid density, U the mean fluid velocity, L the characteristic length and μ the fluid viscosity.[79] As L is related to the channel's cross-section, it is likely that at such small scale, only laminar flow is observed. In laminar flows, lateral mass transfer is only achieved by diffusion. This allows to realize separate flows in one single channel, as shown in Figure 1.4. This property is used for example in hydrodynamic focusing.[80, 81]

Microfluidic devices significantly reduces the quantities of sample needed to be analyzed. Whereas traditional macroscopic techniques require milliliters to perform a quantitative analysis, microfluidics decrease sample consumption down to sub-microliters. Thanks to the miniaturization possibilities, microfluidic devices allow a high degree of parallelization of processes to greatly increase the number of simultaneous observations.[54] This saves both consumables and time and delivers relevant statistics using a minimum flow through. Furthermore, coupling microfluidics to miniaturized bioanalyses created a new field of R&D called "lab on a chip", performing purification, conditioning, separation and multiple analyses of a complex sample all at once within a miniaturized device.[83, 84]

Microfluidic chips used in research and development phase are often made of silicone polymer PDMS (poly-dimethylsiloxane), with channels imprinted by soft lithography, glued on top of a thin glass coverslip (Figure 2.8). PDMS is widely used for its elastic properties, its good biocompatibility, as well as for the relative low complexity of the chip fabrication process.[85] The elastic properties of PDMS can be tuned by varying the amount of curing agent used in the elastomer mixture before polymerization. Tunable elasticity of the polymer is required for multi-layer microchips if pneumatic valves are implemented.[86] PDMS has a remarkable gas permeability, which offers the possibility to culture cells in microchips.[87, 51] Culturing cells directly inside microchannels allows a better control of the growth conditions as well as proper cell adherence to the bottom glass surface of the chip after adequate surface treatment.

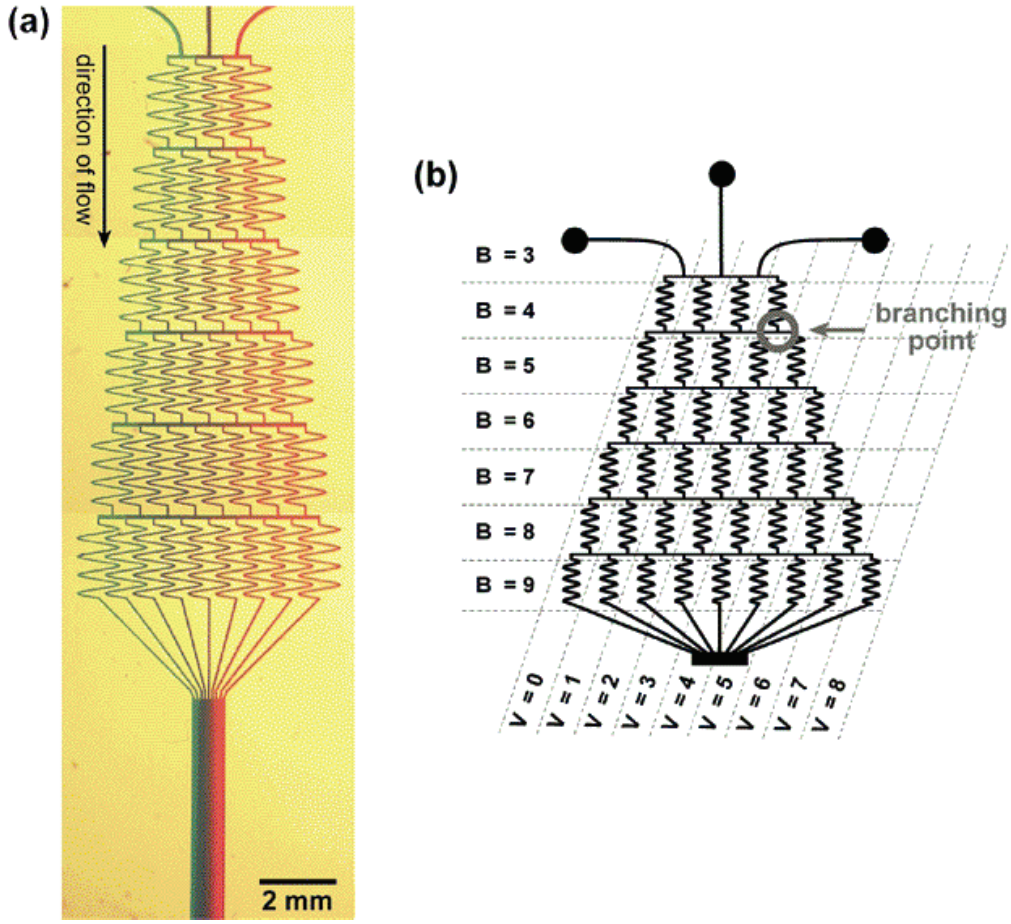

Figure 1.4: Illustration of liquid flowing in a microfluidic channel. *(a) Colored liquid flowing through a microfluidic chip designed for establishing a gradient of three compounds. Three liquids are injected simultaneously in a microfluidic channel array. After mixing in regulated proportions in a mixing area, the resulting eight streams are merged into a single channel where they flow in parallel with very little diffusion only across the interfacial areas of streams. (b) Scheme of the microfluidic chip. Image adapted from [82].*

1.4 Cancer

Cancer has become one of the biggest challenges worldwide.[88, 89] Cancer is the second cause of death in the United States[90] and the fourth cause in the world.[91] Changes in lifestyle, especially of dietary habits, prolonged duration of life, exposition to cancerogenic compounds, environmental factors are a few of the many causes of cancer. Since it has become a major life threatening shadow in the developed countries, it has also drawn the attention of pharmaceutical research, for the potential colossal incomes that can be generated by cancer related drugs, as well as medical related research.

Cancer results from mutations on genomic DNA that control central cellular processes related to cell division, intra- and inter-cellular communication and cell death.[4] Genetic mutations naturally occur with a very low probability.[92, 93] This low rate guarantees a slow process of evolution while maintaining a genetic stability on the time scale of several generations. A gene which has the potential to cause cancer is called "oncogene". A single oncogene mutation is not sufficient to trigger the formation of cancerous lesions, but might accelerate the rate of DNA mutation and produce a long cascade of cellular malfunctions leading ultimately to cell death.[94] In rare occasions, when the mutations are affecting a combination of oncogenes or tumor suppressor genes, cells may develop a cancerous behaviour.[95, 96]

Six main cellular functions are commonly described to play an important role in cancer development.[4] (1) Resistance to cell death implies that the cell becomes insensitive to apoptosis.[97] (2) Resistance to senescence allowing the cell the capability of performing endless replication.[98, 99] (3) Resistance to external growth suppressing signals making the proliferation of cells independent to external mechanisms for holding the unhealthy cells to a normal division rate.[100] (4) In order to proliferate, cancer cells provide growth signal to the cell machinery.[101, 102] (5) To provide the nutrients necessary to growth of cancer cells, angiogenesis is promoted through expression of vascular growth factors.[103, 104] (6) The ability of invading other tissues.[105, 106, 107] p53 is one of the central proteins in relation with cell proliferation and protection of a controlled cell division, as well as with programmed cell death.[108, 109, 5] A mutation on the gene of p53 disrupts its activity in the majority of malignant tumors.[110]

Early detection of cancerous lesions is crucial for patient survival; mortality increases rapidly with malignancy progress, as do healthcare costs.[111, 112] Early cancer diagnosis relies on

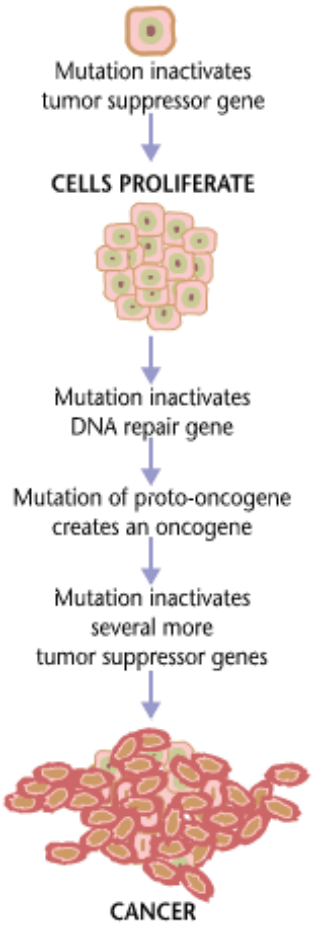

Figure 1.5: Progression from healthy tissue to cancer. *One of the various possible paths of evolution from a healthy tissue to a malignant cancer. A succession of mutations is necessary to break safety barriers to turn a normal cell into an immortal uncontrolled proliferating cancer cell with uncontrolled DNA mutation rate and invasive behaviour. Image from the American National Cancer Institute.*

the detection of biomarkers found in body fluids or in sick tissues.[113, 114, 115] If tumors are treated before reaching a high level of malignancy, they do not spread and remain at a relatively low level of genetic diversity, which makes them easier to erase. Although radiotherapy is widely used for treating a variety of cancers[116], it is limited to the treatment of tumors restrained to small volumes and local areas. Broad spectrum anticancer drugs used for radiation resistant or spread cancers are most often of a high systemic toxicity, especially for kidneys, stem cell-rich tissues and fast replicating cells, making their usage difficult to stand for patients.[117, 118, 119, 120, 121] As such, a complement for making the remission of patients easier is the administration of drugs targeting specifically cancerous cells with as little damages to healthy tissues as possible. The concept of "magic bullet" has been a long time aim of the pharmaceutical industry.[122, 123] A magic bullet is a drug that targets cells

suffering from a specific ailment causing minimum harm to healthy cells. Magic bullets rely on the use of recognitions elements (antibodies, ligands) that have a designed interaction site with biomarkers of cancer cells. It increases the efficiency of the administrated dose while at the same time decreases side effects on fragile organs. Prerequisites to design such a drug is to have reliable methods to detect the molecules indicating a favourable phenotype for the use of a specific drug as well as a good knowledge of a way to deliver efficiently the drug to the targeted cells.

Since one of the features of cancer is phenotypic heterogeneity, it appears necessary to apply detection means on a single-cell basis.[124] It is indeed very common to find multiple populations of cells with various characteristics, each of them having undergone a genetic separation during the evolution process of the genomically instable tumor.[125, 126, 127] New populations have different behaviours in terms of invasiveness, stiffness or drug resistance.[128, 129, 130] The later point renders crucial the deciphering of the tumoral phenotype complex partition in order to eradicate all malignant cells in one single drug treatment, in particular in case of a spread cancer.[131, 132, 133]

Alternative curing strategies are being investigated to greatly decrease the toxicity of treatment agents used in cancer therapy.[134, 135, 136, 137] The choice of one or another depends strongly of the response to the treatment of the cancer itself as well as the response of the patient. Gene therapy is one of those; it relies on the introduction of exogenous genetic material or the silencing of overexpressed proteins in cells of patients.[138, 139] The focus of this technique is on the means for delivering genes to the desired body area. Cargos made of artificial lipid vesicles have already been investigated in that direction, although with limited success so far.[140, 141, 142] Artificial vesicles have to be extensively modified to acquire fusogenic properties as well as prolonged life-time for an acceptable potential efficiency. Adenoviruses have provided promising yields as DNA cargos.[143] Recent observations have underlined the role of extracellular vesicles (EVs) naturally produced by cells with remarkable properties for cellular intercommunication.[144] EVs derived from cancer cells transfer tumor specific proteins and genetic material to the whole body of patients via circulatory systems.[145, 146, 147] There is hope that EVs in body fluids can be used as biomarkers for early detection of diseases such as cancer.[148] Taking advantage from their high performance in modifying behaviour of other cells, the use of EVs as carrier of chemicals of genetic material for gene therapy is a present focus of research groups on the edge of cancer therapy.[149]

2 Probing plasma membranes with optical tweezers

2.1 Introduction

The properties of the plasma membrane are tightly related to the type of cell and to its physiological condition.[150, 151, 152, 153] This implies that not only a cell and its plasma membrane of a given tissue will be different from a cell of another tissue, but also that two cells of apparent identical origin could exhibit different properties according to differences in age and environmental influences like local stress, action of pathogens or epigenetics to mention a few.[154] This chapter concerns the viscoelastic properties of living cells probed by optical tweezers. Recent reports indicate that biological cells can be distinguished by their mechanical properties.[155, 156, 157, 158] Here the invasiveness of cell is compared to their stiffness. The stiffness is measured using stretching lasers [155], magnetic tweezers [156] or atomic force microscopy [157, 158], with the converging observation that the stiffer a cell is, the most invasively it behaves, hence providing a potential mechanical biomarker for cancer evolution. Here we investigate whether it is possible, with the help of optical tweezer technology, to investigate cancer cells from tumors through the viscoelastic properties of their plasma membrane and thereby follow the process of the tumor development. The focus of this study is put on human skin melanoma, a malignant tumor of the skin melanocyte.[159]

2.1.1 The cell membrane

The plasma membrane of a mammalian cell is composed of thousands of different lipids and a plethora of transmembrane proteins.[160, 161, 162, 163] It defines the border of a biological cell and mediates actively the communication between the inside and outside of a cell,

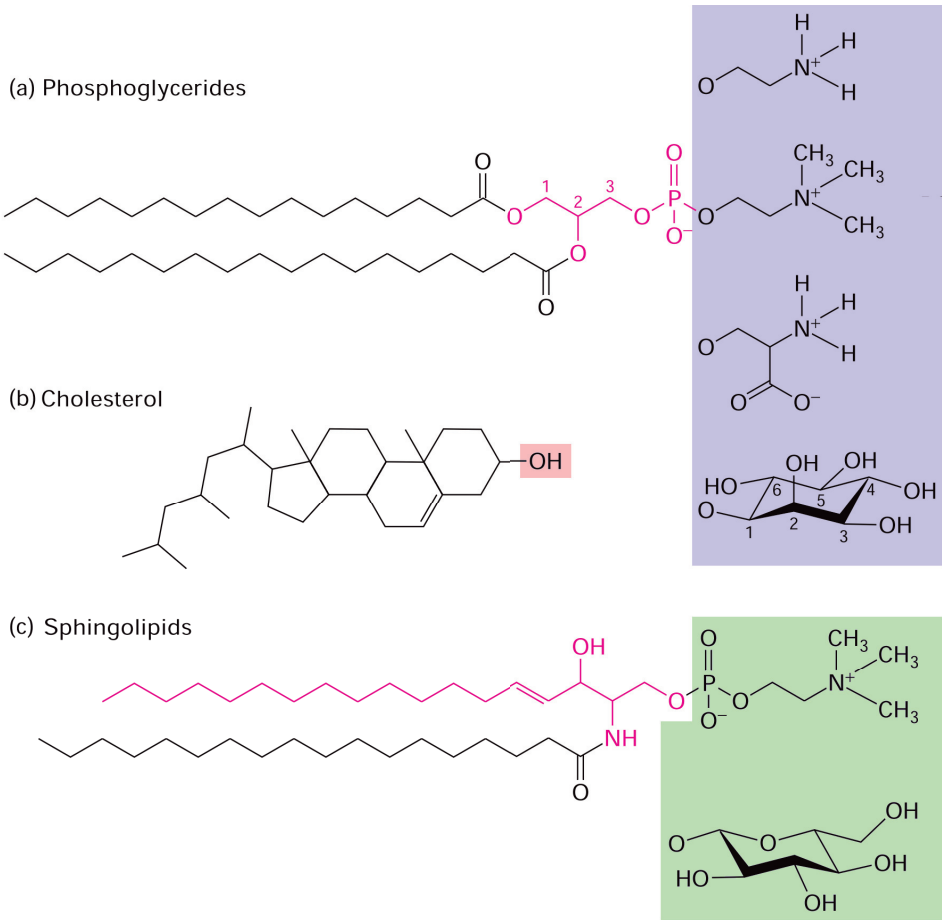

Figure 2.1: The three main lipids constituting the cellular plasma membrane. *(a)* ***Phospholipids*** *(or phosphoglycerides) are made out of two hydrophobic fatty acid chains (black) connected to the polar phosphate head group by a glycerol moiety (magenta). On the blue frame are given a few examples of the many possible moieties found on the phosphate group, here ethanolamine, choline, serine and inositol. (b)* ***Cholesterol*** *is constituted by a four-ring rigid sterol moiety to which are attached a hydrophobic tail and a polar hydroxyl group. (c)* ***Sphingolipids*** *are built from the sphingosine moiety (magenta) to which is attached a fatty acid chain (black) and a polar head group; here are shown sphingomyelin and glycosylcerebroside on the green frame. Image adapted from [1]*

harboring the central cellular signal transduction machineries. Plasma membranes show a very heterogenous composition which varies drastically between different cell types, but are changing very dynamically over time and space even within one single cell.[160, 161, 162] The membrane lipids are organized in form of an asymmetric fluid bilayer, allowing the insertion of transmembrane proteins or the attachment of particular proteins at membrane surface via polar lipid headgroups.[164, 165, 166] The three principal classes of plasma membrane lipids are: **Phospholipids** (Figure 2.1.a) are constituted of two acyl chains anchored to a glycerol group that connects them to a phosphate group; the phosphate group can be functionalized with various polar components, such as choline, ethanolamine or sugar molecules. **Sphingolipids** (Figure 2.1.c) are made of an acyl chain attached to a sphingosine moiety; the polar head can also have various functional groups attached, such as phosphatidylcholine or sugar molecules. **Cholesterol** (Figure 2.1.b) is a sterol that plays a role in the spatial organization of the membrane components.[167, 168, 169] The lipid bilayer functions as a two-dimensional liquid. Its dynamics depend on the temperature, the lipid composition, the presence of cholesterol and other membrane components such as proteins.[170, 171, 172, 173, 162]

Transmembrane proteins mediate communication across the cell membrane to regulate many functions of the cell. Transmembrane proteins contain in their primary structure one or several sequences of hydrophobic amino acids allowing stable incorporation into the lipid bilayer. Transmembrane proteins are integral parts of the plasma membrane and, together with membrane lipids, can form transient microdomains that are important for the organization of the membrane and for activation of biological processes.[171, 162] Since the plasma membrane is highly elastic, it can adopt various shapes that are modulated by a dense network of structural proteins of the cell's cytoskeleton such as microtubules or actin filaments.[174] Cells adopt tissue-specific shapes[175] which, for example during evolution of cancer, are substantially modified.[176]

2.1.2 Probing viscoelastic characteristics of cell membranes

Mammalian cells are continuously changing their shape as they are (i) moving (motility), (ii) probing their environment or contacting neighboring cells via filopodia or membrane nanotubes for exchanging physical and chemical signals, or (iii) undergoing external mechanical stress.[177, 178, 179, 180, 181, 182, 183] Figure 2.2 shows typical examples of cultured cancer cells which continuously are sending out filopodia-like nanotubes to finally establish contact with neighboring cells for intercellular exchange of cellular components and molecules.

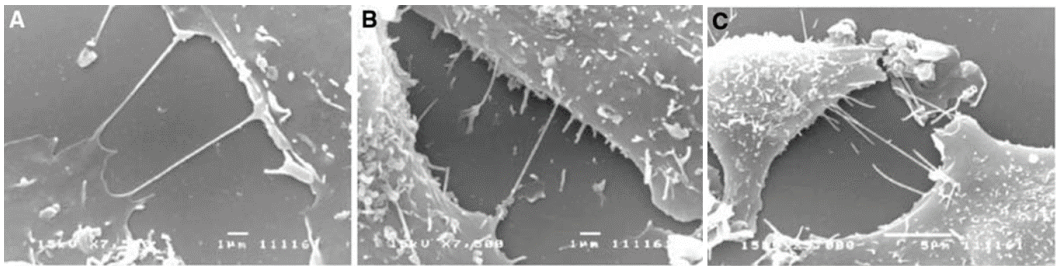

Figure 2.2: Scanning electron micrographs of cultured cancer cells sending out filopodia-like nanotubes. *Some nanotubes make direct contact with a neighboring cell for intercellular exchange of compounds. Image from [179]*

In consequence, cellular membranes, primarily the plasma membranes, are permanently changing their shape. In order to describe these membrane shape changes in physical terms and to assign energies to the different membrane configurations, it is useful to distinguish the different membrane deformations in the framework of continuum elasticity theories (see chapter 11 in [184]). As shown in Figure 2.3, the principal deformations of a cell membrane can be described as stretching of a membrane, bending of a membrane, thickness deformation of a membrane, and shearing of a membrane. In cells, the deformations of plasma membranes are linked to complex processes between membrane proteins, cytoskeleton and motor proteins.[185] It is therefore not surprising that the first experimental approaches to understand the mechanical and viscoelastic properties of membranes are undertaken using model membranes in form of giant unilamellar lipid vesicles (GUVs).[186, 187, 184, 188]

Elastic properties of pure lipid bilayers measured by stretching vesicles

The classical approach introduced by Evans and Needham is based on a micropipette aspiration technique, schematically outlined in Figure 2.4. A glass micropipette is brought in contact with a spherical GUV. The vesicle is then partly sucked into the pipette under controlled pressure, which results in a deformation of the vesicle. On the basis of the measured geometrical parameters using video microscopy and the known pressure difference between the inside of the vesicle and the inside of the pipette, it is possible to determine the membrane tension and the membrane's material properties such as the bending modulus K_b and the area stretch modulus K_a. On the basis of measured geometrical parameters of pipette aspirated vesicles (Figure 2.4) an expression of membrane tension γ and area stretch modulus K_a was derived as [186]:

$$\gamma = \frac{\Delta p}{2} \cdot \frac{R_l}{1 - \frac{R_l}{R_v}} \tag{2.1}$$

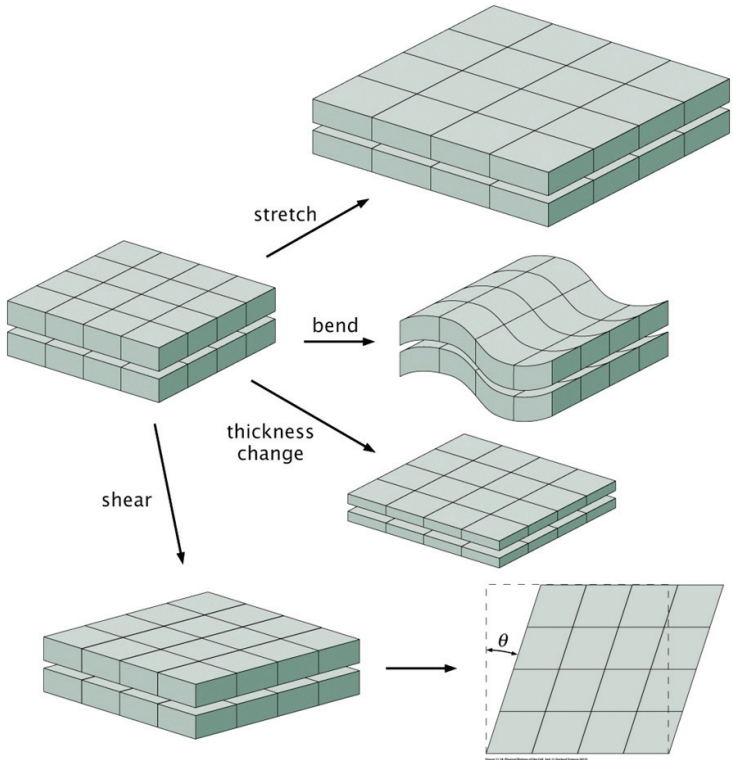

Figure 2.3: Schematic depiction of the principal deformations of a cell membrane. *Cell membranes can be subjected to stretching, bending, thickness changes or shear. Shear deformation is characterized by an angle θ describing the deviation from the undeformed membrane. Image modified from [184]*

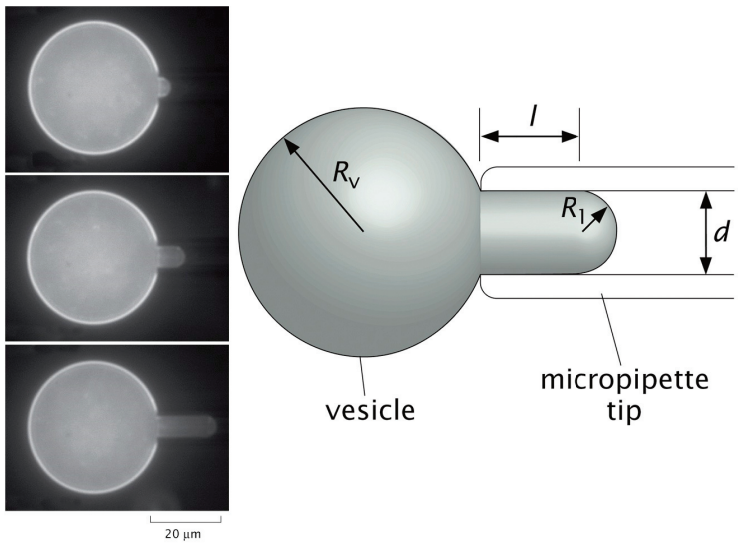

Figure 2.4: Pulling of a membrane tube from an lipid vesicle. *The suction of a micropipette is used to pull a tube out of the membrane of a lipid vesicle. Left: the bigger the aspiration force is, the longer the tube is elongated. Right: the physical parameters used in equations 2.1 and 2.2 for the calculation of the membrane tension γ and stretch modulus. Image adapted from [184]*

where $\Delta p = p_{in} - p_{out}$ is the pressure difference between the inside of the micropipette and the medium surrounding the vesicle;
and

$$\gamma = K_a \frac{\Delta a}{a_0} = K_a \cdot R_l^2 \cdot \frac{1 + l \cdot R_l}{2 \cdot R_v^2} \tag{2.2}$$

where Δa is the membrane area change during vesicle aspiration and a_0 is the area of the vesicle at the resting state.

In the vesicle aspiration experiments, the size and shape of the aspirated membrane tube is constrained by the geometry of the micropipette. However, membrane tubules formed by cells are quite different extending as long, cylindrical structures from the plasma membrane reservoir. Considering a lipid vesicle as the most simplified model of a cell membrane again, the question arises, whether a pulling force applied at a defined point at the vesicle surface will finally produce an extruded membrane tether of micrometer or nanometer diameter. This was realized experimentally by applying a point force on the vesicle surface via a locally attached microbead, which was pulled at a defined force by either an optical or a magnetic tweezer, or by reconstituting molecular motors at the vesicle surface as depicted in Figure 2.5. From these pulling experiments both the bending modulus K_b and the tension γ of the membrane can be determined according to the relation of these properties to the tether diameter r and the pulling force f (see Figure 2.5):

$$r = \sqrt{\frac{K_b}{2 \cdot \gamma}} \tag{2.3}$$

$$f = 2 \cdot \pi \cdot \sqrt{2 \cdot K_b \cdot \gamma} \tag{2.4}$$

The seminal micropipette aspiration and optical tweezer pulling experiments on lipid vesicles revealed for the first time the viscoelastic properties of pure lipid bilayers and opened the door for subsequent experiments on plasma membranes of living cells. In the context of the present thesis chapter, the following findings are of importance. The measured forces required for drawing a membrane tether from a lipid vesicle or from the plasma membrane of a mammalian cell are in the order of 10 pN (Figure 2.5-E). Rewriting equation 2.4 yields $\gamma = f^2/(4 \cdot \pi^2 \cdot 2 \cdot K_b)$. Typical values for the bending modulus are in the order of $K_b \sim 50 \cdot k_b \cdot T$ ($k_b \cdot T = 4 \frac{pN}{nm}$) deduced from K_a values[189] according to $K_b = \frac{1}{12} \cdot K_a \cdot d^2$ where d is the lipid bilayer thickness (this holds for the case of a lipid bilayer with coupled monolayers and uniform stress modulation).[187] Using these data we obtain $\gamma = 0.01 \frac{pN}{nm}$ (or $\frac{mN}{m}$) as a typical order of magnitude for the tension of a lipid bilayer and in turn from equation 2.3 $r \sim 50$ - 100 nm as the diameter of the pulled membrane nanotube which nicely fits to the dimensions

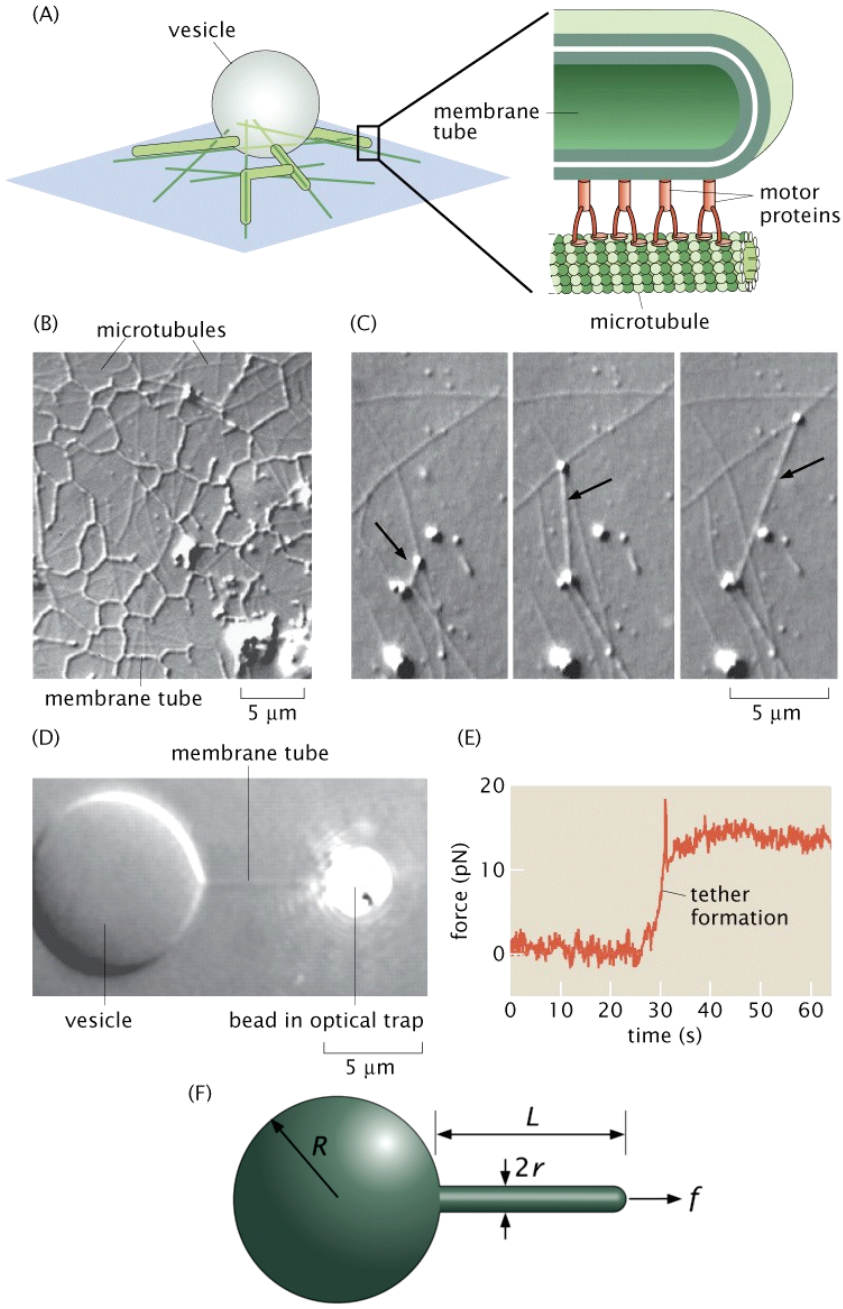

Figure 2.5: Extrusion of tubes by the application of a point force at the membrane of lipid vesicles. *(A) Schematic elongation of membrane tube from a lipid vesicle with the help of molecular motors attached to the membrane and guided by microtubules. (B) Elongation of membrane tubes over a mesh of microtubules. (C) In 11 s, the molecular motors drive the elongating membrane tether along several tracks of microtubule over 10 µm. (D) Elongation of a vesicle membrane nanotube using an optically trapped bead attached to the membrane. (E) Time vs force recording of an experiment such as in (D). The force needed to extract a tether is in the order of 10 pN. Once extracted, the elongation of the tube requires no higher force. (F) Schematic model of a tether elongated by application of a point force on the membrane of a vesicle. Image adapted from [184]*

of plasma membrane nanotubes for cells reported elsewhere.[179, 190]

A nanotube pulled by a point force from an optical or magnetic tweezer can be retracted by switching off the point force. The back-relaxation typically follows single exponential kinetics (see equation 2.6) from which viscoelastic properties of the membrane system can be determined using the following equation:

$$\tau \approx \frac{\eta_m + \eta L_0}{\mu} \tag{2.5}$$

Here τ is the relaxation time for elongation length L_0, η_m the membrane viscosity, η the viscosity of the surrounding aqueous medium and μ the membrane shear modulus. This kinetic description has been used to evaluate viscoelastic properties of the plasma membrane nanotubes of (i) HEK cells drawn with optical tweezers[191] and (ii) RB cancer cells drawn with magnetic tweezers.[190] As underlined by several studies, addition of chemicals impairing the cell's cytoskeleton diminishes the force needed to pull membrane tethers and increases nanotube relaxation time.[192, 193, 191]

2.1.3 Optical tweezers/microfluidic microscope

The optical tweezers microscope used in this thesis was designed by Michael Werner.[53] It consists of a commercial wide field inverted microscope (Axiovert 200M, Zeiss) equipped with different objectives. A couple of lasers for fluorescence excitation at different wavelengths are available. A selected laser is fed into the objective (Plan-Apochromat 100x/1.45 Oil, Zeiss) for a wide field illumination. A 100x objective is particularly suited for the observation of micron-sized objects (membrane nanotubes, beads of chapter 3). The large numerical aperture of this objective ensures a high trapping efficiency of the optical tweezer, as the trapping force depends on it. Typically used lasers have wavelengths at 488 nm (500 mW max output, JDS Uniphase, for excitation of eGFP in chapter 3) and 543.5 nm (5 mW max output, Melles Griot, for excitation of Texas Red in chapter 3). For optical trapping, we used an Ytterbium near infrared laser at 1064 nm TEM_{00} mode (YLD-10-1064-LP, IPG Photonics) with a maximal output power of 10 W. This infrared laser is ideally suited to work on biological samples because of its high penetrative power and low absorption in tissues. Hence, only little energy is dissipated in the living tissues, reducing the risks of photodamaging the plasma membrane. A large portion of the infrared laser power is lost passing the optics, the immersion oil and the glass coverslip; the final output power at the sample is reduced to 2.6% of the output power at

the optical fiber (measured with a power meter model 2930C and a photodiode sensor 818 SL, Newport). Hence, the surface power of the optical trap ranges from 0.24 to $25{\cdot}10^6$ $\frac{W}{cm^2}$ on the 1 μm^2 surface of the optical trap focus. All images, videos and real-time monitoring, in transmission and in fluorescence, are recorded with a CCD camera (Pixelfly, PCO).

Microfluidic components are coupled to the optical tweezer microscope. Two 100 μl glass syringes (Hamilton) are installed on two separate two-syringe pumps (SP 210 IWZ, WPI) to create the main flows of the system. The pumps are controlled by a home made Labview® interface (National Instruments). PTFE tubes (FEP Fluoropolymer Tubing, DuPont) connect the syringes to directional valves. Three-path valves are connected to the syringes on the pumps and to a large-reservoir syringe to fill up the pump syringes which are connected to the microchip. The chip is placed on the sample stage of the microscope to allow direct observation of processes inside the channel such as manipulations performed by the optical tweezer. An output PTFE tube connects the chip to a waste collector.

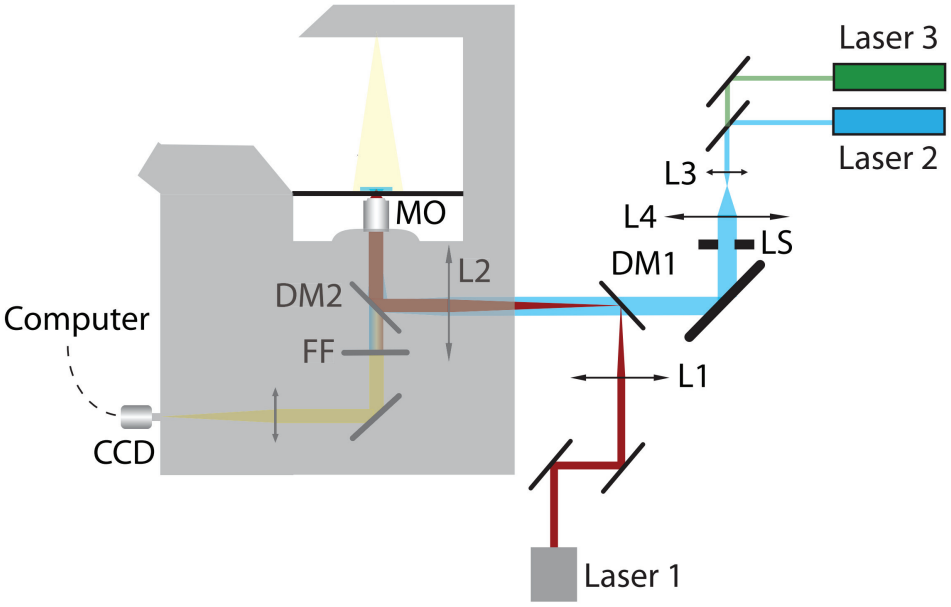

Figure 2.6: Scheme of the optical tweezer, fluorescence microscope setup. Laser 1 *is the 1064 nm TEM_{00} near infrared laser used for optical trapping.* ***Laser 2*** *and* ***Laser 3*** *are fluorescence excitation lasers, emitting light at 488 and 543.5 nm, respectively.* ***L1*** *is the first lens to focus the trapping laser.* ***L1*** *together with lens* ***L2*** *serve as a telescope in order to adapt the diameter of the laser beam such that it slightly overfills the objective's back aperture.* ***L3*** *and* ***L4*** *are controlling the diameters of the beams of* ***Laser 2*** *and* ***Laser 3****.* ***LS*** *is the shutter to control fluorescence excitation.* ***DM1*** *and* ***DM2*** *are dichroic mirrors allowing the superposition of the three lasers into the same optical path of the microscope objective and to isolate the output fluorescence signal of the sample.* ***MO*** *is the microscope objective focussing axcitation and trapping beams and collecting fluorescence.* ***FF*** *are the filters to isolate the fluorescence signal.* ***CCD*** *is the CCD camera to record images of the sample. Figure modified from [194].*

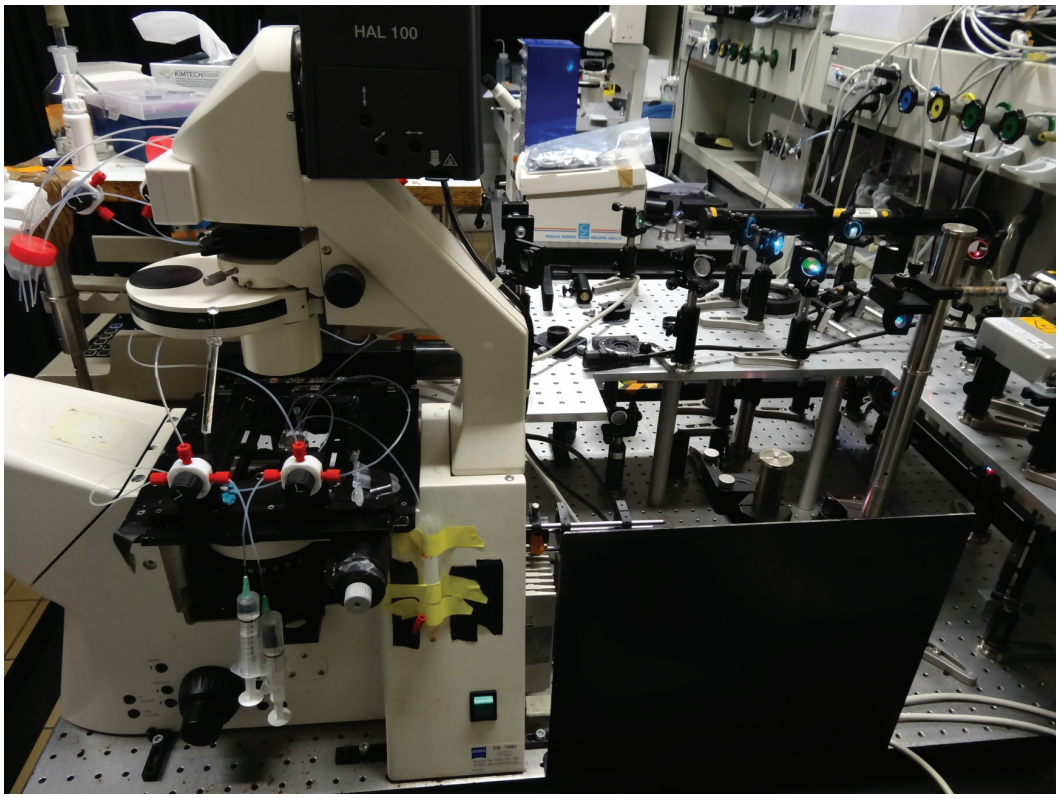

Figure 2.7: Photo of the optical tweezer setup with integrated microfluidic components used in this work. *The upper stage is dedicated to the fluorescence excitation lasers, which join the optical path of the trapping laser on the lower stage before entering in the back side of the microscope. Valves, tubing and syringes are part of the microfluidic components.*

2.2 Experimental

2.2.1 Requirements for optical trapping

As the laser based optical trap generates heat, the medium surrounding the sample is exposed to a temperature gradient that creates a convective flux in the surrounding bulk liquid. Cell culture tends to generate a large amount of micro-debris of organic materials floating all around the cells under consideration. Focusing a laser in a large aqueous medium hence give rise to unwanted liquid displacement which is not only disturbing by itself, but also continuously feeding the laser focal spot with undesired organic material that tends to fuse with soft trapped elements such as cell membranes. To prevent this to occur, all the experiments described in this chapter have been performed in microchannels. The limited size of the volume of the "sample compartment" exposed to the laser insures a locally homogeneous distribution of heat, suppressing any unwanted convective flux and thus preventing cell debris to get transferred towards the optical trap. Hence we performed our analyses in microfluidic channels with the lowest height possible, which turned out to be 50 μm.

All liquids used for the microfluidic experiments have been carefully filtered to prevent large particles clogging the microchannels, especially when using chips with micrometer-sized cross-sections. Liquids also have been carefully degassed in order to avoid the formation of air bubbles in the microfluidic channels. Air bubbles can either clog the channels or destroy the glass bottom of the microchip by extremely fast dilatation when passing in the focus of the laser tweezers.

2.2.2 Cell culture

After taken from the patient's tumor, the primary melanoma tumor cells were cultured in plastic culture flasks (Tissue culture flask, TPP) in Tu 2% medium composed of 79% MCDB 153 medium (Sigma) supplemented with sodium bicarbonate (Sigma), 19% L-15 medium (Sigma), 2% NBCS (Sigma) and 0.5% bovine insulin (from bovine pancreas, Sigma), with the addition 100 $\frac{\mu g}{ml}$ of a preparation of penicillin and streptomycin (AppliChem) in a 34 °C sterile cell culture incubator.

HEK cells were cultured in cell culture medium (DMEM/F-12 GlutaMAX™ Supplement, Life Technologies) supplemented with 10% NBCS, penicillin and streptomycin.

2.2.3 Microchip fabrication

Fabrication of microchips follows the method described by McDonald *et al.*.[195] It starts with the design of the geometry of the channel paths using the software QCad (RibbonSoft) to elaborate the desired microfluidics features. The design is transferred to the software AutoCAD (Autodesk) to be exported as a correct file type (.dwg) that was sent to the Stanford Microfluidic Foundry (Stanford University) for the creation of a negative silica mould which was used for serial chip fabrication. A mixture of PDMS elastomer and curing agent (Sylgard® 184 silicone elastomer kit, Dow Corning) is poured on top of the mould to reach a final layer thickness of approximately 5 mm. Bubbles are removed under vacuum for 2 hrs and the liquid is placed overnight in a 80°C oven for curing. Cured chips are cut from the mould, inlet holes are punched with a custom sharp edge steel tube 1.2 mm diameter. Chips are cleaned by sonication 15 min in ethanol, 15 min in water, 15 min in ethanol and dried under nitrogen stream. Rectangular 24 mm x 50 mm glass coverslips (Menzel-Gläser) are cleaned by sonication three times 15 min in alkaline detergent (Hellmanex® II, Hellma Analytics), three times 15 min in Milli-Q® water, once 15 min in methanol and stored in ethanol. Coverslips are dried under nitrogen stream and put together with dried chips in a plasma cleaner (Harrick Plasma) for final cleaning and surface activation for 1 min. PDMS chips are laid on top of coverslips and pressed to remove air bubbles. Full chips are exposed over 1 hr to UV light for completing PDMS to glass bonding.

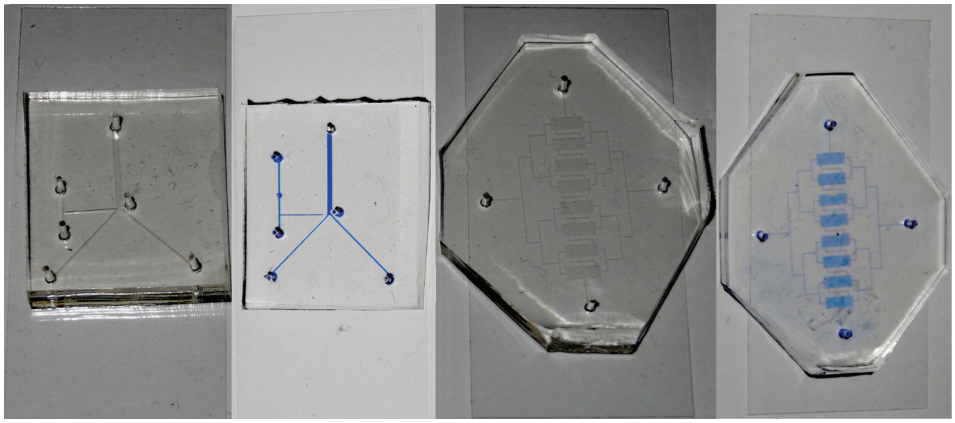

Figure 2.8: Examples of two microfluidic chips, both depicted with empty channels and channels filled with colored liquid. *Left: The chip has a channel height of 50 µm and has been used for the experiments described in chapters 2 and 3. Right: The chip has a channel height of 20 µm and has been designed to make successive dilutions by a factor of two over three orders of magnitude of one component as the other remains at a constant concentration.*

2.2.4 Attaching cells inside microfluidic chip

Microfluidic channels are incubated 1 hr with a poly-L-Lysine solution to promote cell adherence to the glass surface. Cells from a confluent 25 cm^2 culture flask are detached with a 5 mM EDTA solution, centrifuged at 290×g and resuspended in EDTA-free cell culture medium (DMEM, Life Technologies). Cell suspension is injected very slowly with a syringe into the Poly-L-lysine treated microchip with multiple pauses in the injection process for allowing the cells to sediment and adhere to the surface. The syringe is removed and the chip is put in a 37°C cell incubator during several hours for allowing the cells to recover and grow.

2.2.5 Membrane relaxation experiments

The focus of the laser of the optical tweezers is placed on the very edge of the plasma membrane of a cell in a microfluidic channel, slightly above the glass surface of the chip, and the power of the laser is increased until it traps the cell membrane. The plasma membrane is pulled out of the cell. At the maximum elongation distance, the laser tweezer is switched off and the back-relaxation sequence of the plasma membrane is recorded. Data are analyzed with the software ImageJ (Wayne Rasband, National Insitutes of Health). Experiments are done in PBS (Dulbecco's modified phosphate buffered saline, Sigma).

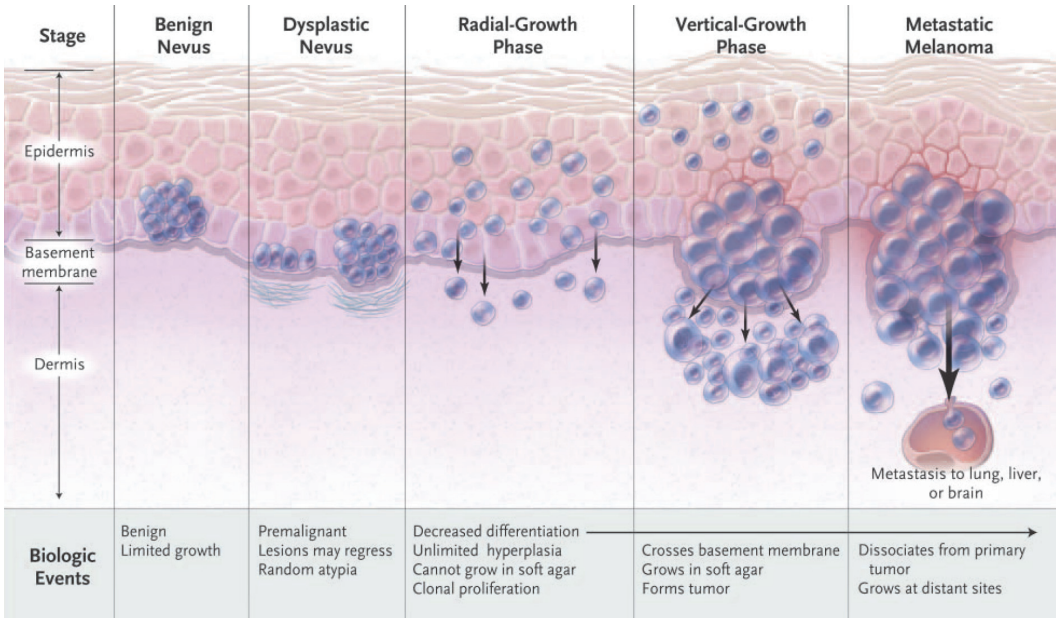

Figure 2.9: Panel of the abnormal behaviour of human skin melanocytes, *from the inoffensive naevus to the lethal metastatic melanoma. Referring to our tumor cell samples, SBCl2 cells are in the radial growth phase, WM115 cells in the vertical growth phase and WM239A cells are lymphatic node metastases. Image from [159]*

2.3 Results and discussions

2.3.1 Melanoma tumor cells

Three different kinds of human skin melanoma cell strains were kindly provided by Dr. Agnese Mariotti (CHUV, Lausanne, Switzerland) and were used to investigate the viscoelastic properties of their plasma membranes. The three different samples of cancer cells have been taken from tumors at different stages of the evolution of a skin melanoma. SBCl2 [196] are primary tumor cells in the radial growth phase. They are typically growing on a local base, sticking to the epidermis, and do not invade neighbouring tissues.[197] WM115 [198] are primary tumor cells in the invasive vertical growth phase. At this growth phase, the tumor cells start to expand through the adjacent layers of skin and become invasive towards neighbouring tissues. WM239A [198] are tumor cells form lymph-node metastases. At this growth phase, malignant cells spread over the patient's body via the circulatory blood and lymphatic systems.[199] When they finally get fixed at a suitable place in a different organ, a secondary, metastatic tumor starts growing.[200]. Both WM115 and MW239A were taken from the same patient. Figure 2.9 shows the evolution of the different phases from a clinically not relevant nevus to a metastatic malignant melanoma. As three samples of tumor cells exhibit substantially differ-

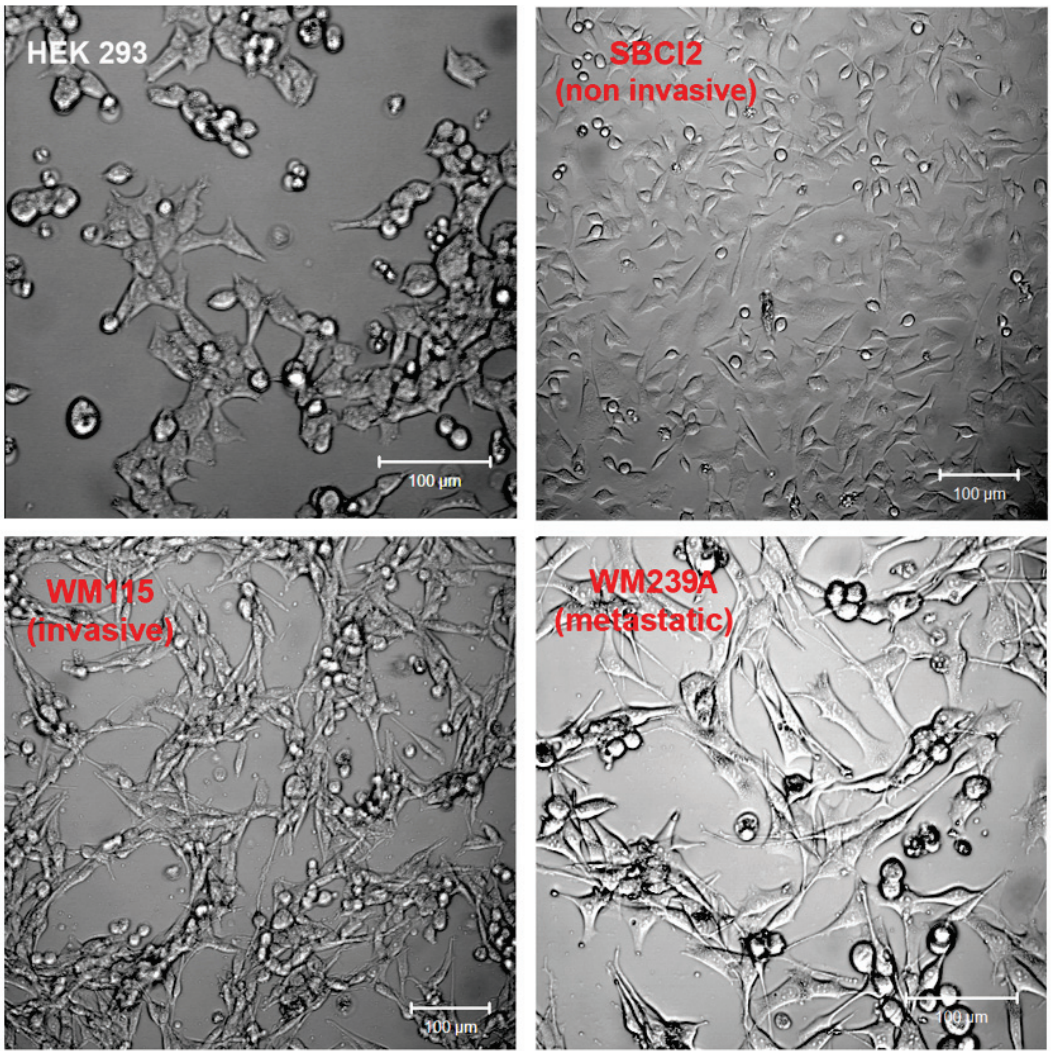

Figure 2.10: Morphological comparison of the three melanoma cells with HEK cells. *The plasma membranes of SBCl2 cells are less optically contrasted than those of the other cells. WM115 cells organize themselves in form of an irregular network.*

ent morphologies, we expected to detect differences in their viscoelastic properties. Figure 2.10 shows the morphological differences of our three different cell types visible in the optical transmission microscopy images; the spatial organization of the cells in different stages of tumor evolution differs substantially. We observed that the WM115 cells never reached 100% surface confluence while cultured, but rather adopted a mesh-like two-dimensional pattern.

2.3.2 Pulling membranes with no handles

The aim of the project was to investigate the capability of discriminating three different cellular states of human skin melanoma cells by observing the relaxation of membrane nanotubes

pulled out from the cellular body by optical tweezers. For this, we used the method developed by Pascoal *et al.*[191] to pull a membrane tube without any external object that could act as a physical handle. The first trials were done by focusing the laser tweezer on bare cells in a large depth culture dish. As explained in section 2.2.1, under these conditions the trapping laser beam generated a convective stream in the surrounding liquid inducing aggregation of cellular micro-debris in the focus of the trapping laser. The decision to perform the experiment in an microfluidic environment allowed to suppress totally the laser-induced convective stream and to prevent accumulation of cellular debris in the trapping laser focus. A slight increase of the temperature in the immediate surrounding of the trapping focus was a minor concern, as the measurements were performed at room temperature and locally produced heat efficiently dissipated to the bulk liquid, glass and PDMS.

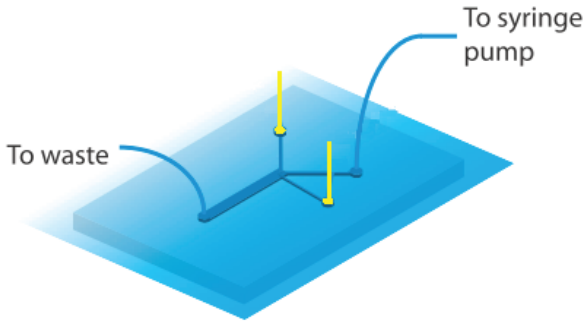

Figure 2.11: Microfluidic chip *in which the membrane pulling and back-relaxation experiments were performed. The two auxiliary side channels were blocked (yellow elements) to leave only one main functional channel in which cells were grown and probed.*

Cells cultured in a microchip as described in section 2.2.4 adhered strongly to the polylysine-treated glass surface. Hence the cell membrane could be manipulated properly under a very gentle liquid flux. To pull a nanotube out of a cell, the trapping laser was directed to the edge of the cell. When switching on the laser, the membrane is attracted to the trap. The focal point of the laser is then moved away over distances ranging from 5 to 45 μm (example of the pulling and relaxation of one nanotube in figure 2.13 (A) and (B)). Up to three different nanotube pulling experiments could be achieved on a single cell without observing cellular damage.

Successful experiments pulling plasma membrane nanotubes were much more frequent and required a lower laser power for WM239A cells than for SBCl2 cells. This is due to a bigger difference in refractive index between the buffer and the metastatic cells than for the cells in radial growth phase (See Figure 2.10). Laser output power of 5 W (approximately 130 mW at the cell) was sufficient to pull rather successfully nanotubes from WM239A cells or WM115,

whereas at least 8 W (approximately 210 mW at the cell) was needed to do so for SBCl2.

When pulling nanotubes from the plasma membrane of cells, they can rupture off after a certain distance resulting in the formation of a spherical vesicle of a size of 1 to 1.5 μm. These cell-derived vesicles comprise part of the cellular membrane and cytoplasm and can be used as closed cargoes for analysis of transmembrane signaling processes.[201] Alternatively to using laser tweezers, native vesicles can be extracted from living cells by exposing the cells to cytochalasin B, which is known to disrupt the interaction of the cell's plasma membrane to the cytoskeleton.[202]

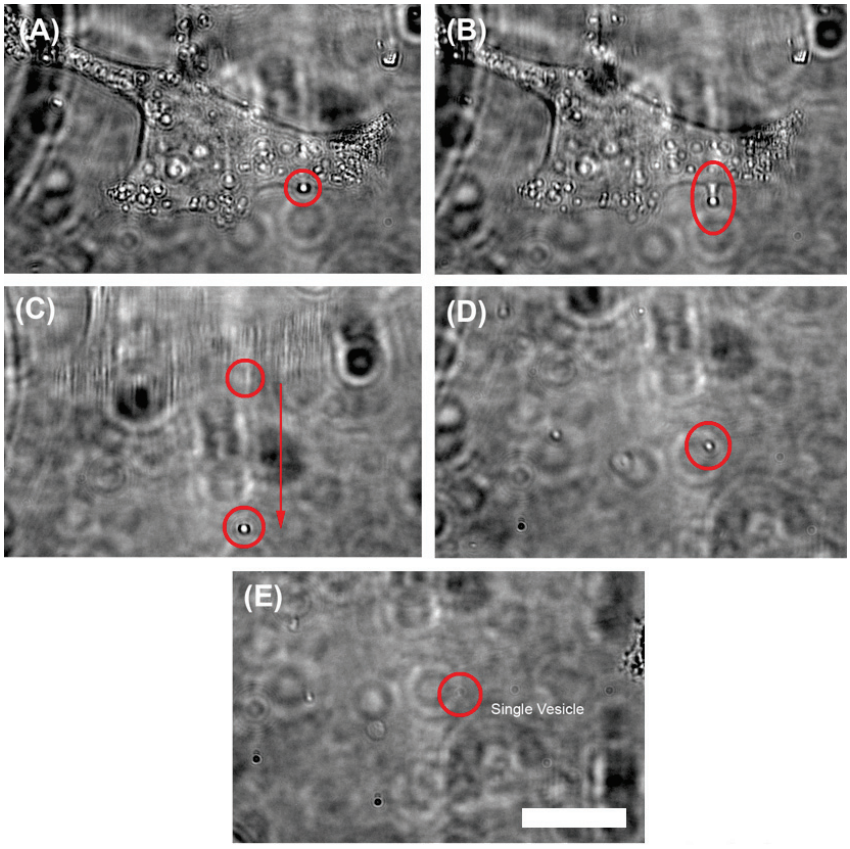

Figure 2.12: Vesicle extraction from a WM239A cell. *If the nanotube is pulled beyond a threshold length, it ruptures off from the cell and reorganizes as a spherical vesicle. Scale bar = 10 μm.*

2.3.3 Back-relaxation of pulled nanotubes

After a membrane nanotube has been pulled out from the surface of a cell and the optical laser trap is switched off, the membrane nanotube retracts (Figure 2.13). The membrane and cellular structural proteins undergo a rearrangement process to recover from the deformation.

This causes the nanotube to quickly retract from its tensed elongated state and shrink back as close as possible to the original resting state of the plasma membrane on the surface of the cell. The time-dependence of the relaxation process follows a monoexponential decay:

$$L(t) = L_0 \exp(\frac{t - t_0}{\tau}) + L_\infty \tag{2.6}$$

L(t) is the length of the nanotube at time t, L_0 the elongation length of the nanotube a time t_0 at which the laser is switched off, τ the characteristic relaxation time for a specific elongation length (see eq. 2.5), and L_∞ the residual length of the nanotube at infinite time. The residual length appears to be related to the large deformation of the membrane and the photodamage occurring sometimes at high laser power. Nanotube relaxation is a process not fully understood yet, but it is highly probable that the tubes contains cytoskeletal elements taking part to the membrane rearrangement.

Relaxation process during retraction of the nanotubes has been measured by monitoring the length of the nanotube as a function of time after switching off the trapping laser. The recordings were processed at 10 frames per second to reach an optimal compromise between visibility of the nanotube extremity and the sampling frequency. The length is measured in pixels with the software ImageJ and converted into micrometers. The three melanoma cell lines, SBCl2, WM115 and WM239A, exhibited a relaxation time linearly correlated with the nanotube elongation length (Figure 2.14). The analysis of variance (ANOVA) [203] shows a significant effect of the elongation length on the nanotube relaxation time ($p\text{-}value = 2.3 \cdot 10^{-6}$). Moreover the analysis shows a statistical relevant distinction between the cancer cell types ($p\text{-}value = 2.49 \cdot 10^{-8}$). A deeper analysis performed by Tukey's honest significant difference (HSD) test [204] reveals a statistical significant distinction between WM115 and SBCl2 ($p\text{-}values = 1.8 \cdot 10^{-5}$) and between WM115 and WM239A ($p\text{-}values = 7.9 \cdot 10^{-5}$). In contrary, there is no statistical significant difference between SBCl2 and WM239A ($p = 0.70$).

The plasma membrane of WM115 cells shows a profile denoting a higher deformability and a longer time to get back to its membrane resting state, whereas the membranes of SBCl2 and WM239A cells are stiffer and relax back faster to the initial position. The viscoelastic parameters calculated from the measured relaxation times using equation 2.5 are depicted in table 2.1. While the membrane viscosities determined here for the melanoma cells are similar as those found for other cells investigating membrane tubes (with the exception of RB cells which show an order of magnitude higher values), the shear moduli of the melanoma cells are considerably lower than those reported for all other cells (Table 2.1). The variation of

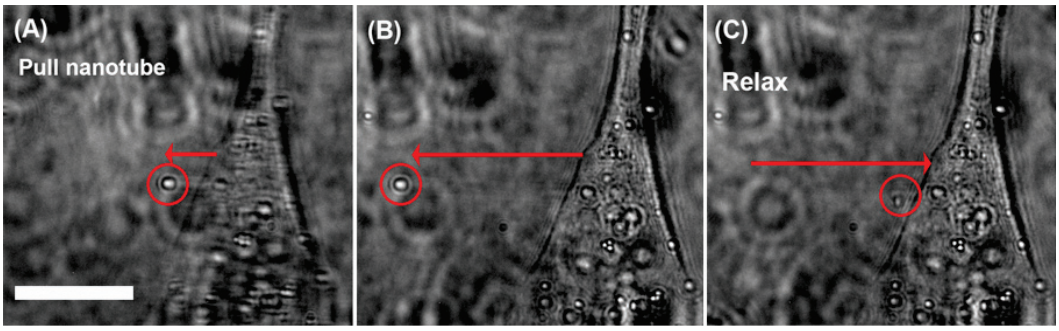

Figure 2.13: Three steps of the pulling and relaxing experiment. *(A) The laser is positioned at the membrane edge and switched on. The optical tweezers become effective and trap the plasma membrane. (B) The membrane nanotube is pulled over a few tens of micrometers. (C) The laser is switched off; the trap is no more effective and the nanotube rapidly relaxes back to its original position at the cell surface. Sometimes, after the relaxation process, a small deformation L_∞ remains at the plasma membrane of the cell surface. Scale bar = 10 µm.*

shear moduli of the different cancer cell types determined by our optical method showed a qualitatively similar trend as the Young's moduli reported by Weder *et al.* [205] on the same cancer cells, but investigated with a different method, (table 2.1). For their experiments, 5 μm glass spheres were glued to the tip of an AFM cantilever and the tip was moved up and down with an amplitude of 500-1000 nm on top of the cell up to a maximal force of 500 pN. Young's moduli were calculated via Hertzian fit of the force-distance curves. This model approximates the entire cell as an isotropic and linear solid. This model is widely used to characterize the elasticity of whole cells although the cell is known to be a highly heterogeneous and anisotropic assembly of biopolymers.[206] In order to compare the the values of the Young's moduli in table 2.1 [205] with the shear moduli of the melanoma cells in table 2.1, we attribute the Young's modulus of a cell exclusively to its two-dimensional plasma membrane. In this approximation we can calculate from Young's modulus Y the membrane shear modulus μ:

$$\mu = \frac{Y \cdot d}{3} \tag{2.7}$$

where d = 6 nm is the thickness of the cell's plasma membrane [207](Chapter 11, p. 339). The corresponding values are depicted in table 2.1. The thus derived values for the shear moduli are about 30-50 times higher than those determined by the membrane nanotube method, indicating that the Young's moduli determined by the AFM method reflects a composition of the cell membrane and all the underlying cellular components as a whole, whereas the nanotube method characterizes primarily the viscoelastic properties of the cellular plasma membrane and the parts of the cytoskeleton directly attached to this membrane. The relative

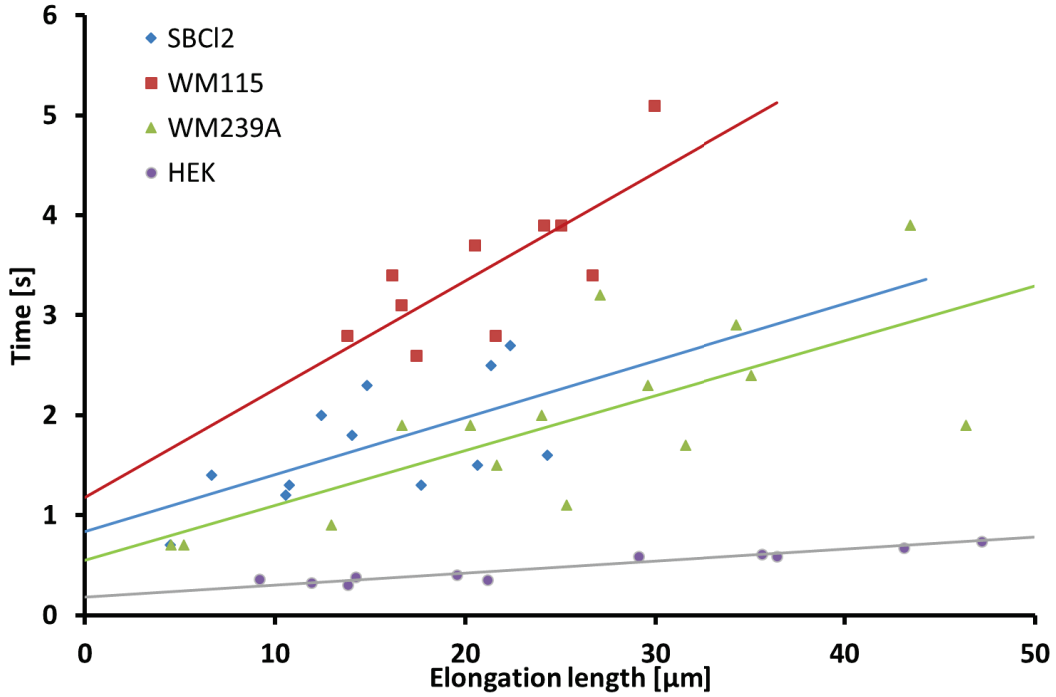

Figure 2.14: Relaxation time vs nanotube elongation length. *The following viscoelastic properties are deduced from this graph:*
SBCl2: $\eta_m = 1.5 \pm 0.4 \cdot 10^{-5}$ *mN·s/m,* $\mu = 1.8 \pm 0.4 \cdot 10^{-5}$ *mN/m*
WM115: $\eta_m = 1.1 \pm 0.1 \cdot 10^{-5}$ *mN·s/m,* $\mu = 9.2 \pm 1.0 \cdot 10^{-6}$ *mN/m*
WM239: $\eta_m = 1.0 \pm 0.2 \cdot 10^{-5}$ *mN·s/m,* $\mu = 1.8 \pm 0.4 \cdot 10^{-5}$ *mN/m.*
For comparison, data measured on HEK cells in another study using the same method [191]:
HEK: $\eta_m = 1.5 \cdot 10^{-5}$ *mN·s/m,* $\mu = 8.3 \cdot 10^{-5}$ *mN/m.*
η_m *is the membrane viscosity and* μ *the membrane shear modulus.*

Cell/vesicle type	Treatment	Membrane viscosity η_m mN·s/m	Shear modulus μ mN/m	Reference
GUVs	SM/Chol 1:1	$7.1{\cdot}10^{-5}$		[208]
GUVs	SOPC	$9{\cdot}10^{-6}$		[208]
GUVs	SOPC/Chol 1:1	$1.2{\cdot}10^{-5}$		[209]
RBC	none	6-8·10^{-4}	$6{\cdot}10^{-3}$	[210]
RBC	none		5-7·10^{-3}	[211]
RBC	none		$2.5{\cdot}10^{-3}$	[212]
RBC	none	$8.8{\cdot}10^{-4}$	$6.1{\cdot}10^{-3}$	[213]
HEK	none	$1.5{\cdot}10^{-5}$	$8.3{\cdot}10^{-5}$	[191]
HEK	Cytochalasin B	$3.5{\cdot}10^{-6}$	$4.9{\cdot}10^{-5}$	[191]
HB	none	1.6 (AFM) or 1.2 (MT) $\cdot 10^{-5}$	$4.5{\cdot}10^{-5}$	[190]
HB	Latrunculin	0.8 (AFM) or 1.1 (MT) $\cdot 10^{-5}$	$8.4{\cdot}10^{-5}$	[190]
CHO	none	2.1 (AFM) or 7.9 (MT) $\cdot 10^{-5}$	$4.9{\cdot}10^{-4}$	[190]
NGC	none	$1.37{\cdot}10^{-4}$		[193]
SBCl2	Grown on PLL	$1.48{\cdot}10^{-5}$	$1.76{\cdot}10^{-5}$	
WM115	Grown on PLL	$1.08{\cdot}10^{-5}$	$9.23{\cdot}10^{-6}$	
WM239A	Grown on PLL	$1.01{\cdot}10^{-5}$	$1.83{\cdot}10^{-5}$	
Weder *et al.* study		**Young's Modulus [Pa] and (μ [mN/m])**		
SBCl2	Grown on PLL	194 Pa ($4.8{\cdot}10^{-4}$ mN/m)		[205]
WM115	Grown on PLL	114 Pa ($2.8{\cdot}10^{-4}$ mN/m)		[205]
WM239A	Grown on PLL	247 Pa ($8.4{\cdot}10^{-4}$ mN/m)		[205]

Table 2.1: Viscoelastic properties of cells *measured under various conditions. Data from red blood cells were collected by observing the suction of membrane tethers inside a micropipette.[211] HB and CHO data were measured both by AFM and magnetic tweezers (MT) nanotube formation and detachment.[190] NGC and vesicle data were calculated from the force needed to pull one tether from the cell membrane. HEK, SBCl2, WM115 and WM239A cells measurements were performed as described in section 2.2.5. Young's moduli were measured by pressing AFM tips to the top of cells.[205]*
GUVs: giant unilamellar vesicles, SM: sphingomyelin, Chol: cholesterol, SOPC: 1-stearoyl-2-oleoyl-sn-glycero-3-phosphatidylcholine, RBC: red blood cells, HEK: human embryo kidney, HB: human brain tumor, CHO: Chinese hamster ovary, NGC: neuronal growth cone, PLL: Poly-L-lysine

stiffness as measured here by the membrane shear moduli of the different melanoma cell types is directly related to the progress of the melanoma tumor state. WM239 cells could be expected to be the most mobile and most deformable ones as they are the most invasive ones among the three cell types investigated.[156, 214] Cells of this type circulate in the blood and lymph systems and undergo severe deformations to penetrate tissues at remote locations to establish metastatic nodules.[215] These nodules, once established, form a new cancer cell colony, adapting the surrounding tissue to its growth needs. The creation of a dense network of blood vessels and the resilience needed to resist to the compression consecutive to its self growth explains the increased stiffness of the metastatic cells.[216] It appears that growing metastatic nodules in a non-native environment exert a mechanical pressure on their surrounding and, in return, are being compressed themselves; hence to survive, cells with the most resistive mechanical abilities are selected over the softer ones and give to metastases a more cohesive character. This may explain why the WM239A cells analyzed here display a higher stiffness, as they have been extracted from a lymph-node metastatic tumor and were no more in the blood circulation.

2.3.4 In-flow immobilizing microchip

A specific chip has been designed for the in-flow immobilization of cells to increase the processing throughput of membrane probing. Inspired from the cell-docking microchip of Skelley *et al.*[54], the microstructural element is placed in the centre of the main chamber of the chip (Figure 2.15). It is designed to dock one single cell and a hole is left on the downstream extremity to allow access to the membrane for pulling membrane nanotubes. After nanotube back-relaxation, the cell is expected to be removed with the help of the optical tweezers, from the dock and released in one of the two lateral streams, where a potential sorting step could be implemented. After several trials, the PDMS docking element was observed to be a much too sticky structure as it was impossible to move the cell out of the microfluidic channel once it was in contact with the PDMS surface. Protective coatings such as BSA were applied with no effect. A potential way to solve this challenge would be to add to the microchip a pneumatic valve-controlled docking element to have a temporary immobilizing structure that can be pushed in and out from a superior extra-thin PDMS layer as described by Araci *et al.*[217]. Another strategy could be to implement this microstructural element in a highly parallelized microchip to immobilize a large number of cells at once and probe them on an automated base. This would require a high precision in the docking of the cell to make it easy enough for

the a programm to recognize the membrane edge to switch correctly on the trapping laser. Substantial increase in complexity in microfluidic chip fabrication can now be achieved using 3D-printing.[218]

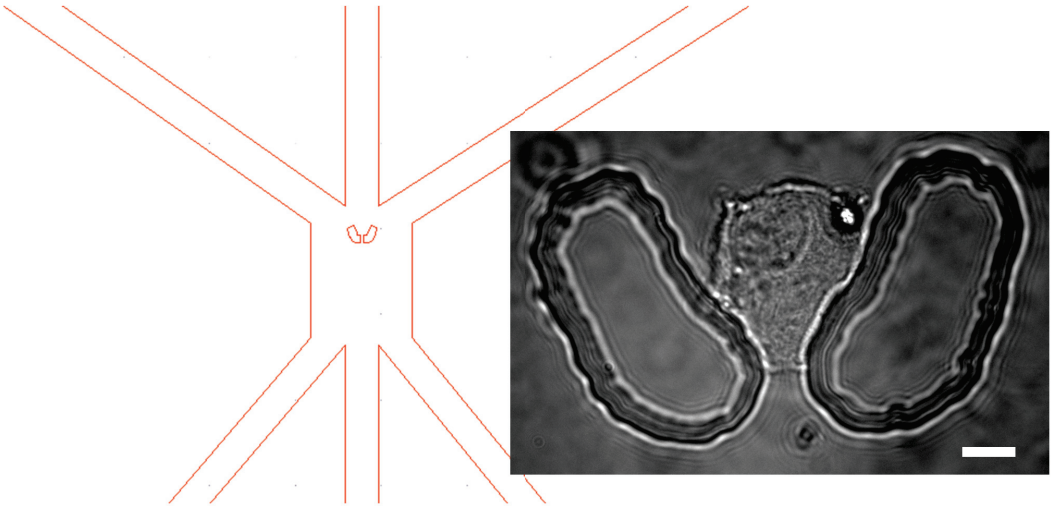

Figure 2.15: Cell immobilized in the microsized funnel-shaped PDMS dock. *Cell is docked into the PDMS microstructural element and a membrane nanotube can be pulled from it. Scale bar = 10 μm.*

2.4 Conclusions and outlook

The results of our plasma membrane tube experiments are promising to be used in the future in a microfluidic platform for the analysis of the progression state of tumors. The cancer cell line WM115, originating from a tumor at a specific malignancy, could be discriminated from other cells of the same type of cancer at different progression states. Yet some challenges still have to be overcome to achieve relevant efficiency and reliability for clinical diagnostics. Much higher throughput should be achieved by using a microfluidic chip that would be able to process cells in suspension instead of having them attached to an immobile solid support. Multiple external factors are known to disturb the membrane biophysical properties of the plasma membrane, such as cell cycle or atmospheric pressure. This emphasizes the necessity to performs such analyses in a tightly controlled environment and to record large amounts of data, especially in the crucial goal of diagnosis.

Limitations arise from the success rate of the pulling of nanotubes, which is at the moment low. We remain confident that automation of the process will provide a more precise positioning of the optical trap on plasma membrane. Although the microfluidic chip fabricated from PDMS did not fulfill all requirements for real application yet, it opened the way for future improvements, for example towards either parallelization or on-demand activatable cell trap with an lateral access to perform the pulling and back-relaxation measurements while the cell remains still.

The beauty of the method lies in the fact that there is no need of binding the probed cell to a bead or similar objects, which would influence the measurements of the biophysical parameters. Cells remain unmodified and can withstand several nanotube pulls at predefined positions at the cell surface, thus opening the possibility to establish a non-invasive tomogram of the viscoelastic properties of a cell surface. This also accounts for the vesicle extraction, which would allow single cell selective analysis of membrane derived attoliter carriers from predefined locations in/on a cell, comparable to a sub-micrometer sized biopsy from a living cell for further proteomic or functional analyses.

3 Single-cell analysis with affinity beads

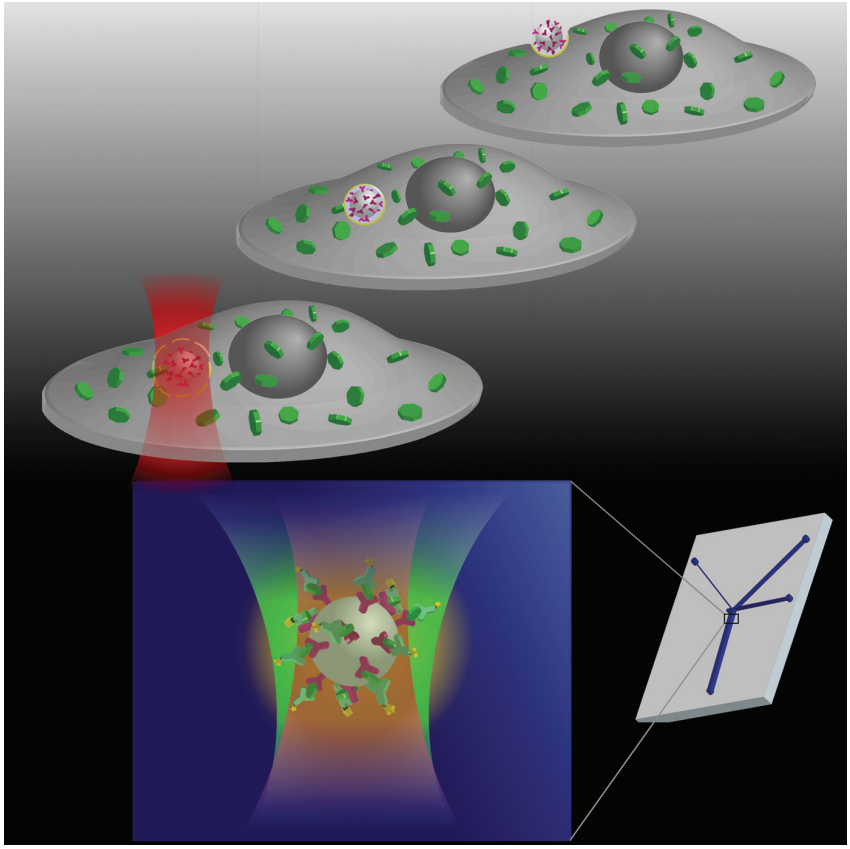

Figure 3.1: Single-cell analysis with affinity beads. *A bead, prior deposited on top of a cell, is internalized by phagocytosis. Protected from contact with cytoplasmic elements by a phagosome, photoactivation of an added photosensitizer is used to break this protective layer. The bead can then be extracted out of the cell with the help of an optical tweezer and the target molecules, bound to the specific capturing coating of the bead, can be analyzed by fluorescence microscopy. Frontispiece of Small, volume 11, issue 22 (2015).*

3.1 Introduction

Rapid, accurate and relevant analysis of miniaturized biological samples is a central objective of "lab-on-a-chip" concept, combining microfluidics and other miniaturized bioanalytical methodologies to offer platforms enabling functional single-cell analysis.[219, 220, 221, 222] In this context, two major hurdles have to be overcome: First, one or several molecular species have to be specifically quantified in each cells. Second, a large number of cells has to be processed to sample also rare cell phenotypes and to properly evaluate their functional significance. A good compromise between throughput, precision and complexity of the analysis is difficult to reach, if single-cell resolution is required. Flow cytometry is a powerful classical method able to process thousands of single cells per second.[223] Despite the enormous potential flow cytometry offers due to a fully automated processing of the cells and a large range of accessible wavelengths of excitation and emission, limitations arise from the need for bright organic fluorescent dyes as reliable probes.[224] This requires either molecules of interest to be located at the extracellular membrane surface by post-translational labeling for example using fluorescently labeled antibodies, or to pre-treat cells by insertion of specific labels in their cytoplasm before analysis. High contrast organelles and relatively large cellular elements can be observed during flow cytometry analysis by light scattering without the help of labels, but this application is limited to only a few cases.[225] **Chemical cytometry**, represents a more generally applicable approach: a single cell is lysed, the target analyte is separated from other contents in the cellular lysate, usually by capillary electrophoresis, followed by specific detection and quantification of the target analyte for example by laser-induced fluorescence.[226, 227] The deciphering of complex metabolic pathways requires to determine picomolar concentrations inside cells; for a HeLa cell with an average volume of 3700 μm^3[228], proteins have been quantified to range from 6000 to 20,000,000 copy number, which corresponds to 2.7 nM and 9 μM respectively.[31] Of importance in this context is the miniaturization of biological analysis processes into micro- and nanoscale operating platforms, so called "lab-on-a-chip" devices. Their possibilities of high spatial and temporal flow control as well as the sensible shortening of analysis time make them promising biomedical tools.

In the method described in this chapter, lab-on-a-chip concepts have been used to up-concentrate the molecules of interest onto the surface and into pores of micron-sized silica beads specifically coated with interacting molecules designed to capture analytes.[194, 53]

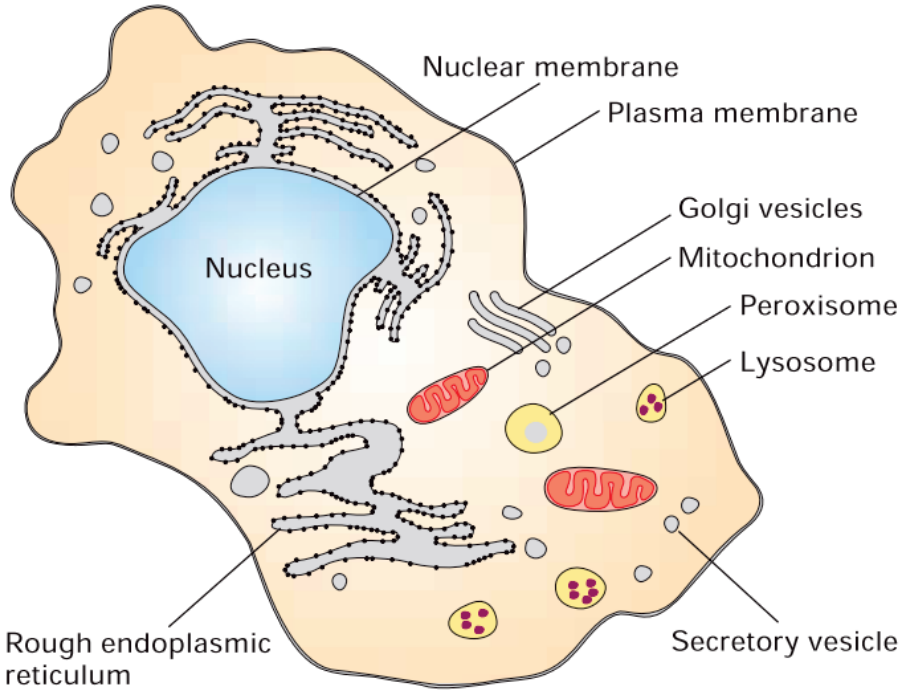

Figure 3.2: Anatomy of a cell. *The organizational complexity of a cell, containing numerous organelles and displaying heterogenous distribution of cellular components, makes it a challenge to analyze and understand the various biochemical processes occurring in the smallest individual unit of living organisms. Image from [229].*

Capturing target analytes circumvents the dilution issue appearing in numerous other single-cell methods, which rely on cell lysis. Concentrating the target analyte on a bead makes it possible to transfer the bead together with the analytes with minimal loss to different places in the microfluidic chip. Capturing cytoplasmic molecules or intracellular components however requires to access the cytoplasm of single cells. Small objects (such as microbeads) inserted into the cytoplasm are typically captured by the cell by endocytosis or phagocytosis.[230, 231, 232] Advantage has been taken of this process by dispersing a suspension of microbeads over cells and waiting overnight to let them be internalized into cells via endocytosis. Silica beads of 3 μm in diameter have been selected as they are easily phagocytosed.[233] Furthermore, beads of this size are very well suited for microscopic manipulation and observation and do not disturb significantly the cell after integration. Silica beads have a higher refractive index than most internal components of cells, which makes it easier to observe them in bright field microscopy and more convenient to trap them optically.

Once functionalized beads have been internalized into the cell, they remain protected from direct contact with the cytoplasm by integration into small closed containers called phagosomes.[234] In order to access the target analytes, the beads must be released from the phagosomes. The

most appealing method for this specific application happened to be photochemical internalization (PCI), chosen for its membrane destabilization capabilities.[235, 236] Here we used the photosensitizer $TPPS_{2a}$ as a membrane destabilizing element to liberate the beads from their enclosing phagosomal membrane. Upon irradiation at 405 nm, reactive oxygen, mainly singlet oxygen[237], is produced by $TPPS_{2a}$, which causes the surrounding phagosomal membrane to get damaged allowing to access the beads. PCI has been used so far to release naturally internalized molecules from endosomes such as nucleic acids, proteins and therapeutic drugs.[236] In our present case, analytes have to reach and bind the capture agents located on the bead surface and in the bead pores and to be up-concentrated. Pores in the microbeads allow binding a high concentration of analytes; furthermore, high density of capture agent on the microbeads promotes rebinding of the analyte after dissociation, which tends to keep target analyte trapped on the bead in a similar way as in the case of affinity chromatography. Concentrating analytes onto a bead also prevents unwanted adsorption on the walls of the microchannel. As a single cell may incorporate several beads, cells should be prior sorted and only the ones containing a single liberated bead should be analyzed to keep single-cell resolution. Optical trapping has been used here to analyze *in situ* a selected bead by fluorescence microscopy. The developed procedure is described in detail in section 3.2.5. Fluorescence microscopy is a fast and reliable analytical technique that can be implemented together with optical tweezers on the same setup, as described in section 2.1.3. *In situ* measurements prevent loss of analyte molecules related to transfer into an external analysis unit.

This method may find applications in the diagnostics field, especially for cancer diagnosis. As cancer is characterized by uncontrolled gene product expression, capability to detect key molecules or proteins is crucial for the selection of the most efficient treatment of cancer.[238] Highlighting of specific molecules is a great indicator for discrimination of drug targets in case of administration of highly powerful chemotherapy agents.

3.2 Experimental

3.2.1 Preparation of mixed Ni-NTA-antibody functionalized beads

Silica beads (Sicastar 3 μm, Micromod) coated with protein A and Ni-NTA are suspended in PBS at a concentration of 10^9 particles per ml. A 15 μl solution of 1 $\frac{mg}{ml}$ polyclonal anti-RFP antibody against red fluorescent protein (ab28664, Abcam) is added to 250 μl suspension of beads and the suspension is incubated for 1 h at room temperature under gentle agitation. Free antibodies are removed by washing three times with 0.2 M sodium borate at pH 9.0, afterwards the beads are resuspended in 250 μl borate buffer. 1.25 mg of dimethyl pimelimidate is added to cross-link bound antibodies and protein A. After 30 min incubation at room temperature under gentle agitation, ethanolamine is added to a final concentration of 0.2 M to quench excess dimethyl pimelimidate. After another 2 h of incubation, the beads are washed three times with PBS and suspended in PBS in a final volume of 250 μl. The beads are stored at 4°C and are ready for use.

3.2.2 Cell transfection and bead internalization

HEK cells are grown on 8-well dish (Lab-Tek® II chambered coverglass, Nunc) in a 37 °C incubator. One day after splitting, they are transfected with the particular plasmid following either the standard procedure of Lipofectamine mediated transfection (Lipoefctamine® 2000 Transfection Reagent, Invitrogen) or according to a calcium phosphate transfection protocol. Second day after splitting, a suspension of functionalized beads (to a final concentration of $4 \cdot 10^5$ - $2 \cdot 10^6$ beads par ml) together with photosensitizer $TPPS_{2a}$ (PCI biotech, to a final concentration of 0.7 $\frac{\mu g}{ml}$) are added on top of the cells (Figure 3.3). After another 24 h of incubation at 37 °C, the cells have internalized the beads by phagocytosis and are ready for use in further experiments.

3.2.3 Phagosomal escape

Cells containing both $TPPS_{2a}$ and phagosome internalized beads are exposed to 405 nm light (laser pointer) at a power of approximately 5 $\frac{mW}{cm^2}$ for 5 min. To optimize the illumination, the cell-containing dish is placed on top of a reflecting surface (aluminum foil). Cells can then be suspended in PBS for microfluidic analysis or observed directly in the 8-well dish under microscope.

3.2.4 Cell trapping

After illumination, cells are detached from the culture surface and suspended in PBS. They are injected with a 10 μl syringe (Hamilton) in the microfluidic system to the microchip (Figure 3.4). The observation setup is described in detail in section 2.1.3. The flow rate is adapted to the needs of the experiment, usually at 0.1 μl, which is optimal to quickly discriminate dead cells from healthy ones and to select a cell comprising one single affinity bead. Cells are injected in a channel of 100 μm wide and 50 μm high merging with the lysis and analysis channels to form together a channel of 400 μm width. In a typical protocol, a cell containing one bead is immobilized in the optical trap. Since the trapping force is proportional to the difference in refractive index between the medium and the object [65] and the refractive index of the silica bead is higher than the rest of the cell (silica bead: 1.45 [239], cell membrane: 1.40 [240], PBS: 1.34 [241]), the bead is trapped in the laser focus. As it is tightly embedded in the internal cellular structure, the whole cell moves as the optical trap is displaced.

3.2.5 Cell analysis

Once trapped, the cell of interest is dragged to the lysis channel, where buffer containing 0.1% SDS (Sigma) is flowing. The cell lyses in a few seconds and all its constituents are carried away by the buffer flow, leaving only the bead and all what is attached on it. The bead is moved further to the analysis channel where a detection agent can be added if needed. Fluorescence measurement of the probe molecules is performed to detect and quantify the amount of protein of interest captured by the bead.

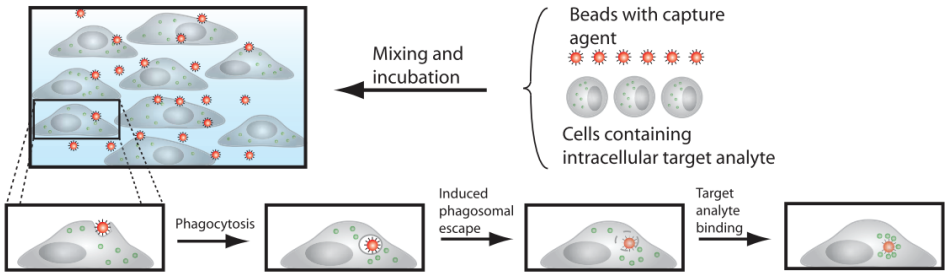

Figure 3.3: Single-cell cytometry: internalization of beads into cells. *After internalization of beads, cells are exposed to 405 nm light inducing phagosomal $TPPS_{2a}$ mediated disruption, giving access of the beads to the cytoplasm.*

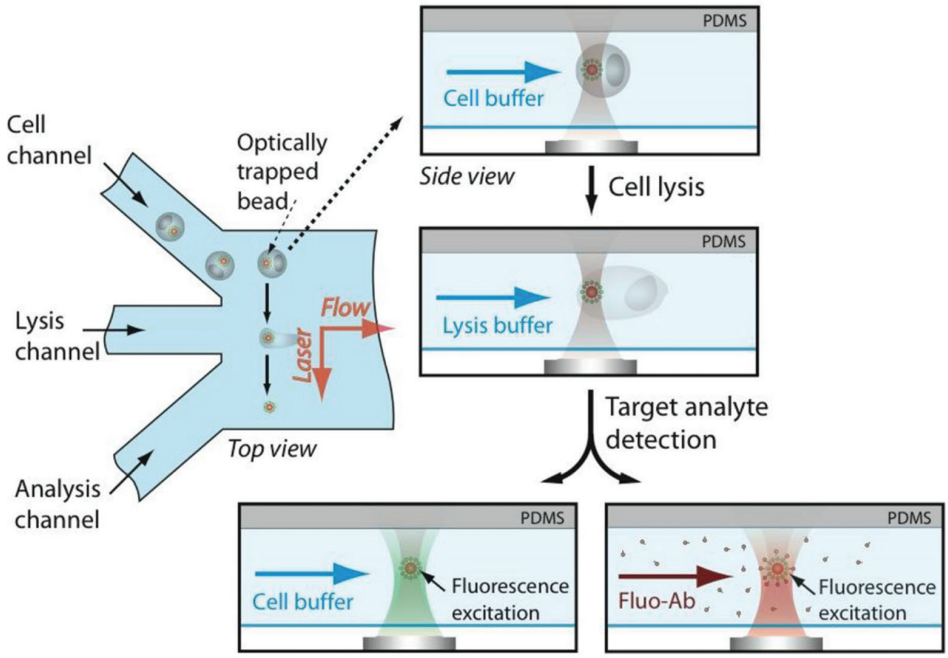

Figure 3.4: Single-cell bead analysis. *After the cells have been exposed to UV light, they are injected into the microfluidic chip where the internalized bead, and in turn the cell, gets trapped by the optical tweezer. The immobilized cell is dragged to the lysis channel where a stream of detergent solution dissolves the plasma membrane and organelles of the trapped cell to leave in the optical trap only the bead with bound protein analyte. The bead is then dragged to the analysis channel. If the target protein is fluorescent by itself, it can be directly detected and quantified by fluorescence microscopy; if not, a fluorescent antibody or a selective fluorescent ligand provided by the analysis channel makes it detectable and quantifiable.*

3.3 Results and discussion

3.3.1 Phagocytosis in multiple cell lines

Although phagocytosis is a process belonging principally to the behaviour panel of phagocytes, other cell types are capable of absorbing external elements in a less aggressive and active fashion. 3 μm beads have been deposited on top of several cell lines, HEK cells, BHK cells, MCF7 human breast cancer cells, MIN6 pancreatic beta cells, SBCl2 human radial growth phase melanoma and WM239A lymph node metastatic cells of human skin melanoma, to observe their ability to internalize into the cells mediated by scavenger receptors. After overnight incubation, 2 mM eGFP-His10 was added to the cell medium, so that the non-internalized beads bind massively the green fluorescent protein. 12 hours are necessary to observe good phagocytosis yields as no signaling molecule mediates the process, which is only directed by scavenger-type receptors.[242] Only beads protected intracellularly did not display green fluorescence (Figure 3.5). As eGFP-His10 does not penetrate the cell, beads inside phagosomes cannot bind it. It has also been shown that once internalized, beads are wrapped inside endosomal vesicles and are not in contact with the cytoplasm of cells.[194] Hence we consider as that phagocytosis is a cellular process that can be used reliably in our method for the internalization of affinity beads.

3.3.2 Capture of a single analyte

The experiments on beads with a single type of coating and the capture of a single analyte were designed in collaboration with Michael Werner and Raghavendra Palankar.[194, 53] Briefly it has been demonstrated that it was possible to insert a fluorescent bead coated with Ni-NTA groups into HEK cells by phagocytosis in combination with $TPPS_{2a}$, a photosensitizer that liberates singlet oxygen molecules upon 405 nm light irradiation. Once phagocytosed, the beads are liberated from the lipid capsule with a short exposure to a 405 nm laser and can access the cytoplasm of the cell. Histidine-tagged eGFP binds to the bead, which is then extracted from the cell inside a microfluidic chip. The presence of eGFP can be detected by fluorescence microscopy and the fluorescence signal is proportional to the initial concentration of eGFP in the cell.[194]

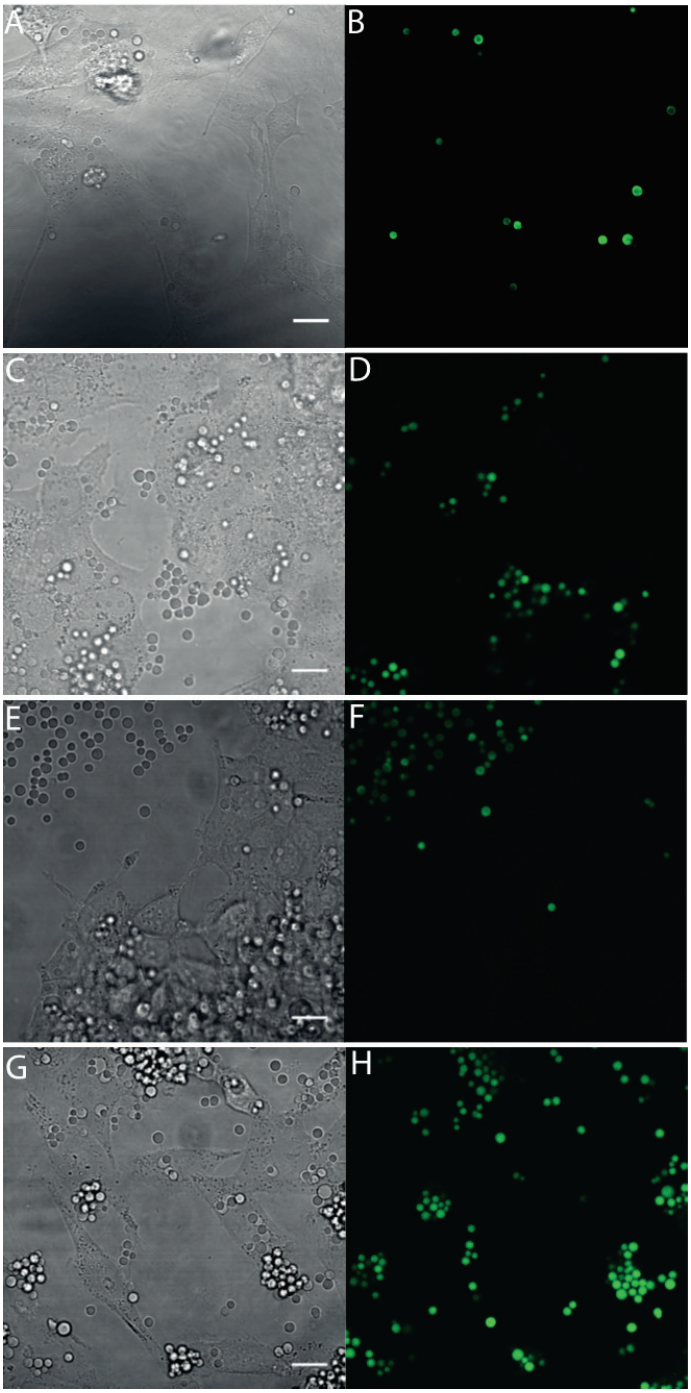

Figure 3.5: Phagocytosis of Ni-NTA coated silica beads by multiple cell lines. *Beads deposited on top of (A, B) BHK cells, (C, D) MCF7 human breast cancer cells, (E, F) MIN6 pancreatic beta cells, and (G, H) SBCl2 human melanoma cells. To distinguish internalized from non-internalized beads, eGFP-His10 was added to the cell medium prior to analysis by confocal microscopy. Accordingly, beads not internalized by cells were able to bind eGFP-His10 in the extracellular medium. (A, C, E, F) Transmission micrographs of the different cell types with internalized and non-internalized silica beads. (B, D, F, H) Corresponding confocal fluorescence micrographs facilitating the discrimination between internalized beads (non-fluorescent) and non-internalized beads (green fluorescent). Scale bars: 15 µm.*

3.3.3 Simultaneous capture of two orthogonal analytes

In order to demonstrate the possibility to multiplex the number of proteins that can be detected using single-cell analysis with affinity beads, we have chosen two orthogonal capture systems allowing to bind two spectrally distinct autofluorescent proteins: eGFP[243] and mCherry.[244] eGFP is expressed with a N-terminal 10-histidine tag, hence Ni-NTA is used on the bead as the first capturing agent as it has a natural affinity for nickel ions.[245] As mCherry does not bear a specific tag, we have chosen a capturing antibody (ab28664, abcam) which specifically bind mCherry but does not bind eGFP. 3 μm beads are used comprising a mixed coating of Ni-NTA groups and protein A to which various proteins can be attached. After completing the coating, the beads together with $TPPS_{2a}$ are spread over HEK cells expressing simultaneously tagged eGFP and mCherry. After 12 hrs incubation, many cells contain at least one non-fluorescent bead, indicating that the bead is indeed inside the cell and protected from direct contact with the fluorescent cytoplasm enclosed in a phagosome (Figure 3.6, top line). The cells are illuminated with 405 nm laser light to promote phagosomal escape of the beads. It is not clear yet whether the phagosomes are entirely disrupted or if they are only destabilized to allow permeability of proteins and other solutes through their membrane, although evidences in section 4.3.3 seem to indicate permeability increase at such low concentrations of $TPPS_{2a}$. After illumination, we observe a gradual increase of the fluorescence signal on the capturing beads. 3 minutes are needed for mCherry to reach the maximum fluorescence level, whereas 10 minutes are necessary for maximal binding of eGFP. Both proteins are bound simultaneously on the beads (Figure 3.6, bottom line).

After illumination, cells containing beads with both mCherry and eGFP are suspended into PBS and injected into the microfluidic chip for bead isolation and fluorescence detection. A cell is immobilized by the optical trap via its internalized bead (Figure 3.7, top line). The cell is then dragged into the lysis channel to be dissolved by detergent, leaving only the bead and the captured proteins in the optical trap. The bead is then transferred to the analysis channel where the presence of eGFP and mCherry is observed by fluorescence imaging. The whole process takes approximately 30 seconds to 1 minute. This demonstrates that the two orthogonal proteins can be bound on mixed functionalized beads and that more than two simultaneous binding events might be technically feasible, with the only limits that the signals must be distinguishable. The multiplexing potential thus relies on the surface concentration capability as well as on the fluorescence properties of the target analyte.

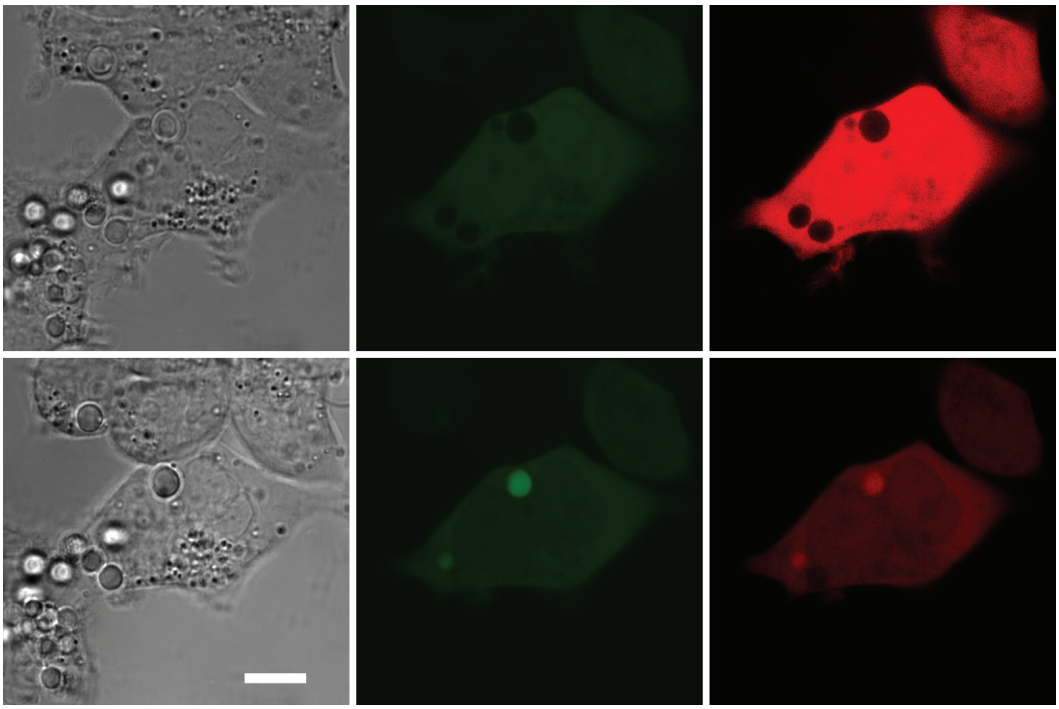

Figure 3.6: Beads comprising a double-coating inside a HEK cell before and after UV illumination. *A bead was deposited on top of a cell and absorbed by phagocytosis, together with the photosensitizer $TPPS_2a$. Before UV illumination (top line), none of the cytoplasmic fluorescent proteins is detected on the bead surface. After 5 minutes of illumination at 405 nm, and further 10 minutes incubation (bottom line), both eGFP (middle column) and mCherry (right column) have bound to the bead. Scale bar = 10 µm.*

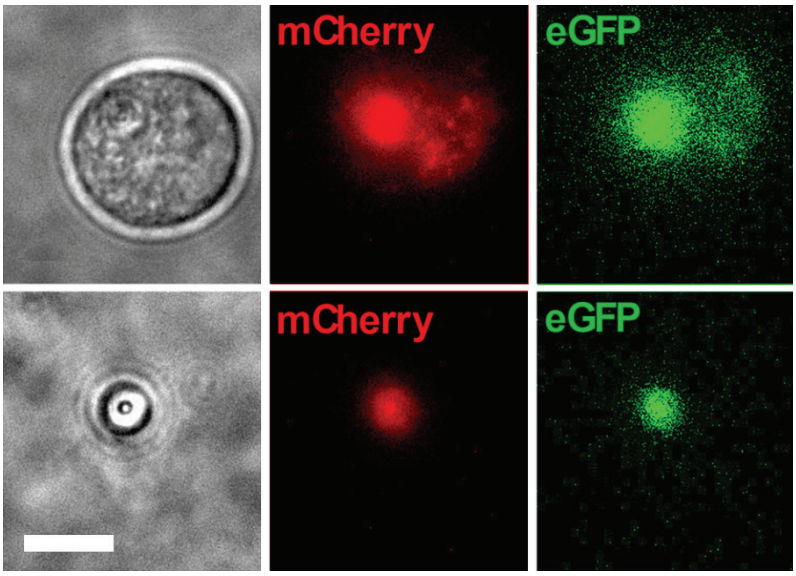

Figure 3.7: eGFP and mCherry captured on an optically trapped bead, *before (top) and after (bottom) lysis of the surrounding cell. The bead is coated with both Ni-NTA and anti-mCherry antibody captured simultaneously and efficiently the two proteins from the cytoplasm of a cell. After the cell is transferred into the lysis channel, the entire cell is dissolved by detergent and the remaining bead is moved into the analysis channel for fluorescence readout. The presence of both eGFP and mCherry indicates that a bead can capture two different sorts of analyte using orthogonal capturing agents. Scale bar = 10 µm.*

3.3.4 Maximal imidazole concentration in analysis buffer

The binding of His-tagged proteins to Ni-NTA groups is based on the specific interaction of imidazole groups with multivalent transition metal ions.[246] Taking advantage of the chelating effect, the affinity to polyhistidine sequences is superior over imidazole monomers.[247] Typically decahistidine tags on proteins are optimal for binding to Ni-NTA groups on microbeads. The addition of small quantities of monomeric imidazole in the washing buffer removes those molecules which are poorly bound to the affinity bead surface while not disturbing these which are specifically bound to polyhistidine groups.[248] This is especially true in the case of using a secondary molecule to characterize the presence of the initial captured protein. As we want to keep as much specific binding of the protein of interest on the affinity beads, our goal is to find the upper limit concentration of imidazole at which the fluorescence intensity of eGFP-His10 immobilized on the bead is not decreased compared to imidazole-free conditions. To approximate the maximal concentration of imidazole in solution that would not interfere with the binding of His-tagged eGFP, beads coated with Ni-NTA groups were immersed in solution of 100 nM of eGFP-His10 in PBS. Imidazole added in separate compartments to concentrations varying from 1 to 50 mM, then followed by an overnight incubation to give

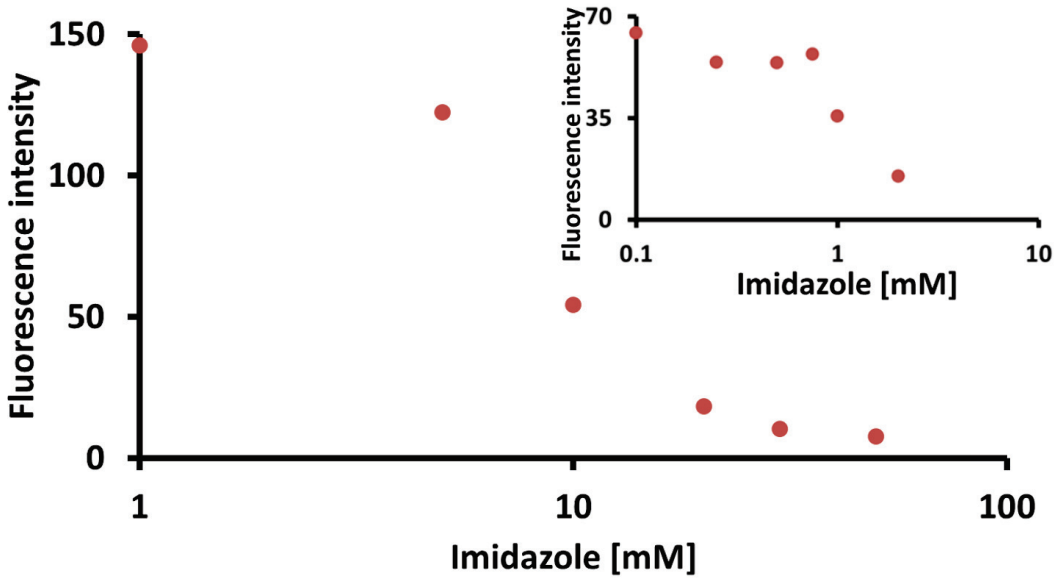

Figure 3.8: Fluorescence intensity of eGFP-His10 on beads vs free imidazole concentration in bulk medium. *As the concentration of free monomeric imidazole in the bulk increases, the recorded fluorescence intensity (arbitrary units) of eGFP-His10 bound to capturing beads is decreasing. Enhanced resolution (insert, top right corner) shows that the maximal imidazole concentration at which eGFP signal is not altered is 1 mM.*

enough time to the system to reach equilibrium. eGFP fluorescence is recorded by confocal fluorescence microscopy. As we observed that the fluorescence intensity of bead-bound eGFP started decreasing around 1mM of imidazole, we refined the observed concentrations from 0.1 to 2 mM with the same procedure. A clear decrease in fluorescence of eGFP bound on beads was detected at 1 mM imidazole, while the fluorescence signal remained constant up to 0.75 mM imidazole (Figure 3.8). We thus established the maximum concentration of free monomeric imidazole that can be used in buffers during the experiments of secondary detection without disturbing the binding of eGFP to the affinity beads being 0.75 mM.

If the binding partners were as in our case polyhistidine and Ni-NTA groups, the most suitable molecule for preventing non-specific interactions is imidazole. In the case of other capturing agents, a coherent choice of non-specific interaction blocker has to be found in order to minimize false positives and to better correlate the labeling molecule with the analyte of interest.

3.3.5 Correlation of eGFP fluorescence on the bead with eGFP concentration in the cell

The correlation between the fluorescence intensity of eGFP-His10 bound to Ni-NTA coated beads with the concentration of eGFP in surrounding buffer solution has been established elsewhere by immersing beads in a solutions of different eGFP-His10 concentrations.[194] (supplementary information) This works well as a proof of concept, however it does not reflect the reality of a confined, material-limited and crowded intracellular environment. The establishment of a precise correlation between in-cell eGFP concentration and on-bead eGFP fluorescence is an absolute necessity if quantification of analytes should be achieved. Since the numerous trials to perform UV phagosome liberation in microfluidic chips with beads immobilized in the optical trap did not give satisfactory results, notably because of flow instability, enhanced photobleaching or microexplosions of microscopic air bubbles in the microchannel, the measurements are finally performed in a traditional culture dish with a fluorescence confocal microscope.

To proceed, we cultured HEK cells in 1 cm^2 compartments and transfected them as described in section 3.2.2 with peGFPN1 plasmids (Clonetech). After incubation varying from a few hours to 4 days, beads are dispersed over the cells with $TPPS_{2a}$ and incubated at 37 °C overnight, bringing the total incubation time for eGFP-His10 production to 1-5 days. A large range of incubation times increases the range of resulting intracellular concentrations of eGFP. Finally the culture medium is replaced by a PBS solution containing 1 μM eGFP-His10 that serves as internal standard for evaluation of the cytoplasmic concentration of fluorescent protein in cells. After a final incubation time of 90-180 minutes, microscopic images of the cell population are recorded to find those individual cells which have internalized only one single affinity bead inside a non-damaged phagosome (Figure 3.9, left column, arrows). The cells are then illuminated with 405 nm light for four minutes. Several minutes after illumination, microscopic images are recorded again to observe the fluorescence intensity of eGFP-His10 on beads captured by Ni-NTA groups on the beads. It is important to note that only cells comprising a single bead having undergone photochemical liberation from phagosome are taken into consideration (Figure 3.9, right column, arrows).

Figure 3.10 shows a linear correlation between the eGFP fluorescence intensity on individual beads and the free intracellular eGFP concentration ranging from 1-25 μM. The fluorescence intensity of eGFP-His10 bound on beads has been translated into a virtual equivalent concen-

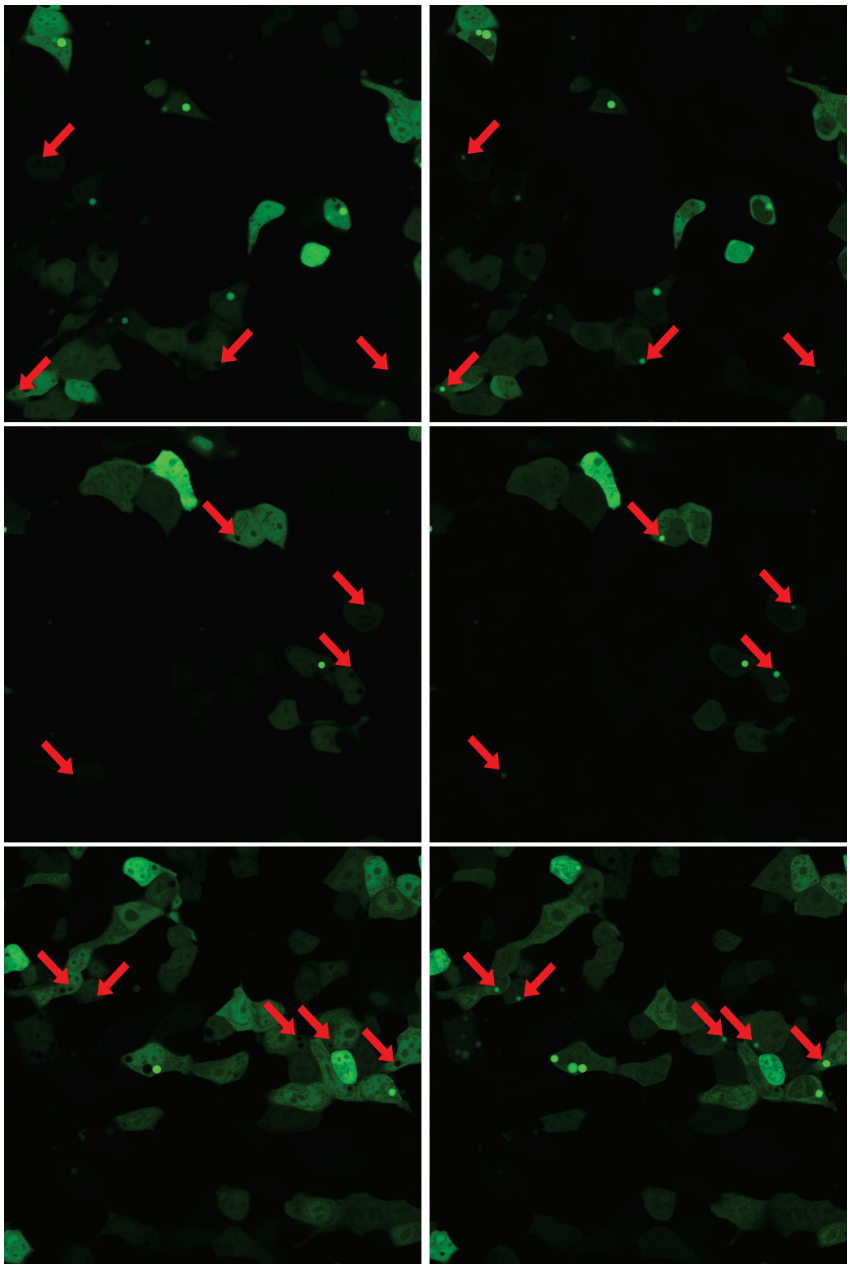

Figure 3.9: Cells expressing eGFP-His10 with beads inside phagosomes before and after UV illumination. *Cells expressing eGFP-His10 having phagocytosed Ni-NTA-coated beads. The beads were resting inside of phagosomes and thereby were protected from direct contact with cytoplasmic content (left column, arrows). After UV illumination, the phagosomes are destroyed allowing access of cytoplasmic eGFP-His10 to the Ni-NTA groups on the beads. Beads become fluorescent in parallel to decreasing intensity of eGFP fluorescence of the cell cytoplasm. Only cells containing one single bead having gone from dark to bright state have been considered (right column, arrows).*

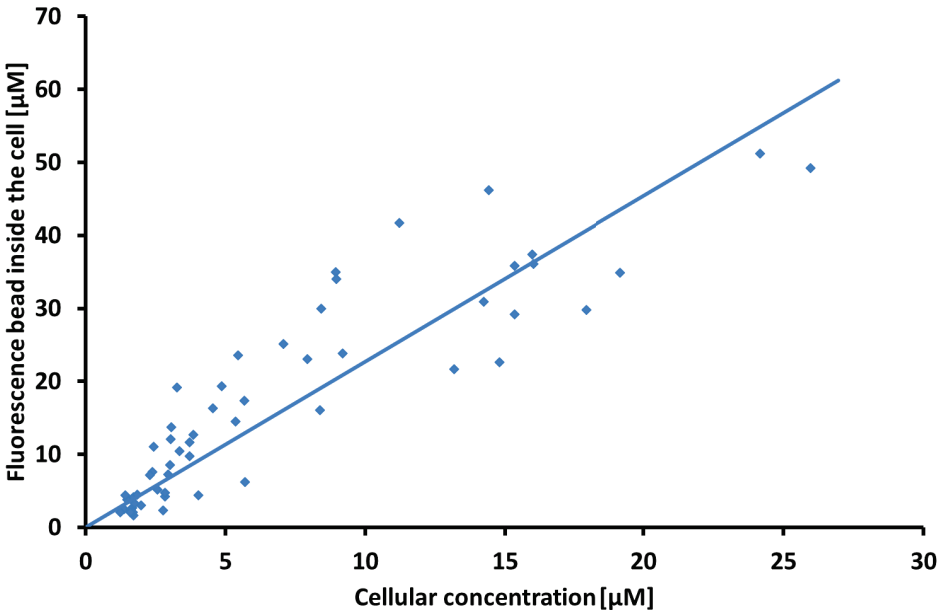

Figure 3.10: Fluorescence intensity of eGFP-His10 on beads vs intracellular concentration of eGFP-His10. *Fluorescence intensity of eGFP-His10 bound to affinity beads versus the concentration of fluorescence intensity of cellular eGFP-His10 prior photochemical opening of the phagosomes. The linear relation allows quantification of the eGFP content of a cell from the eGFP fluorescence bound to a bead.*

tration of free eGFP by dividing the recorded signal by the surrounding background signal displaying the fluorescence of 1 μM of free eGFP. This correlating factor can be applied to other systems. In our case, the correlation coefficient is 2.27, which is the average ratio between the fluorescence of the bead and the fluorescence of the cell before the bead binds eGFP-His10. This method of calibration is however only valid for fluorescent analytes. Precise calibration for non-fluorescent proteins would require to work in parallel with other quantitative methods.

3.3.6 Detection of an analyte on microbeads using a secondary antibody

The procedures described in sections 3.3.2 and 3.3.3 are only valid for analytes displaying intrinsic fluorescence. For non-fluorescent proteins, it is necessary to label the protein with a suitable probe to achieve proper detection. Several options are available with different degrees of complexity. Mass spectrometry analysis of the beads would require mass tags on the target protein.[249, 250, 251] For this approach, the precision, throughput and multiplexing possibilities are actually very promising. However, the use of mass spectrometry associated to our method would substantially increase the complexity of our microfluidic platform as the beads must be transported outside of the chip for analysis. This causes problems, such as the

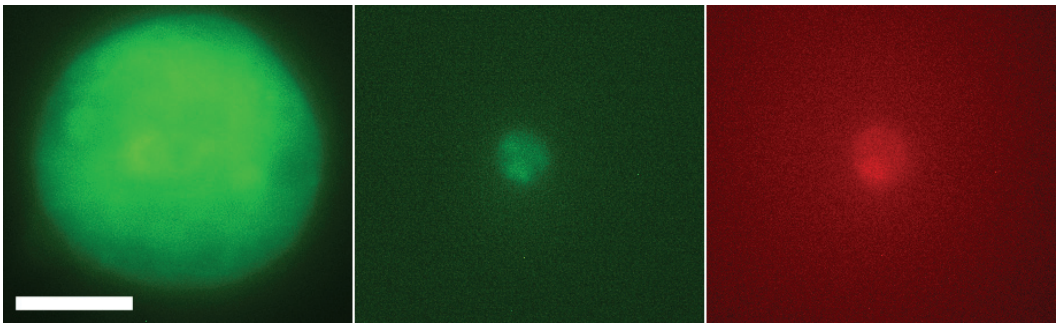

Figure 3.11: Extraction of a bead from a suspended cell followed by the addition of fluorescent antibody. *Left: a suspended cell expressing eGFP-His10 and containing a Ni-NTA-coated bead that has already bound eGFP after having previously been illuminated by UV light. Middle: eGFP-His10 fluorescence of the bead after lysis of the cell. Right: Labeling antibody fluorescence on top of eGFP-His10 molecules bound to the Ni-NTA groups of the bead. Scale bar = 10 µm.*

potential loss of beads or the loss of material captured on the bead. The implementation of micro-droplet generation[252] would also be an interesting alternative, however, associated with very complicated handling in the absence of full automation of the system.

A much simpler alternative is based on the use of a secondary binding element, typically an antibody or a ligand, comprising a fluorescent probe that can be detected by fluorescence microscopy. This approach is chosen here to demonstrate its feasibility to allow rapid and direct *in situ* observation of the selected analyte. Its implementation is straightforward as the optical tweezer setup is integrated in a fluorescence microscope and because many versatile fluorescent probes for labeling antibodies are commercially available. To demonstrate the feasibility of the approach, we have chosen to use Ni-NTA beads (Sicastar 3 μm, Micromod) to capture histidine tagged eGFP from transfected HEK cells and to further mark eGFP with a red fluorescent anti-eGFP antibody (ab6660, abcam). As both the target protein and the antibody are fluorescent, it is possible to determine whether the technique is suitable for quantification of the target protein by quantification of the antibody, as the two different fluorescence signals deliver independent means for quantification of the target protein on the bead.

To keep the system as simple as possible, we applied the fluorescent antibody in the analysis channel of the microchip at a relatively low concentration (10 $\frac{\mu g}{ml}$). The freshly extracted eGFP-His10 comprising bead from the cell quickly accumulates the antibody probe to reach a maximal signal after about ten seconds. Exciting the bead at 488 and 543.5 nm yielded fluorescence signals of both target proteins eGFP-His_{10} and the antibody probe labelled with Texas Red, allowing comparison of both signals. Figure 3.12 shows a linear correlation (t-test, $p\text{-}value = 1.2 \cdot 10^{-5}$) between the concentration of intracellular eGFP-His10 measured

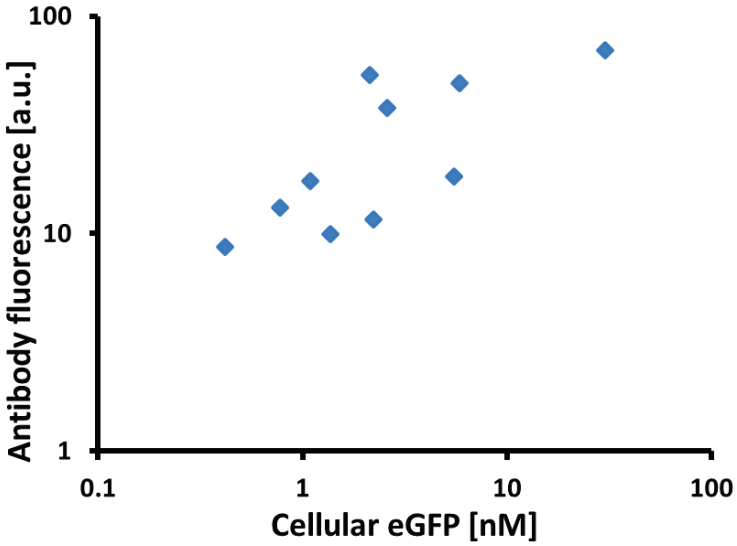

Figure 3.12: Correlation between the fluorescence signal of bead bound fluorescent anti-GFP antibody with the intrinsic fluorescence of bead bound eGFP-His10. *Fluorescence of the Texas-red-labeled anti-GFP antibody against the concentration of intracellular eGFP-His10 calculated from the fluorescence intensity of eGFP bound to the bead after cell lysis. The correlation is significant (t-test, p value* $= 1.2 \cdot 10^{-5}$*).*

from the fluorescence intensity of eGFP bound and the bead after cell lysis (Figure 3.12), demonstrating the potential to quantify analytes with fluorescently labeled binding molecules such as antibodies. This is a proof of concept that soluble analytes can be collected from a single cell onto an affinity bead and subsequently analyzed by fluorescence microscopy after a short on-chip labeling step following the lysis of the cell.

3.4 Conclusion and outlooks

Up until now, rapid cell lysis by crossing microfluidic streams was restricted to the separation of large, micrometer- sized analytes such as bacterial chromosomes.[253] Our method is principally amenable for investigating any type of cytosolic analyte. In contrast to prior microfluidic single-cell analysis methods involving cell lysis and therefore dilution of intracellular species over several orders of magnitude, our method comprises target analyte enrichment on the bead surface. This is due to the strong interaction between the analyte and the capture agent, and the high local concentration throughout the volume of the beads. Consequently, rebinding dominates over dissociation and escape. A similar situation is present during affinity-column purification of proteins using porous beads with capture groups, where washing steps can be performed with virtually no loss of bound material. Another advantage compared to other single-cell analysis methods is that analyte binding in individual cells can be executed simultaneously for a large number of cells. Given this high degree of parallelization for target analyte binding, the throughput of the method is mainly determined by the bead extraction and analysis procedure, which for our present experimental configuration is at the order of 1–2 cells per minute. This low throughput is determined by the fact that all experimental steps starting from optical trapping of a bead-comprising cell to fluorescence imaging of the extracted bead were conducted manually. The entire workflow, however, could be readily automatized as has been demonstrated for other cases on optical trapping.[254, 255] For such conditions the throughput would be mainly limited by the time required for cell lysis. Here, cell lysis occurred in less than 3 s enabling a potential throughput of about 20 cells per minute. Faster methods, such as optical[256] or electrical lysis[257] proceeding on a millisecond timescale, might further increase the throughput considerably.

Taking advantage of recent technological progress in the fabrication and manipulation of microscopic particles we here developed a novel integrated concept for the chemical analysis of single cells. Although still at an early stage we proved that our method enables extraction and analysis of specific intracellular contents from individual cells, at reasonable throughput and virtually no sample dilution. Therefore, this method has the potential to evolve into a sensitive platform for investigating fundamental aspects of cellular physiology and into a powerful single-cell technology for routine applications in molecular diagnostics. A few limitations of this method, intrinsic to its basic principles, require attention before selecting it for a specific application. Non intrinsically fluorescent analytes require a prior calibration

strategy to be able to faithfully quantify them with a labeled antibody. Natural phagocytosis of the affinity beads is a prerequisite to reduce stress the target cells; hence this could become a time-limiting step once the analysis procedure is fully automated.

Full automation of the lysis-detection process would increase the rate of analysis to higher throughput, with cell lysis and labeling procedure as time-limiting steps. Up to 20 cells per minutes could be processed in a single analysis units, meeting with a higher versatility the rates of the actual fastest methods available.[44] Full automation opens the way to a massive parallelization that would furthermore increase the throughput up to those of conventional flow cytometry. Our method offers novel opportunities in single-cell diagnostics for diseases affecting metabolism or protein expression to identify and quantify biomarkers with the perspective to provide to patients personalized therapies.

4 Exosomes as potential vectors of drugs and DNA for medical treatment

4.1 Introduction

4.1.1 Extracellular vesicles

Biological cells have a wide variety of communication tools to transfer information to one another. They can communicate with their direct neighbours through gap junctions or via synaptic connections [258, 259, 260, 261], with cells of their close vicinity by diffusion of small chemical molecules or ions [262, 263, 264] and with partners located at much larger distances, over the range of the whole organism with more complex biologically active molecules, with a long lifetime in the circulation of blood.[265, 266, 267] As these communication procedures are the result of million years of evolution, one expects them to have reached a very high level of efficiency. For example hormones can induce dramatic changes in an organism at low blood concentrations thanks to a very powerful signaling machinery.[268, 269] Another signal and material transmission machinery used by organisms are extracellular vesicles (EVs). EVs are small vesicles excreted by cells and contain various cellular components in their lumen as well as on their surface.[144] They transport cargo of genetic material and can propagate diseases such as cancer.[270, 271, 149]

Extracellular vesicles, first observed in 1996 [272], are proteoliposomes ranging 50 to 1000 nm that are excreted by nearly all eukaryotic cells. Thought at first having no other biological function than transporting cellular waste, they were recently shown to play an important role in intercellular communication. They have been often referred as apoptotic bodies, the vesicular structures with a signaling role created by cells undergoing programmed cell death.[273] But then it was found that they are produced also by many healthy cells. EVs have two main

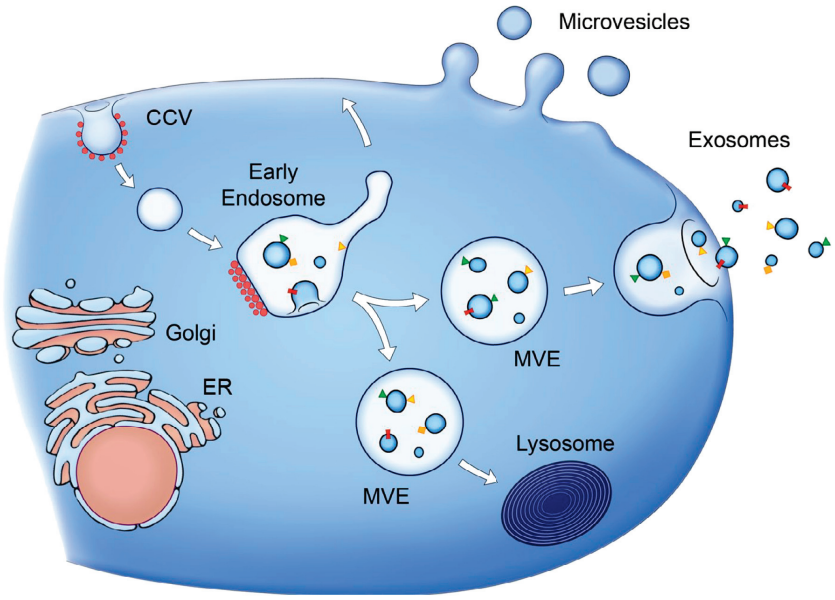

Figure 4.1: Formation of two different kinds of extracellular vesicles: microvesicles and exosomes. *Microvesicles are shed from the surface of the cell, with a membrane composition directly issued from the plasma membrane of the cell and an internal compartment originating from the cellular cytosol. Exosomes are formed by internal budding inside multivesicular bodies. Smaller in size than microvesicles, they are excreted when their endosome container fuses with the plasma membrane and liberates them in the extracellular medium. Image taken from [144].*

origins (Figure 4.1). Microvesicles are formed by exocytotic budding of the plasma membrane. Their diameter ranges from 0.1 to 1 micrometer. Exosomes are smaller-sized vesicles, with a diameter between 50 and 200 nm. They are formed by a budding process inside multi-vesicular bodies and are released by cells when the surrounding endosome fuses with the plasma membrane (Figure 4.1). The membrane of exosomes is rich in various transmembrane proteins. Unlike their membrane of origin, exosomes appear to be strongly enriched in transmembrane proteins of the tetraspanin family [274], which serve as markers of choice for detection or immobilization of exosomes. The membrane of exosomes comprises a high proportion of saturated and mono-unsaturated lipids, as well as, in some cases, cholesterol.[275] Markers at the surface seem to direct exosomes towards targeted cell types[276, 277] using different mechanisms, depending both on the exosome and on the recipient cell; permanent docking, fusion with the recipient membrane or endocytosis are possible.[278]

EVs have been reported to transfer information in numerous various biological processes. For example, EVs harvested from mouse embryonic stem cells have been shown to increase the survival and growth of hematopoietic stem cells to preserve the pluripotency of the cells.[279] Vesicles also exhibit healing properties; rats, to which acute post-ischemic injuries have

been inflicted to kidneys, showed a remarkable recovery after intravenous injection of EVs derived from human mesenchymal stem cells.[280] Furthermore, it seems in this case that EVs prevented kidneys from suffering of chronical diseases after acute injury. The action of blood circulating EVs derived from monocytes and macrophages has been highlighted to help coagulation by selectively fusing with activated platelets and activating a coagulation factor.[281] Meanwhile, EVs are also implied in the transmission and propagation of impairing conditions from diseased to healthy cells.

EVs help to transmit characteristics of certain cancer cells to surrounding cells in diverse ways.[282] For example, oncogenic proteins transported by EVs can affect the biological function of surrounding cells. Brain gliomas use this mechanism to transfer oncogenes produced by a small subset of cells to neighboring cells to foster the growth of the tumor.[283] EVs also function as an important cell-to-cell transport system for genetic material. mRNA and miRNA have been found in microvesicles isolated from glioblastoma cells.[284] mRNA of microvesicles has been shown to be translated in the receiving cell which initially was lacking the corresponding protein. Since oncogenes are expressed in a very abundant way, they are prone to be contained in EVs that are disseminating around their cell of origin, hence propagating genetic material for the production of oncogenic proteins. These features make EVs a very efficient tool for the so-called “horizontal” propagation of cancer, where proteins and genetic material are exchanged between cells as a driving force of the progression of tumors. Healthy cells suffer from a prolonged exposition to EVs produced by nearby malignant tumors, as they inevitably absorb them and integrate their content. Biological functions are directly altered by the transferred proteins and unwanted genetic material can alter the proteome of the recipient cell. Long-term exposition can lead to cell reprogramming or cell death.[285] Among transferred proteins, growth factor membrane receptors are found to modify the biology of neighbouring cells by artificial activation of transforming pathways.[286] Numerous pathways of oncogenic proteins are concerned with EV transmission to close-by cells.

Cancer-derived EVs are present in body fluids of patients, especially in blood, were they can reach concentrations as high as 10^{10} EVs per ml. This abundance added to the relatively high number of characteristic proteins or pieces of genetic material make them candidates of choice for the detection and specification of cancer.[284] EVs can be isolated by a combination of ultracentrifugation, ultrafiltration and size-exclusion chromatography.[287, 288]

4.1.2 Liposomes as carriers of material and information to cells

For several year, research has focused on the elaboration of spherical lipid vessels to deliver chemicals and drugs in the organism.[289, 290, 291] If regular liposomes have a poor efficiency in delivery, selectivity, life-time and or mechanical resistance, substantial improvements can be achieved by chemical or biological modifications. Circulation life-time can be improved by adding of protective molecules such as long polymers preventing access of degrading enzymes to liposomes circulating in blood and preventing their aggregation.[292, 293] Targeting a specific cell type with artificial liposomes can be achieved to a certain extent by including affinity molecules, such as antibodies or ligands, on the outer layer.[294, 295] The delivery of vesicles to the target cell can be optimized by attaching fusogenic molecules to the vesicle surface. These molecules can be fusogenic proteins, such as SNAREs, which carry the natural fusion capabilities to mediate actively or increase the fusion probabilities of the liposomes with targeted cells.[296, 297] Objects as complex as living cells have been shown to fuse under the action of SNAREs. The fusion is operated by specific interaction of v-SNAREs (vesicular SNAREs) with t-SNAREs (target membrane SNAREs), two complementary sets of specific partners respectively located on the vesicle and the target membrane, which actively wrap around each other. This causes the vesicle to come closer and closer of the membrane up to fusion of both entities.[298] Positively charged artificial lipids, such as DOTAP (1,2-dioleoyl-3-trimethylammonium-propane chloride) or DDAB (dimethyldioctadecylammonium bromide), can be incorporated in the lipid membrane of liposomes to take benefit from the negatively charged plasma membrane of cells to increase the fusion capabilities of the liposomes, with a fusion process based on the attraction of opposite electrical charges.[299, 300] Transfection methods such as Lipofectamine® are based on the spontaneous attraction of positively charged charged lipids with negatively charged genetic material.[301, 302]

EVs are body's own specialized way to diffuse genetic information from cell to cell with potentially both high specificity and fusogenic abilities. Investigating them for transport of specific exogenous material into targeted cells and transforming them for increased targeting and fusion capabilities is an opportunity to hijack nature for medical purpouse.[278, 303] In this chapter, we explore the first steps towards the use of EVs with enhanced fusion capabilities encapsulated in giant vesicles as potential curing agents. From the modification of the lipid composition of EVs to the different methods for triggering the releases of proteoliposome as large as 250 nm, the first steps in the direction of a potentially powerful healing method are explored.

4.2 Experimental

4.2.1 Isolation of extracellular vesicles

Extracellular vesicles were isolated and purified as described by Wyss *et al.*[288]. Briefly, particular cells are cultured in 150 ml plastic tissue culture flasks (TPP) up to surface confluence in standard culture medium supplemented by NBCS and antibiotics. The culture medium is then replaced by NBCS-free medium and incubated for two days. The culture medium is centrifuged at 300 g to pellet cell debris and the supernatant is passed through a 0.2 μm filter. The filtrate is concentrated in a ultracentrifugation concentrator with a 100 kDa cutoff. The concentrate is passed through a 0.2 μm centrifugal filtration unit, then through a Sephacryl S-500 HR (GE Healthcare Life Sciences) size-exclusion chromatography column with PBS as eluent. The fractions containing EVs are collected and if necessary frozen in liquid nitrogen for further use.

4.2.2 Modification of the lipid composition of extracellular vesicles

Lipid composition of EVs is modified according to a protocol described elsewhere.[202] The corresponding lipids dissolved in chloroform are transferred into a 1 ml glass bottle and dried under a flow nitrogen and 1 h vacuum. The lipid film is solubilized in ethanol by strong stirring. A small volume of lipid solution (typically a few microliters) is added to the purified EV dispersion to a final concentration of 10 μg/ml and incubated under gentle shaking for 30 minutes. Under these conditions, the exogenous lipids are spontaneously inserting into the membrane of the EVs. The modified EVs are then ready to be used.

4.2.3 Insemination of mammalian cells with extracellular vesicles

HEK cells are cultured in 8-well coverglass dishes. As they reach 30% confluence, modified EVs purified from eGFP-producing HEK cells are added with a EVs suspension/culture medium ratio of 1:20. The cells are then incubated 2 days at 37 °C. After detachment from the coverglass, washing and resuspension in PBS, the cells are analyzed by flow cytometry on a CyAn ADP high-performance flow cytometer (Beckman Coulter). Fluorescent events are measured by laser excitation at 488 nm and emission at 510-550 nm.

4.2.4 Giant unilamellar vesicle (GUV) fabrication

GUVs are produced by electroformation.[304] A solution of lipids in chloroform (1 $\frac{mg}{ml}$) is transferred into a 5 ml round bottom flask. Chloroform is evaporated first with a stream of nitrogen, then under vacuum for 1-2 h yielding a dry lipid film. Single unilamellar vesicles (SUVs) are produced by adding 1 ml of deionized water to the lipids and sonicating the sample with a metal-tip sonicator (Vibra-Cell VCX 750 Watts, Sonics) for 5 minutes. 10 μl drops of the suspension of SUVs are placed onto a ITO-coated conducting glass slide, inside a 1 mm, 250 μl PDMS chamber and dried under vacuum for 2 h. The film of lipids is gently rehydrated with a 200 μM sucrose solution and the chamber is closed with a second ITO-coated glass slide. Each slide is connected to a current generator electrode applying for 90 minutes an alternating electrical potential of 1.2 V at 10 Hz to the ITO electrode and subsequently for 30 minutes an additional alternating potential of 2.5 V at 4 Hz. The chamber is then opened and the GUVs are carefully collected with a pipette tip with an enlarged diameter and stored at 4 °C.

To prepare GUVs in physiological buffer, the protocol established by Montes *et al.*[305] was followed since under these conditions the previous method does not yield a satisfactory production of vesicles. SUVs suspended in water are carefully deposited on two platinum wire electrodes of 1 mm diameter placed at 2.5 mm distance sealed in a home-made PTFE chamber (Figure 4.2). Water is removed by placing the chamber in vacuum for 1 h. Once the lipids are dried, the chamber is filled up with physiological buffer and sealed tightly with glass supported Parafilm M (Bemis North America). Each wire is connected to a power supply. An alternating voltage of 106 mV at 500 Hz is applied for 5 min, then increased to 940 mV for 20 min and finally up to 2.61 V for 90 min. The chamber is opened, the GUVs are carefully collected with a pipette tip with an enlarged diameter and stored at 4 °C.

4.2.5 Controlled opening of GUVs

12 μl of a suspension of GUVs are pipetted into the inner well of a μ-Slide Angiogenesis (ibidi$_{\textcircled{R}}$). A circular piece of 20 μm nylon mesh (Millipore) with adapted size is placed on top of the vesicle sample (Figure 4.5). The top compartment of the well is filled with the buffer solution to equilibrate with the GUVs. The stability of the GUVs is monitored over time with a confocal LSM at the proper excitation/emission wavelengths.

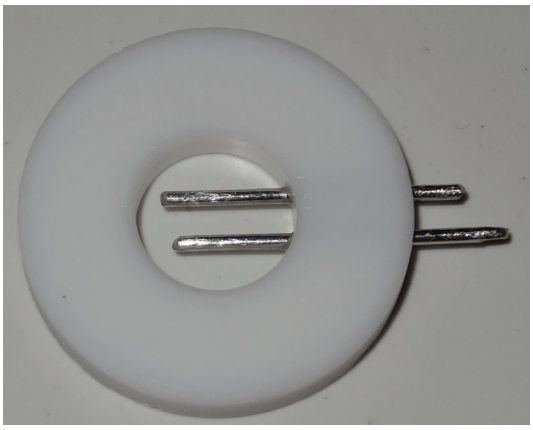

Figure 4.2: PTFE chamber comprising platinum wire electrodes for the electroformation of GUVs at high salt concentration.

4.3 Results and discussion

4.3.1 Cell insertion of EVs carrying genetic material

Based on the observation that genetic material can be transferred from cell to cell via exosomes and extracellular vesicles, we isolated EVs from HEK cells expressing eGFP to transfect non fluorescent HEK cells. EVs are produced and isolated as described in section 4.2.1. After isolation, the presence of EVs in solution is confirmed by fluorescence confocal microscopy, since the vesicles contain part of the expressed intracellular eGFP. The membrane composition of EVs is modified by addition of positively charged lipids according to the protocol described in section 4.2.2. The lipid-modified EVs are then added to a cell culture that express no eGFP and incubated at 37 °C over two days. In parallel, non-modified EVs are added to cultured cells as a control. After incubation, the cells have been first observed by a confocal microscopy; the two samples did not show significant differences. The cells of the two samples are therefor analyzed by flow cytometry to provide a statistically relevant amount of single-cell eGFP expression levels. With this approach, it was possible to detect small, but statistically significant differences of expressed eGFP between the two samples (Figure 4.3).
As expected, the addition of DOTAP in the membrane of EVs increased the fluorescence level of the analyzed cells as compared to the fluorescence level of control cells stably expressing the membrane receptor neurokinin 1 receptor (NK_1R) fused to eGFP. EVs were modified with several concentrations of DOTAP. The isolate of EVs from six 150 ml culture flasks (TPP) was divided into three equal fractions, completed to 100 ul with PBS, modified with a final concentration of respectively 0, 0.2 and 0.4 $\frac{mg}{ml}$ of DOTAP. Lower concentrations were tested with no significant fluorescence increase observed, whereas higher concentrations led to a high cell death rate. After two-day incubation, the amount of eGFP produced by the infected cells was maximal. No significant increase in fluorescence has been observed after longer incubation time. The obtained results are in agreement with those reported by Grasso *et al.* under different conditions.[202]

4.3.2 Encapsulation of microparticles in GUVs

In a next step, we encapsulated particles with an average diameter of 100 nm in giant unilamellar vesicles. As EVs are not stable in water and GUVs are difficult to produce in salt buffer conditions, we focused firstly on the encapsulation of fluorescent SUVs, with a diameter similar to that of EVs, inside GUVs formed in 200 mM sucrose solution. GUVs were electro-

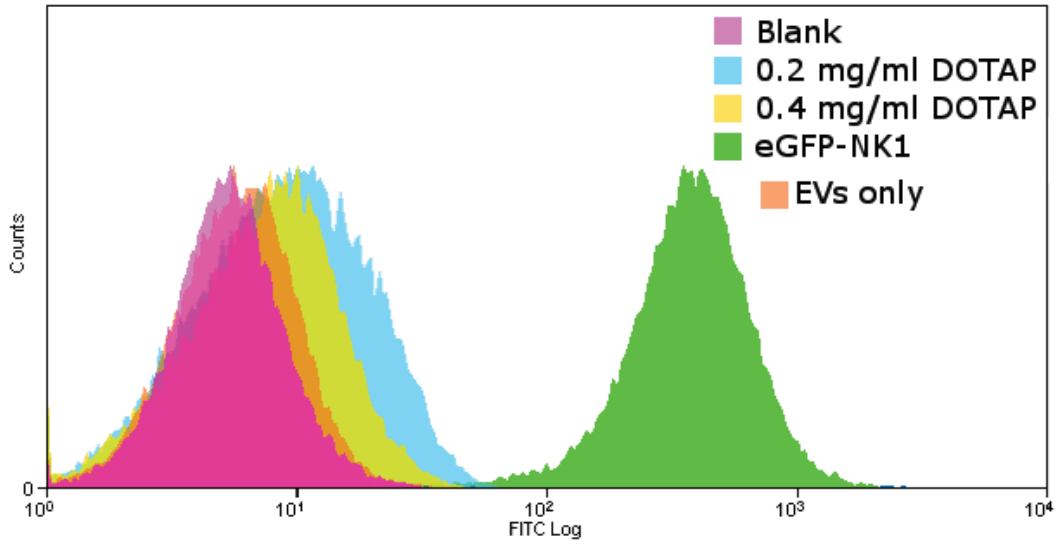

Figure 4.3: Flow cytometry of HEK cells transfected with DOTAP-EVs containing eGFP RNA. *Normalized fluorescence signals of HEK cells transfected with EVs comprising eGFP mRNA and different concentrations of DOTAP. In the absence of DOTAP ("EVs only"), only subtle increase of fluorescence of cellular eGFP is observed. In the presence of 0.2 $\frac{mg}{ml}$ of DOTAP in the bulk of EVs suspension, the fluorescence containing cells increased substantially. A further increase of the DOTAP concentration to 0.4 $\frac{mg}{ml}$ in the bulk of EVs suspension further increases the number of cells comprising fluorescence, but has a depleting effect on the survival rate of HEK cells. In pink, fluorescence unmodified HEK cells; in green, fluorescence level of HEK cells stably expressing NK_1R-eGFP membrane receptor as a comparative control.*

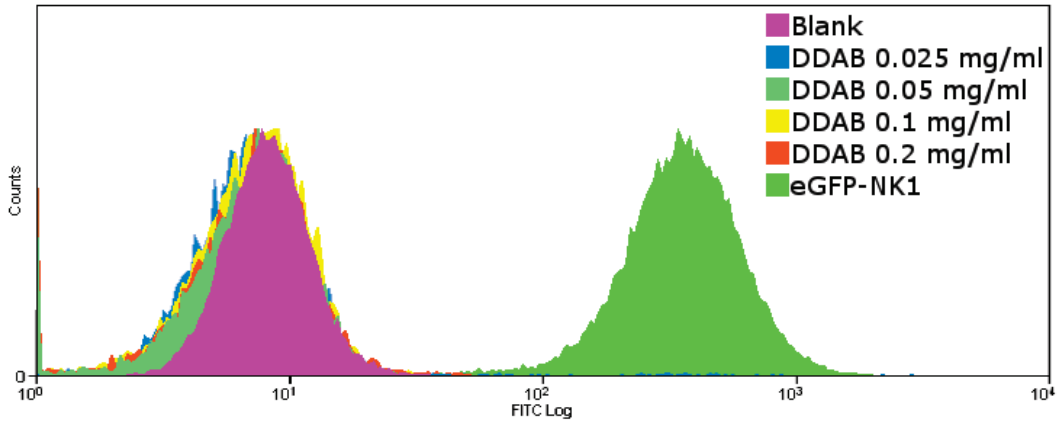

Figure 4.4: Flow cytometry of HEK cells transfected with DDAB-EVs containing eGFP RNA. *Normalized fluorescence signals of HEK cells transfected by EVs containing eGFP mRNA and different concentrations of DDAB added. No clear increase in fluorescence is observed within the range of DDAB concentration used for EV modification.*

formed according to the protocol of Angelova.[304] SUVs and GUVs were made from a mixture of 90% POPC, 9% DOPG and 1% of fluorescent lipid, either Liss-Rhod-PE (red) or NBD-PE (green). Suspension of SUVs was made from 1 mg of lipid mixture dissolved in chloroform, dried in a 5 ml glass bulb and resuspended in 1 ml of deionized water or 200 mM sucrose and then vortexed and either tip-sonicated (5 minutes) or extruded (100 nm pore-size filters, Miniextruder from Avanti Polar Lipids). The stock preparation of SUVs is diluted at a 1:500 ratio in 200 mM sucrose and used for electroformation of GUVs. If, during the formation of GUVs, SUVa are present in the surrounding bulk solution, they are finally in the lumen of GUVs.

Since we eventually want to observe the release of SUVs, the remaining non-trapped SUVs in the bulk must be removed from the GUVs. A procedure developed during my master thesis was used for this purpouse.[306] Twelve μl of GUVs are placed in the bottom of a compartmented plastic coverglass with a "well-in-a-well" structure (μ-slide Angiogenesis, ibidi$_{®}$) with a micropipette of which the tip has been cut to a larger diameter. A 20 μm nylon mesh (Millipore), cut to the exact dimensions to cover the inner well of the μ-slide, is carefully placed on top of the GUV suspension, while avoiding trapping air bubbles under the mesh. An iso-osmotic solution to the one in which the GUVs were formed is pipetted on top of the mesh in the main well. The top and bottom solution will mix reaching, equilibrium in about 30 minutes. The solution on the top can be easily exchanged by micropipetting without disturbing the mechanically sensitive GUVs underneath the mesh. After several dialysis operations, the GUV outer medium is cleaned from SUVs and GUVs containing SUVs can be easily observed (Figure 4.6).

To be noted, the GUV permeabilization protocol developed elsewhere[306] does not allow the SUVs to pass through the membrane of GUVs as the local destabilized membrane regions are too small.

4.3.3 Giant vesicle disruption

Release of the GUV content may be initiated by various processes such as pH change, photochemical processes, mechanical stress, acoustic waves, temperature change or addition of chemicals.[307, 308, 309, 310, 311] In many cases, the content release is mediated by a local destabilization in the GUV membrane. As we aim to trigger the release of large objects of more than 100 nm, small defects that let small molecules flow out of the GUVs are not suitable to meet our objective. We thus focus on methods that are able to completely open or destroy the

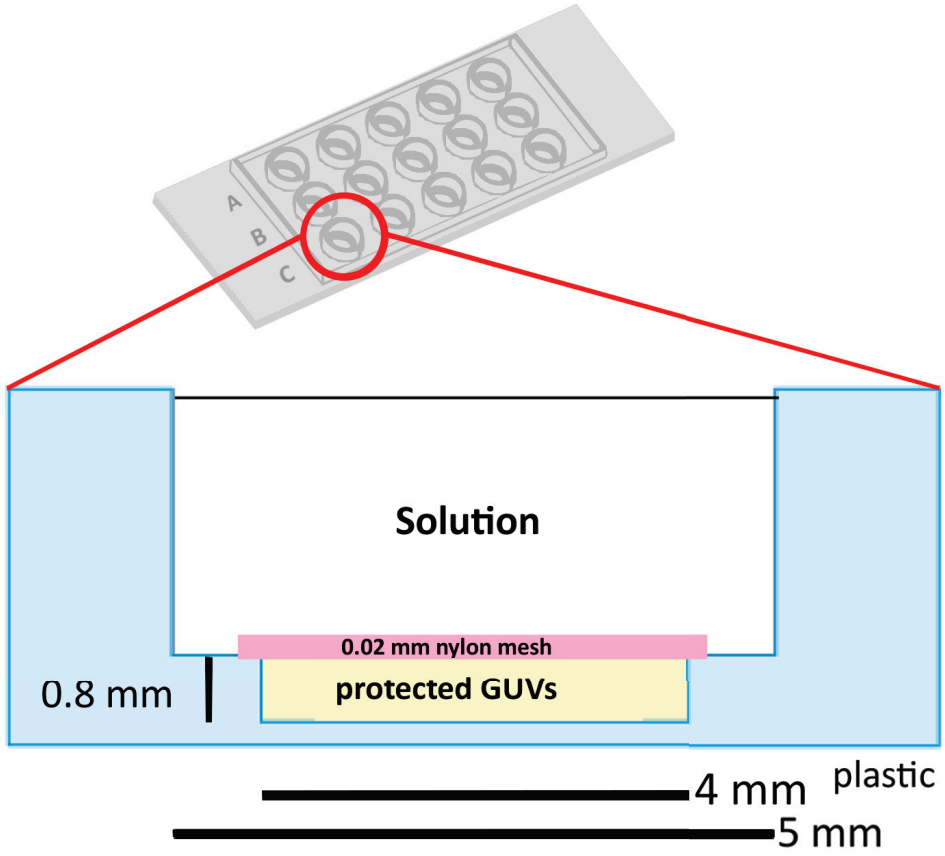

Figure 4.5: Scheme of the system used for exchanging solution surrounding GUVs with minimal perturbation. *The system for buffer exchange is made from a compartmented plastic coverglass with a "well-in-a-well" structure (µ-slide Angiogenesis, ibidi®). Each individual well contains a smaller well, originally used for a gel matrix supporting cells growing on top. GUVs are carefully deposited in the inner well, which is then covered by a nylon mesh (in our case, a 20 µm mesh) that allows passive diffusion between the inner and the top well while keeping the GUVs protected from mechanical perturbations such as convective stress created by pipeting liquid in the top well. The liquid of choice can be pipetted safely in the large top well to create a diffusive flux that will dilute the solution of the inner well into the upper well's liquid by a factor of 6-7 in about 30 minutes. This microdialysis procedure can be repeated several times to formally replace the initial bulk solution surrounding the GUVs by a solution of choice. Interesting to note is that high ionic strength buffers can be used as exchange solution. However, a permeabilization procedure is necessary to change the GUV inner liquid as well to avoid osmotic shock.[306] Image modified from ibidi® µ-slide Angiogenesis description webpage (http://tinyurl.com/zu76hng).*

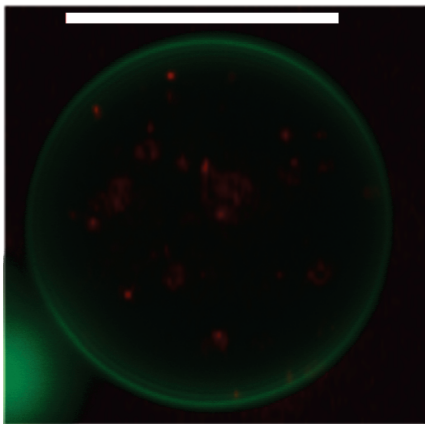

Figure 4.6: Green fluorescent GUV comprising red fluorescent SUVs trapped inside *are made of a mixture of 90% POPC, 9% DOPG and 1% of respectively NBD-PE and Liss-Rhod-PE. Non-trapped SUVs in the outer bulk phase bulk have been removed by repeated microdialysis to permit the observation of the release of SUVs from the inside of GUVs. Scalebar = 10 µm.*

GUVs while keeping the SUV intact. pH-sensitive liposomes have been considered for quite a long time as potential selective vehicles for therapeutic molecules.[312] Spatial bidimensional reorganization of lipids according to their charge have the potential to destabilize liposomes, inducing the collapse of the spherical structure. Methods using detergents are excluded as we aim to release the GUV content nearby living cells, and ultimately in living organisms while causing minimum damage. Temperature-sensitive lipids, although extremely interesting for the release, are very sensitive the most subtle change in experimental conditions, especially regarding the relative osmolarity of the solutions inside and outside the GUVs, and were not tested here. The use of chemicals in the surrounding of GUVs is prohibited, unless it does not harm living cells. A few chemicals fulfill this requirement in the tested conditions and may be candidates for release of EVs. Light-reactive compounds are of interest since they allow a precise control in space and time of the triggering of photochemical response.

pH-sensitive lipids as destabilizing agents

Growing tumors often show locally decreased pH values.[313] A change in pH can trigger the release of vesicle cargoes which could be used to release locally therapeutic agents to treat cancer.[314] In this context, the pH-sensitive lipid DODAP (1,2-dioleoyl-3-dimethylammonium-propane) is of interest. It is neutral at physiological conditions and protonated at its tertiary amino group at low pH, forming a positively charged lipid headgroup. The positive charges destabilize the membrane of the GUVs. By addition of HCl to the surrounding medium, the GUVs are destabilized and are able to release the enclosed SUVs. Vesicles containing 10%

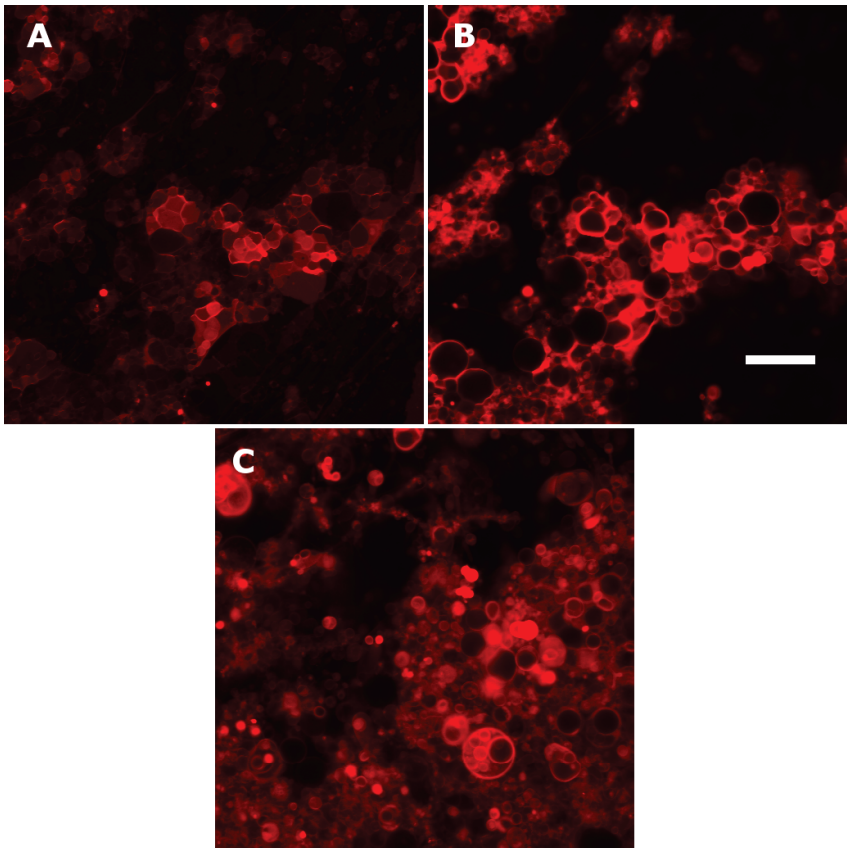

Figure 4.7: Fluorescent micrographs of GUVs composed of 90% POPC, 10% DODAP. *The 10% DODAP-containing vesicles are aggregated at pH 7 and are separated as individuals at pH 3 after HCl addition. A, time = 0 s; B, time = 20 s; C, time = 450 s after addition of HCl; Liss-Rhod-PE is used as fluorescent probe; Scalebar = 50 µm.*

DODAP are aggregated at pH 7. Addition of 100 mM HCl to reach a final pH of 3 separates the vesicles as individuals, without however breaking them in a noticeable way (Figure 4.7).

An alternative to DODAP is DGS (1,2-dioleoyl-sn-glycero-3-succinate), another pH-sensitive lipid. Here a carboxylic group is the functional group which can be protonated; therefore DGS is negatively charged at pH 7 and will become neutral at low pH values, which in turn leads to fusion and leakage of GUVs.

Diyne-PC containing vesicles

Here we report on experiments to destabilize GUVs by using the photopolymerizable lipid diyne-PC, used to trigger the release of small molecules from SUVs.[315, 316] The release of vesicle content relies here on two-dimensional aggregation and polymerization of lipids containing photoactivatable carbon-carbon triple bonds that crosslink upon illumination

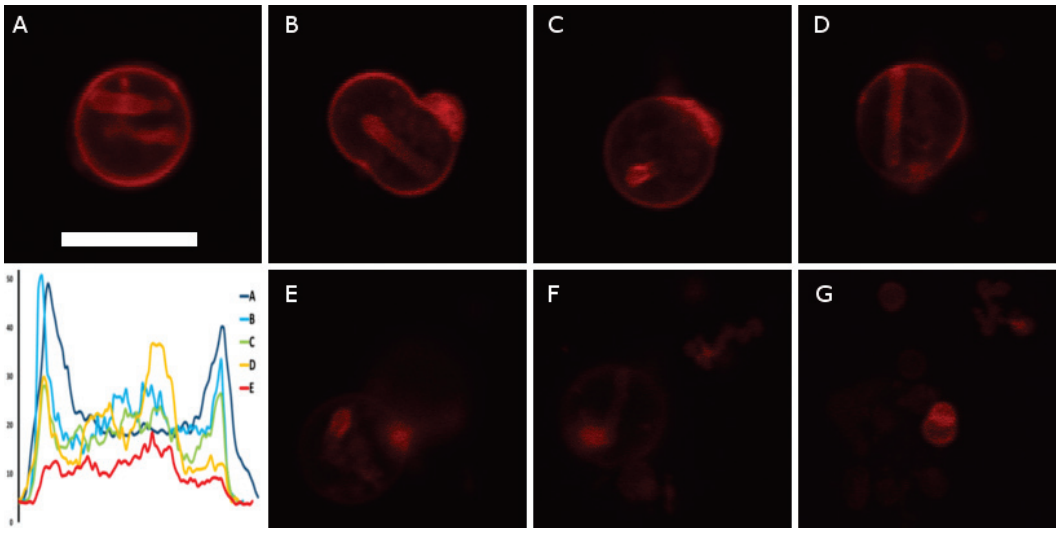

Figure 4.8: Fluorescent micrographs of GUVs composed of 90% POPC, 10% DGS. *A giant multilamellar vesicle containing DGS undergoes progressive loss of its external lipid bilayers at pH 3 after addition of HCl. The most external bilayer is pealed away after 3 minutes (B, C), the second bilayer 25 seconds later (D, E) and the last one after 5 minutes (F, G), releasing the entrapped lipid aggregates. The graph depicts the fluorescence intensity of the vesicle edges, showing the progressive loss of the external layers, one by one, in an unwrapping fashion. A, time = 0 s; B, time = 164 s; C, time = 184 s; D, time = 207 s; E, time = 209 s; F, time = 325 s; G, time = 336 s after addition of HCl; Liss-Rhod-PE is used as fluorescent probe; Scalebar = 10 µm.*

by UV light. Photocrosslinking induces phase transition that permeabilizes the lipid bilayer and releases the vesicle content. Molar ratios of diyne-PC of 5%, 10% and 15% in vesicles composed of a 9:1 mixture of POPC:POPG were tested. Under these conditions, we never observed GUVs. This might result from a destabilizing effect of the diyne-PC partly due to its length of the carbon chains made of 23 atoms whereas POPC and POPG are shorter with acyl chains of 18 and 16 carbon atoms. Another destabilizing contribution might arise from the relative rigidity of the hydrocarbon chains of diyne-PC containing both two carbon-carbon triple bonds. This rigid rod-like structure contrasts with the highly flexible acyl chains of surrounding lipids, which are more prone to form a stable two-dimensional fluid bilayer.

Addition of epigallocatechin gallate to the vesicle surrounding buffer

Epigallocatechin gallate is a catechin ester molecule, from the flavonoid family, found in abundance in green tea extract and exhibiting an antibacterial activity.[317] Epigallocatechin gallate interacts with lipid vesicles by progressively reducing their size until it totally destroys the initial spherical vesicle structure.[318] Epigallocatechin gallate forms holes in

lipid bilayers[317] which are large enough to enable the release of SUVs from GUVs.

Using the system described in figure 4.5, we incubated GUVs in solution with epigallocatechin gallate at a concentration of 700 μM. Since the migration of molecules through de nylon mesh is limited by diffusion, no effect could be observed on the GUVs during the first 15 minutes. Afterwards vesicles start to decrease in size and irregular, less stable lipidic structures appear and stick to GUVs. After 20 minutes, GUVs suddenly collapse forming large lipid clumps, releasing the content of the collapsed GUVs (Figure 4.9). HEK cells survived over several hours in the presence of a concentration of 1 mM epigallocatechin gallate, indicating a potential *in vivo* use.

Photochemical disruption of GUVs using $TPPS_{2a}$

In the following, we investigated whether $TPPS_{2a}$ encapsulated inside GUVs can be used for photochemically induce the release of SUVs from the GUVs.[319, 194] Giant vesicles are electroformed in the presence of both fluorescent SUVs and $TPPS_{2a}$ at high concentration. The formed GUVs are placed in the microdialysis system to remove non-encapsulated SUVs while keeping the $TPPS_{2a}$ concentration in the outer medium at 7 $\frac{\mu g}{ml}$. PBS is used for the final dialysis step to remove $TPPS_{2a}$ from the solution. The vesicles are observed with a confocal microscope thanks to 1% fluorescent lipids. Illumination of the vesicles containing the photosensitizer with a 5 mW laser pointer (405 nm) initiates the photochemical process. Thereby a part of the GUVs were disrupted remarkably quickly, between 15 seconds and 1.5 minute, releasing their cargo (Figure 4.10). SUVs released from GUVs can be seen in figure 4.10.H. Yet only a fraction of the total GUVs were found to open upon illumination.

As light can be easily and precisely controlled over time and space, the use of light-triggered release of EVs from GUVs appears not only to be the most efficient, but also the most applicable method among the ones tested for future *in vivo* tests, since it does not require a high blood concentration of $TPPS_{2a}$.

4.3.4 Towards EV liberation from GUV cargos

In the following, we report experiments to transfect HEK cells with SUVs comprising eGFP plasmids and containing DOTAP. We first tried to encapsulate the full length pEGFP-N1 plasmid (Clonetech), but neither sonication, nor extrusion of SUVs resulted in detectable eGFP expression after incubation with cells. We believe it is due to the size of the plasmid, which

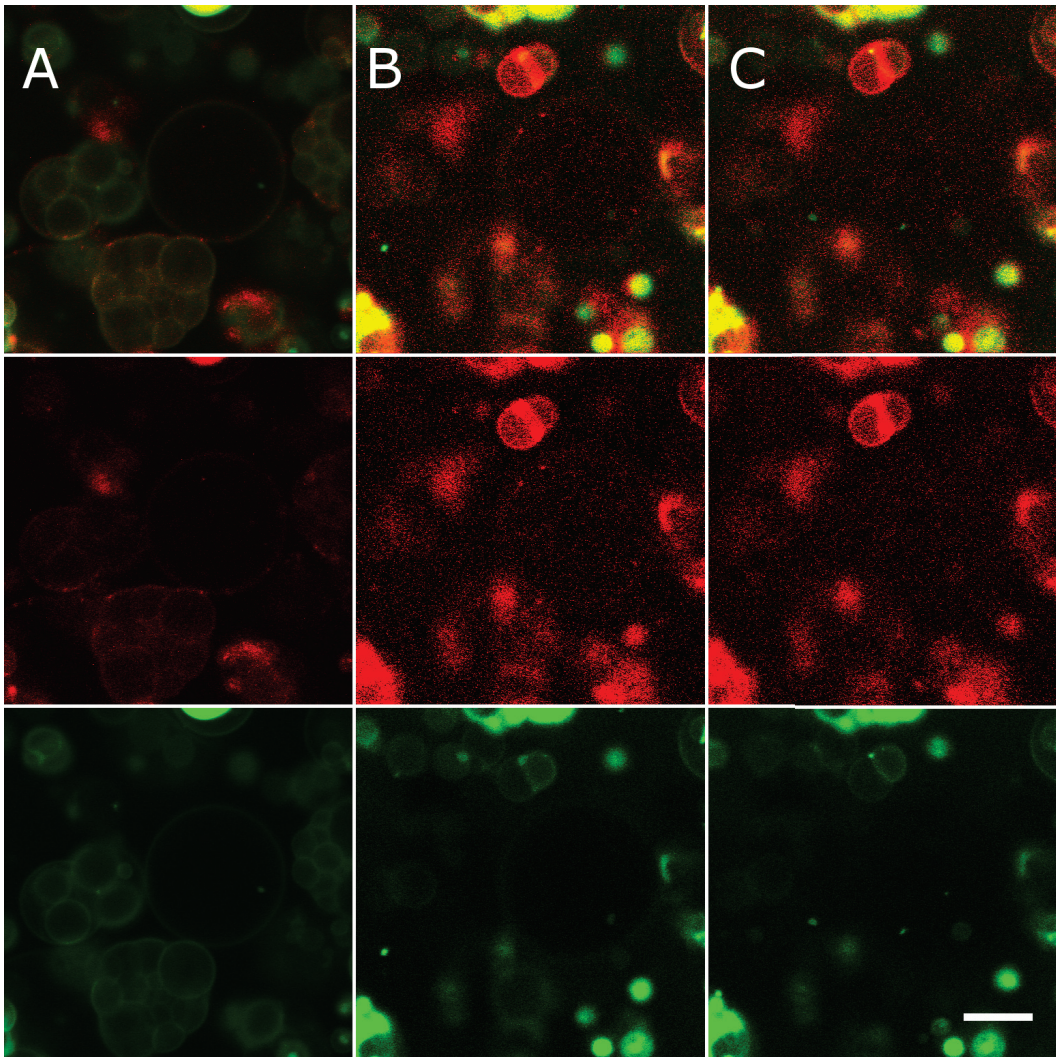

Figure 4.9: Fluorescent GUVs (90% POPC, 9% DOPG, 1% NBD-PE (green fluorescent)) containing SUVs (90% POPC, 9% DOPG, 1% Liss-Rhod-PC (red-fluorescent)) during addition of epigallocatechin gallate to a final concentration of 700 μM. *Using the system depicted in Figure 4.5, vesicles (A) are exposed to epigallocatechin gallate by slow diffusion. The vesicles start to collapse approximately 1200 seconds after the addition of epigallocatechin gallate. Within less than a minute, the content of a vesicle is released. Image series taken at 1 frame every 20 seconds. A, time = 77 s; B, time = 1179 s; C, time = 1230 s after addition of epigallocatechin gallate. B and C have been contrast enhanced to compensate photobleaching caused by laser excitation of the fluorescent probes. Scale bar = 10 μm.*

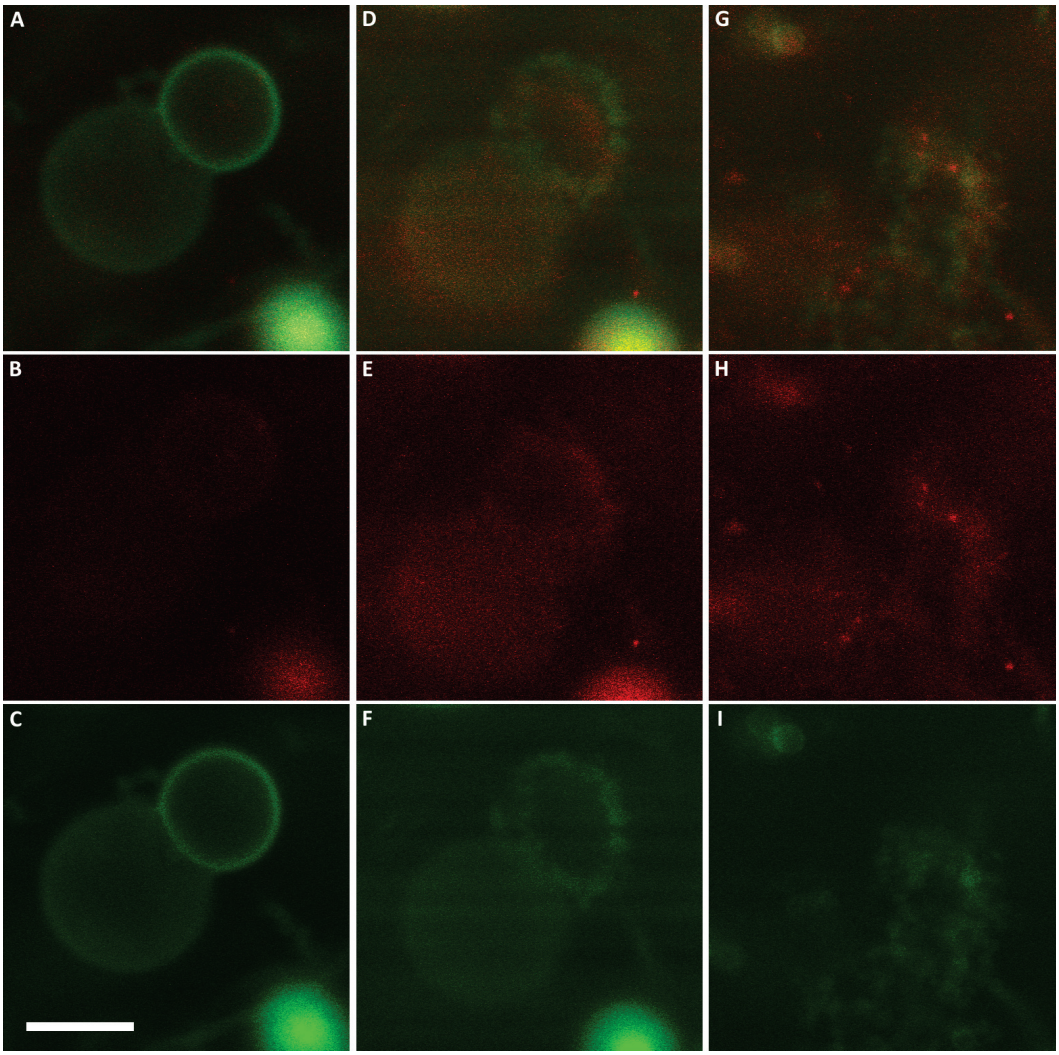

Figure 4.10: Green fluorescent GUVs (90% POPC, 10% DOPG, 1% NBD-PE) containing red fluorescent SUVs (90% POPC, 10% DOPG, 1% Liss-Rhod-PC) and TPPS$_{2a}$ irradiated by UV light. *Green fluorescent GUVs containing red fluorescent SUVs are destroyed photochemically. The first vesicle breaks after 15 s of light irradiation, the second breaks after 45 s. Released SUVs are visible in H. Images during irradiation exhibit more intense fluorescence because of the additional excitation light input provided by the illuminating laser. A, B, C, time = 0 s; D, E, F, time = 15 s; G, H, I, time = 45 s of irradiation. Scale bar = 10 µm.*

might be too large to integrate into SUVs. The plasmid is composed of 4700 base pairs which might finally form a compact structure of 500 nm.[320] We then tried smaller DNA fragments of the plasmid, but obtained no conclusive results.

We finally focused on a method to encapsulate green fluorescent EVs inside GUVs as described in section 4.2.4 using EV-containing solution during GUV formation. It has been shown that vesicles derived from erythrocyte ghosts did not loose their inner content upon formation under physiological conditions. After formation, vesicles have been observed, most of them multilamellar with a low proportion of unilamellar vesicles. No clear evidence of encapsulated EVs could be found, despite some GUVs displaying a unusually high green (fluorescent reporter of GUV lipid mixture) to red (eGFP encapsulated in EVs) fluorescence ratio at the vesicle membrane, suggesting that EVs are fusing with the lipid film during the vesicle electroformation process.

We will now discuss alternative methods that were not tested in this thesis. The method of Horger *et al.* [321], designed to make giant vesicles from a lipid film deposited on ultra-low melting agarose in saline buffer, could be a potential candidate, provided EVs can diffuse through agarose.
Shear-stress sensitive vesicles, made of the artificial lipid Pad-PC-Pad, may take advantage of the local pressure created *in vivo* by a growing tumor to trigger automatically the release of nano-sized cargoes in the area of interest.[322] Release of microvesicles remains however to prove possible, since the shear-stress release is suspected to occur via transient pores rather than vesicle disruption.
Two last methods consist in encapsulating EVs inside larger vesicles in microfluidics by formation of droplets of an EV suspension in a lipophile liquid containing lipids.[323, 324] These methodologies circumvent the problem of the high ionic strength of physiological media and insure both homogenous size and unilamellarity. They furthermore ensure a high yield of encapsulation and are less limited in the choice of the lipids used for making the GUVs. Replacing the lipophile solvent to make the GUV suspension *in vivo*-compatible remains a problem and can be possibly solved by dialysis. Yield, size and encapsulation efficiency of the vesicles are directly proportional to the microfluidic parameters, in particular flow rate and channel dimensions.

4.4 Conclusion and outlook

There is an ever increasing demand for technological advances in the context of precision medicine. In this chapter, we explored the possibilities to use extracellular vesicles as nano-sized cargoes for the delivery of native material into cells. We have shown that if the fusion of EVs with target cells is inefficiently mediated by surface proteins, the addition of the positively charged lipid DOTAP to the bilayer of EVs make them more prone to release their content into cells, which have an overall negatively charged plasma membrane. Genetic material enclosed in EVs can be translocated and subsequently be expressed in the recipient cell to palliate for example a lack of critical protein for therapeutic purpose. It is important to keep in mind that the genetic material contained in EVs is mRNA, which has a limited lifetime in cells and can be translated into proteins only a limited amount of times. Hence it is critical to overload the EV-producing cells with the desired mRNA sequence to achieve reasonable effect to the target cells.

We have shown that SUVs, a size and composition equivalent model of EVs, can be encapsulated in giant unilamellar vesicles and then released upon various trigger reactions. This approach could become of interest to efficiently deliver biological material, including genetical material, into diseased cells in a controlled manner. The use of characteristic features of a disease, such as tissue compression, local low pH, or increased body temperature, could be considered as trigger factors. Exogenous opening of GUVs induced by light provides a high spatial and temporal control of releasing the content of GUVs. Interesting possibilities to release vesicles up to about 1000 nm are: (1) DGS, a pH-sensitive lipid that can be inserted into the membrane of GUVs. (2) Epigallocatechin gallate, a tea catechin that destroys GUVs while preserving living cells. (3) $TPPS_{2a}$, a photosensitizer that destabilizes GUVs from the inside upon UV illumination.

Using the body's own cargo system to transport desired molecules or genetic material may revolutionize the way to administer treatments in specific areas of the body. Production of EVs with selected recruitment and fusion proteins in large quantities could provide standardized man-engineered natural magic bullets, containing genetic material able to be delivered on demand. Though it is not yet realized in concrete application, targeting medicine offers interesting possibilities for future medication for curing and healing purposes.

5 Overall conclusion

Micro-sized devices are gaining increasing importance in many fields of bioanalysis as they offer single-cell applications which are difficult or impossible to reach with classical technologies. Usually, experimental data are obtained from the study of large numbers of cells, whereas results are represented and interpreted on the basis of consensus average properties of a single cell. However, increasing experimental evidences on the biochemical and functional variability between individuals in populations of cells demonstrate that a one-cell prototypical property does not properly represent a whole cell population. Consequently, to elucidate a cell's functional or, in the context of a disease, dysfunctional state, genetic or phenotypic characteristics of individual cells have to be measured within the cell population. Here we have developed bioanalytical methods for probing the biochemical composition and mechanical properties of single cells and for delivering compounds into cells.

The single-cell methods developed within this thesis probe various properties of single cells. The investigations methods presented here are targeting two specific locations of a cell and aim at (i) the determination of local viscoelastic properties of a cell's plasma membrane and (ii) the quantification of intracellular analytes. Both methods yield important information about the functional state of each observed cell. These novel ways of probing individual cells are directed to two constitutive aspects of a cell, the plasma membrane and the cytoplasm content, to harvest information of distinct sources and provide a broader biomedical profile of a specific disease if used in combination.

First we have investigated the mechanical properties of human skin melanoma cells originating from patients at different stages of cancer development. We demonstrated that the back relaxation of nanotubes of plasma membranes pulled out of cancer cells with the help of

laser tweezers yields important information of the viscoelastic properties of the cells and are able to distinguish cancer cells at different stages of tumor development. This opens novel possibilities in diagnosing the functional state of tumor derived cancer cells.

Further, we developed an alternative concept of chemical cytometry in microfluidics employing micron-sized particles as intracellular probes. Our approach addresses inherent limitations of present chemical cytometry methods by (i) preventing dilution of target analytes upon cell lysis, and (ii) by parallelization of the analyte separation step. Here we used micrometer sized silica beads coated with high-affinity receptors to capture a specific analyte. The affinity beads are adsorbed on top of cells, internalized by phagocytosis and then, using the photosensitizer $TPPS_{2a}$, the phagosomes were broken upon illumination at a wavelength of 405 nm to allow direct contact with the components of the cytoplasm. Finally, target analytes were captured by the accessible affinity beads. Cells were then processed through a microfluidic chip where cells containing a bead are captured by an optical trap. The cells were lysed, and the bead, with target analytes attached to it, were characterized by a specific marker. Our method analyzes 1-2 cells per minute with manual operation and could increase greatly its throughput by automation. Parallel binding of multiple analytes to beads has been shown, opening the way for very efficient multiple analyte detection with single-cell resolution. In summary, our bead-based analysis presented here offers interesting novel opportunities for single-cell analyses in diagnostics and therapy towards personalized medicine. An attractive future development would be a platform combining the two latter methods. This would allow to first analyze to first analyze the viscoelastic properties of the plasma membrane of a single and subsequently its biochemical content, for example concerning cancer markers. Such sequential analyses would provide simultaneously critical information about the type of cancer and its progression state with a single-cell resolution.

Finally, we explored the potential how cell-derived extracellular vesicles could be enclosed as cargo in giant unilamellar vesicles (GUVs), and, after controlled release, might be used as cell modifying agents. We first showed that EVs enriched on their membrane surface with positively charged DOTAP lipids were capable to deliver genetic material derived from their mother cell into a target cell leading to the expression of a particular protein. We then showed in a separate step that SUVs, a size and composition equivalent model of EVs, could be first enclosed into and then released from giant vesicles using a photochemical trigger. This tool has the potential to be used within gene therapy as a complementary tool to the previous methods, regarding the development of a personalized, highly individual specific biomedical process of diagnosis and treatment of diseases such as cancer or chronical inflammatory

diseases, which display a high cell-to-cell heterogeneity.

The relevance of the single-cell methodologies developed in the present thesis are becoming obvious from the following few examples out of many: (i) Cell differentiation in multicellular organisms is known since the beginning of cell biology; single-cell analysis would discover differences and heterogeneity of protein profiles and their biological relevance between and within the various cell types, including rare ones such as the different forms of stem cells, which are of central importance for generation, homeostatic regeneration and repair of tissues. Single-cell analysis will have a big impact to understand stem cell behavior, which is essential for potential therapeutic applications. (ii) Cellular gene expression is known to occur stochastically; this leads to massive cell-to-cell variations in the concentration of rare proteins many of which play an important role in cell functioning and signaling. (iii) Cancer tumors show enormous variability which is manifested in a large heterogeneity of signaling profiles between individual cells; these variations might be of importance for cancer cell survival and pathology and a deeper understanding of such processes is of utmost medical relevance. Consequently, the methods developed in this thesis overcome limitations of presently used ensemble measurements and might in the future be used in the context of the examples mentioned before.

Bibliography

[1] Harvey Lodish, Arnold Berk, Paul Matsudaira, et al. *Molecular Cell Biology*. Freeman, W. H. & Company, 5th edition, 2003.

[2] Jeremy M Berg, John L Tymoczko, and Lubert Stryer. *Biochemistry - Chapter 3 - Protein Structure and Function*. W. H. Freeman, New York, 5th edition, 2002.

[3] Niels Gregersen, Peter Bross, Søren Vang, and Jane H. Christensen. Protein Misfolding and Human Disease. *Annual Review of Genomics and Human Genetics*, 7(1):103–124, 2006.

[4] Douglas Hanahan and Robert A. Weinberg. Hallmarks of cancer: the next generation. *Cell*, 144(5):646–74, 2011.

[5] Karen H. Vousden and David P. Lane. p53 in Health and Disease. *Nature Reviews Molecular Cell Biology*, 8(4):275–283, 2007.

[6] B. Drouet, M. Pinçon-Raymond, Jean Chambaz, and T. Pillot. Molecular basis of Alzheimer's disease. *Cellular and Molecular Life Sciences*, 57:705–715, 2000.

[7] Joseph B. Martin. Molecular basis of the neurodegenerative disorders. *The New England Journal of Medicine*, 340(25):1970–1980, 1999.

[8] Raya S. Brown and Richard L. Wahl. Overexpression of Glut-1 glucose transporter in human breast cancer: An immunohistochemical study. *Cancer*, 72(10):2979–2985, 1993.

[9] Jian-Yu Wu, Anne-Therese Vlastos, Marie-Françoise Pelte, et al. Aberrant expression of BARD1 in breast and ovarian cancers with poor prognosis. *International Journal of Cancer*, 118(5):1215–1226, 2006.

[10] Wen-Jian Meng, Hui Yan, Bin Zhou, et al. Correlation of SATB1 overexpression with the progression of human rectal cancer. *International Journal of Colorectal Disease*, 27(2):143–150, 2012.

[11] Michael M. Malim, Joachim Hauber, Randy Fenrick, and Bryan R. Cullen. Immunodeficiency virus rev trans-activator modulates the expression of the viral regulatory genes. *Nature*, 335:181–183, 1988.

[12] S. Fujino, A. Andoh, S. Bamba, et al. Increased expression of interleukin 17 in inflammatory bowel disease. *Gut*, 52(1):65–70, 2003.

[13] Ibtisam E. Tothill. Biosensors for cancer markers diagnosis. *Seminars in Cell & Developmental Biology*, 20(1):55–62, 2009.

[14] Gengfeng Zheng, Fernando Patolsky, Yi Cui, Wayne U. Wang, and Charles M. Lieber. Multiplexed electrical detection of cancer markers with nanowire sensor arrays. *Nature Biotechnology*, 23(10):1294–1301, 2005.

[15] Savka I. Stoeva, Jae Seung Lee, Steven T. Rosen, and Chad A. Mirkin. Multiplexed detection of protein cancer markers with biobarcoded nanoparticle probes. *Journal of the American Chemical Society*, 128(26):8378–8379, 2006.

[16] Michael S. Wilson and Weiyan Nie. Multiplex measurement of seven tumor markers using an electrochemical protein chip. *Analytical Chemistry*, 78(18):6476–6483, 2006.

[17] Paul K. Horan and Leon L. Jr. Wheeless. Quantitative single cell analysis and sorting. *Science*, 198(4313):149–157, 1977.

[18] Westbrook M. Weaver, Peter Tseng, Anja Kunze, et al. Advances in high-throughput single-cell microtechnologies. *Current Opinion in Biotechnology*, 25:114–123, 2014.

[19] Jing Yu, Jing Zhou, Alex Sutherland, et al. Microfluidics-based single-cell functional proteomics for fundamental and applied biomedical applications. *Annual Review of Analytical Chemistry*, 7:275–295, 2014.

[20] Yuliang Deng, Yu Zhang, Shuai Sun, et al. An Integrated Microfluidic Chip System for Single-Cell Secretion Profiling of Rare Circulating Tumor Cells. *Scientific Reports*, 4:7499, 2014.

[21] André A. Adams, Paul I. Okagbare, Juan Feng, et al. Highly efficient circulating tumor cell isolation from whole blood and label-free enumeration using polymer-based microfluidics with an integrated conductivity sensor. *Journal of the American Chemical Society*, 130(27):8633–8641, 2008.

[22] S. Riethdorf, H. Fritsche, V. Muller, et al. Detection of Circulating Tumor Cells in Peripheral Blood of Patients with Metastatic Breast Cancer: A Validation Study of the CellSearch System. *Clinical Cancer Research*, 13(3):920–928, 2007.

[23] Sunitha Nagrath, Lecia V. Sequist, Shyamala Maheswaran, et al. Isolation of rare circulating tumour cells in cancer patients by microchip technology. *Nature*, 450(7173):1235–1239, 2007.

[24] Shannon L. Stott, C.-H. Chia-Hsien Hsu, Dina I. Tsukrov, et al. Isolation of circulating tumor cells using a microvortex-generating herringbone-chip. *Proceedings of the National Academy of Sciences of the United States of America*, 107(43):18392–18397, 2010.

[25] E. Ozkumur, A. M. Shah, J. C. Ciciliano, et al. Inertial Focusing for Tumor Antigen-Dependent and -Independent Sorting of Rare Circulating Tumor Cells. *Science Translational Medicine*, 5(179):179ra47, 2013.

[26] Lotien Richard Huang, Edward C. Cox, Robert H. Austin, and James C. Sturm. Continuous particle separation through deterministic lateral displacement. *Science*, 304(5673):987–990, 2004.

[27] H. Christina Fan, Jianbin Wang, Anastasia Potanina, and Stephen R. Quake. Whole-genome molecular haplotyping of single cells. *Nature Biotechnology*, 29(1):51–57, 2011.

[28] Frank B. Dean, John R. Nelson, Theresa L. Giesler, and Roger S. Lasken. Rapid Amplification of Plasmid and Phage DNA Using Phi29 DNA Polymerase and Multiply-Primed Rolling Circle Amplification. *Genome Research*, 11(6):1095–1099, 2001.

[29] Chenghang Zong, Sijia Lu, Alec R. Chapman, and X Sunney Xie. Genome-wide detection of single-nucleotide and copy-number variations of a single human cell. *Science*, 338(6114):1622–1626, 2012.

[30] Wibke Hellmich, Christoph Pelargus, Kai Leffhalm, Alexandra Ros, and Dario Anselmetti. Single cell manipulation, analytics, and label-free protein detection in microfluidic devices for systems nanobiology. *Electrophoresis*, 26(19):3689–3696, 2005.

[31] Marlis Zeiler, Werner L. Straube, Emma Lundberg, Mathias Uhlen, and Matthias Mann. A Protein Epitope Signature Tag (PrEST) library allows SILAC-based absolute quantification and multiplexed determination of protein copy numbers in cell lines. *Molecular & Cellular Proteomics*, 11(3):O111.009613, 2012.

[32] Shoji Ohkuma and Brian Poole. Fluorescence Probe Measurement of Intralysosomal pH in Living Cells and Perturbation of pH By Various Agents. *Proceedings of the National Academy of Sciences of the United States of America*, 75(7):3327–3331, 1978.

[33] Roger Y. Tsien. The Green Fluorescent Protein. *Annual Review of Biochemistry*, 67:509 – 544, 1998.

[34] Thamani Dahoun, Luigino Grasso, Horst Vogel, and Horst Pick. Recombinant Expression and Functional Characterization of Mouse Olfactory Receptor mOR256-17 in Mammalian Cells. *Biochemistry*, 50(33):7228–7235, 2011.

[35] Emmanuelle Astoul, Sandra Watton, and Doreen Cantrell. The Dynamics of Protein Kinase B Regulation during B Cell Antigen Receptor Engagement. *The Journal of Cell Biology*, 145(7):1511–1520, 1999.

[36] L S Barak, S S Ferguson, J Zhang, and M G Caron. A beta-arrestin/green fluorescent protein biosensor for detecting G protein-coupled receptor activation. *The Journal of Biological Chemistry*, 272(44):27497–27500, 1997.

[37] Kevin Truong and Mitsuhiko Ikura. The use of FRET imaging microscopy to detect protein-protein interactions and protein conformational changes in vivo. *Current Opinion in Structural Biology*, 11(5):573–578, 2001.

[38] Marco Mank, Dierk F Reiff, Nicola Heim, et al. A FRET-Based Calcium Biosensor with Fast Signal Kinetics and High Fluorescence Change. *Biophysical Journal*, 90(5):1790–1796, 2006.

[39] Bas Ponsioen, Jun Zhao, Jurgen Riedl, et al. Detecting cAMP-induced Epac activation by fluorescence resonance energy transfer: Epac as a novel cAMP indicator. *EMBO Reports*, 5(12):1176–1180, 2004.

[40] Samuel T. Hess, Thanu P. K. Girirajan, and Michael D. Mason. Ultra-high resolution imaging by fluorescence photoactivation localization microscopy. *Biophysical Journal*, 91(11):4258–4272, 2006.

[41] Michael J. Rust, Mark Bates, and Xiaowei Zhuang. Sub-diffraction-limit imaging by stochastic optical reconstruction microscopy (STORM). *Nature Methods*, 3(10):793–795, 2006.

[42] Thomas A. Klar, Stefan Jakobs, Marcus Dyba, Alexander Egner, and Stefan W. Hell. Fluorescence microscopy with diffraction resolution barrier broken by stimulated emission. *Proceedings of the National Academy of Sciences of the United States of America*, 97(15):8206–8210, 2000.

[43] Hazel M. Davey and Douglas B. Kell. Flow cytometry and cell sorting of heterogeneous microbial populations: the importance of single-cell analyses. *Microbiological Reviews*, 60(4):641–696, 1996.

[44] Maxine A. McClain, Christopher T. Culbertson, Stephen C. Jacobson, et al. Microfluidic devices for the high-throughput chemical analysis of cells. *Analytical Chemistry*, 75(21):5646–5655, 2008.

[45] J. Scott Mellors, Kaveh Jorabchi, Lloyd M. Smith, and J. Michael Ramsey. Integrated Microfluidic Device for Automated Single Cell Analysis Using Electrophoretic Separation and Electrospray Ionization Mass Spectrometry. *Analytical Chemistry*, 82(3):967–973, 2010.

[46] Bo Huang, Hongkai Wu, Devaki Bhaya, et al. Counting Low-Copy Number Proteins in a Single Cell. *Science*, 315(5808):81–84, 2007.

[47] Wibke Hellmich, Dominik Greif, Christoph Pelargus, Dario Anselmetti, and Alexandra Ros. Improved native UV laser induced fluorescence detection for single cell analysis in poly(dimethylsiloxane) microfluidic devices. *Journal of Chromatography A*, 1130(2):195–200, 2006.

[48] Dominik Greif, Lukas Galla, Alexandra Ros, and Dario Anselmetti. Single cell analysis in full body quartz glass chips with native UV laser-induced fluorescence detection. *Journal of Chromatography A*, 1206(1):83–88, 2008.

[49] Mian Yang, Tzu-Chiao Chao, Randall Nelson, and Alexandra Ros. Direct detection of peptides and proteins on a microfluidic platform with MALDI mass spectrometry. *Analytical and Bioanalytical Chemistry*, 404(6):1681–1689, 2012.

[50] Mian Yang, Tzu-Chiao Chao, Randall Nelson, and Alexandra Ros. Protein identification and quantification for single cell analysis by coupling a microfluidic platform with MALDI-TOF. In *17th μTAS Proceedings*, pages 1039–1041, 2013.

[51] Paul J. Hung, Philip J. Lee, Poorya Sabounchi, Robert Lin, and Luke P. Lee. Continuous perfusion microfluidic cell culture array for high-throughput cell-based Assays. *Biotechnology and Bioengineering*, 89(1):1–8, 2005.

[52] Michael Werner, Fabrice Merenda, Joachim Piguet, René-Paul Salathé, and Horst Vogel. Microfluidic array cytometer based on refractive optical tweezers for parallel trapping, imaging and sorting of individual cells. *Lab on a Chip*, 11(14):2432–9, 2011.

[53] Michael Werner. *Optical Trapping in Microfluidic Channels for Functional and Chemical Analysis of Single Cells*. PhD thesis, EPFL, 2011.

[54] Alison M. Skelley, Oktay Kirak, Heikyung Suh, Rudolf Jaenisch, and Voldman Joel. Microfluidic control of cell pairing and fusion. *Nature Methods*, 6(2):147–152, 2009.

[55] Shia-Yen Teh, Robert Lin, Lung-Hsin Hung, and Abraham P. Lee. Droplet Microfluidics. *Lab on a Chip*, 8(2):198–220, 2008.

[56] J. Sun, M. D. Masterman-Smith, N. A. Graham, et al. A Microfluidic Platform for Systems Pathology: Multiparameter Single-Cell Signaling Measurements of Clinical Brain Tumor Specimens. *Cancer Research*, 70(15):6128–6138, 2010.

[57] Assieh Saadatpour, Shujing Lai, Guoji Guo, and Guo-Cheng Yuan. Single-Cell Analysis in Cancer Genomics. *Trends in Genetics*, 31(10):576–586, 2015.

[58] James R. Heath, Antoni Ribas, and Paul S. Mischel. Single-cell analysis tools for drug discovery and development. *Nature Reviews Drug discovery*, 15(3):204–216, 2015.

[59] Robert Barer. Microscopes, microscopy, and microbiology. *Annual Review of Microbiology*, 28:371–389, 1974.

[60] Douglas Magde, Eliott Elson, and W. W. Webb. Thermodynamic fluctuations in a reacting system - measurement by fluorescence correlation spectroscopy. *Physical Review Letters*, 29(11):705–708, 1972.

[61] Yan Chen, Li-Na Wei, and Joachim D. Müller. Probing protein oligomerization in living cells with fluorescence fluctuation spectroscopy. *Proceedings of the National Academy of Sciences of the United States of America*, 100(26):15492–15497, 2003.

[62] Clement E. Blanchet and Dmitri I. Svergun. Small-angle X-ray scattering on biological macromolecules and nanocomposites in solution. *Annual Review of Physical Chemistry*, 64:37–54, 2013.

[63] Arthur Ashkin. Acceleration and trapping of particles by radiation pressure. *Physical Review Letters*, 24(4):156–159, 1970.

[64] Arthur Ashkin, J. M. Dziedzic, J. E. Bjorkholm, and S. Chu. Observation of a single-beam gradient force optical trap for dielectric particles. *Optics Letters*, 11(5):288–290, 1986.

[65] Arthur Ashkin. Forces of a single-beam gradient laser trap on a dielectric sphere in the ray optics regime. *Biophysical Journal*, 61(February):569–582, 1992.

[66] Steven M. Block, Lawrence S. Goldstein, and Bruce J. Schnapp. Bead movement by single kinesin molecules studied with optical tweezers. *Nature*, 348:348–352, 1990.

[67] Thomas T. Perkins, Stephen R. Quake, Douglas E. Smith, and Steven Chu. Relaxation of a single DNA molecule observed by optical microscopy. *Science*, 264(5160):822–826, 1994.

[68] Eugene Hecht. *Optics*. Addison-Wesley, 4th edition, 2002.

[69] Iva M. Tolić-Nørrelykke, Leonardo Sacconi, Chiara Stringari, Isabel Raabe, and Francesco S. Pavone. Nuclear and Division-Plane Positioning Revealed by Optical Micromanipulation. *Current Biology*, 15(13):1212–1216, 2005.

[70] Chris Hawes, Anne Osterrieder, Imogen A. Sparkes, and Tijs Ketelaar. Optical tweezers for the micromanipulation of plant cytoplasm and organelles. *Current Opinion in Plant Biology*, 13(6):731–735, 2010.

[71] S. Bayoudh, M. Mehta, H. Rubinsztein-Dunlop, N. R. Heckenberg, and C. Critchley. Micromanipulation of choloroplasts using optical tweezers. *Journal of Microscopy*, 203(June 2000):214–222, 2001.

[72] Martin L. Bennink, Sanford H. Leuba, Gregory H. Leno, et al. Unfolding individual nucleosomes by stretching single chromatin fibers with optical tweezers. *Nature Structural Biology*, 8(7):606–610, 2001.

[73] Yasuharu Arai, Ryohei Yasuda, Ken-ichirou Akashi, et al. Tying a molecular knot with optical tweezers. *Nature*, 399(6735):446–448, 1999.

[74] Furqan M. Fazal, Cong A. Meng, Kenji Murakami, Roger D. Kornberg, and Steven M. Block. Real-time observation of the initiation of RNA polymerase II transcription. *Nature*, 525(7568):274–277, 2015.

[75] George M. Whitesides. The Origins and the Future of Microfluidics. *Nature*, 442(7101):368–373, 2006.

[76] Yongtae Kim and Robert Langer. Microfluidics in Nanomedicine. *Reviews in Cell Biology and Molecular Medicine*, 1(2):127–152, 2015.

[77] Shelley Lynn Anna. Droplets and Bubbles in Microfluidic Devices. *Annual Review of Fluid Mechanics*, 48(1):285–309, 2016.

[78] Adam Bange, H. Brian Halsall, and William R. Heineman. Microfluidic immunosensor systems. *Biosensors and Bioelectronics*, 20(12):2488–2503, 2005.

[79] H. A. Stone, A. D. Stroock, and Armand Ajdari. Engineering Flows in Small Devices. *Annual Review of Fluid Mechanics*, 36(1):381–411, 2004.

[80] Gwo-Bin Lee, Chen-I Hung, Bin-Jo Ke, et al. Hydrodynamic Focusing for a Micromachined Flow Cytometer. *Journal of Fluids Engineering*, 123(3):672, 2001.

[81] Claire Simonnet and Alex Groisman. Two-dimensional hydrodynamic focusing in a simple microfluidic device. *Applied Physics Letters*, 87(11):22–25, 2005.

[82] Stephan K W Dertinger, Daniel T Chiu, Noo Li Jeon, and George M Whitesides. Generation of Gradients Having Complex Shapes Using Microfluidic Networks. *Analytical Chemistry*, 73(6):1240–1246, 2001.

[83] Hsih Yin Tan, Keong Loke, Teng Tan, and Nam-trung Nguyen. A Lab-on-a-Chip for Detection of Nerve Agent Sarin in Blood. *Lab on a Chip*, 8:885–891, 2008.

[84] Barry L Ziober, Michael G Mauk, Erica M Falls, et al. Lab-on-a-chip for oral cancer screening and diagnosis. *Head & Neck*, 30(1):111–121, 2008.

[85] Teruo Fujii. PDMS-Based Microfluidic Devices for Biomedical Applications. *Microelectronic Engineering*, 61-62(2002):904–914, 2000.

[86] Klaus Eyer, Phillip Kuhn, Conni Hanke, and Petra S. Dittrich. A microchamber array for single cell isolation and analysis of intracellular biomolecules. *Lab on a Chip*, 12(4):765–772, 2012.

[87] Matthias Mehling and Savaş Tay. Microfluidic Cell Culture. *Current Opinion in Biotechnology*, 25:95–102, 2014.

[88] A. Jemal, R. Siegel, E. Ward, et al. Cancer Statistics, 2008. *CA: A Cancer Journal for Clinicians*, 58(2):71–96, 2008.

[89] Ahmedin Jemal, Rebecca Siegel, Jiaquan Xu, and Elizabeth Ward. Cancer Statistics, 2010. *CA: A Cancer Journal for Clinicians*, 60(5):277–300, 2010.

[90] David S. Jones, Scott H. Podolsky, and Jeremy A. Greene. The Burden of Disease and the Changing Task of Medicine. *New England Journal of Medicine*, 366(25):2333–2338, 2012.

[91] Rafael Lozano, Mohsen Naghavi, Kyle Foreman, et al. Global and regional mortality from 235 causes of death for 20 age groups in 1990 and 2010: a systematic analysis for the Global Burden of Disease Study 2010. *The Lancet*, 380(9859):2095–2128, 2012.

[92] Aimee L. Jackson and Lawrence A. Loeb. The mutation rate and cancer. *Genetics*, 148(4):1483–1490, 1998.

[93] Franziska Michor, Yoh Iwasa, and Martin A. Nowak. Dynamics of cancer progression. *Nature Reviews Cancer*, 4(3):197–205, 2004.

[94] Lawrence A. Loeb, Keith R. Loeb, and Jon P. Anderson. Multiple mutations and cancer. *Proceedings of the National Academy of Sciences of the United States of America*, 100(3):776–781, 2003.

[95] Gerard I. Evan and Karen H. Vousden. Proliferation, cell cycle and apoptosis in cancer. *Nature*, 411:342–348, 2001.

[96] I. P. Tomlinson, M. R. Novelli, and W. F. Bodmer. The mutation rate and cancer. *Proceedings of the National Academy of Sciences of the United States of America*, 93(25):14800–14803, 1996.

[97] Scott W. Lowe and Athena W. Lin. Apoptosis in cancer. *Carcinogenesis*, 21(3):485–495, 2000.

[98] N. W. Kim, M. A. Piatyszek, K. R. Prowse, et al. Specific association of human telomerase activity with immortal cells and cancer. *Science*, 266(5193):2011–2015, 1994.

[99] C. B. Harley, N. W. Kim, K. R. Prowse, et al. Telomerase, Cell Immortality, and Cancer. *Cold Spring Harbour Symposia on Quantitative Biology*, 59:307–315, 1994.

[100] Russell G. Jones and Craig B. Thompson. Tumor suppressors and cell metabolism : a recipe for cancer growth. *Genes & Development*, 23:537–548, 2009.

[101] Michael B. Sporn and Anita B. Roberts. Autocrine growth factors and cancer. *Nature*, 313(14):745–747, 1985.

[102] Herbert Yu and Thomas Rohan. Role of the insulin-like growth factor family in cancer development and progression. *Journal of the National Cancer Institute*, 92(18):1472–1489, 2000.

[103] Peter Carmeliet and Rakesh K. Jain. Angiogenesis in cancer and other diseases. *Nature*, 407(6801):249–257, 2000.

[104] Judah Folkman. Angiogenesis in cancer, vascular, rheumatoid and other disease. *Nature Medicine*, 1:27–30, 1995.

[105] George Poste and Isaiah J. Fidler. The pathogenesis of cancer metastasis. *Nature*, 283:139–146, 1980.

[106] Garth L. Nicolson. Cancer metastasis: Organ colonization and the cell-surface properties of malignant cells. *Biochimica et Biophysica Acta*, 695(2):113–176, 1982.

[107] Isaiah J. Fidler. The pathogenesis of cancer metastasis: the 'seed and soil' hypothesis revisited. *Nature Reviews Cancer*, 3:1–6, 2003.

[108] Arnold J. Levine, Jamil Momand, and Cathy A. Finlay. The p53 tumour suppressor gene. *Nature*, 351:453–456, 1991.

[109] Alejo Efeyan and Manuel Serrano. p53: Guardian of the genome and policeman of the oncogenes. *Cell Cycle*, 6(9):1006–1010, 2007.

[110] M. Hollstein, K. Rice, M.S. Greenblatt, et al. Database of p53 gene somatic mutations in human tumors and cell lines. *Nucleic Acids Research*, 22(17):3551–3555, 1994.

[111] Lee Hartwell, David Mankoff, Amanda Paulovich, Scott Ramsey, and Elizabeth Swisher. Cancer biomarkers: a systems approach. *Nature Biotechnology*, 24(8):905–908, 2006.

[112] Ruth Etzioni, Nicole Urban, Scott Ramsey, et al. The case for early detection. *Nature Reviews Cancer*, 3(4):243–252, 2003.

[113] Samir M. Hanash, Sharon J. Pitteri, and Vitor M. Faca. Mining the plasma proteome for cancer biomarkers. *Nature*, 452(7187):571–579, 2008.

[114] Jürgen Wittmann and Hans-Martin Jäck. Serum microRNAs as powerful cancer biomarkers. *Biochimica et Biophysica Acta*, 1806(2):200–207, 2010.

[115] Sabarni K. Chatterjee and Bruce R. Zetter. Cancer biomarkers: knowing the present and predicting the future. *Future Oncology*, 1(1):37–50, 2005.

[116] Paul Symonds, Charles Deehan, Catherine Meridith, and John A. Mills. *Walter and Miller's textbook of radiation therapy*. Churchill Livingstone, London, 7th edition, 2012.

[117] Micheal T. Shaw, Monroe H. Spector, and A. J. Ladman. Effects of cancer, radiotherapy and cytotoxic drugs on intestinal structure and function. *Cancer Treatment Reviews*, 6(3):141–148, 1979.

[118] F. Ries and J. Klastersky. Nephrotoxicity Induced by Cancer Chemotherapy With Special Emphasis on Cisplatin Toxicity. *American Journal of Kidney Diseases*, 8(5):368–379, 1986.

[119] Rachel J. Gibson and Dorothy M. K. Keefe. Cancer chemotherapy-induced diarrhoea and constipation: mechanisms of damage and prevention strategies. *Supportive Care in Cancer*, 14(9):890–900, 2006.

[120] Franck G. A. Jansman, Dirk T. Sleifer, Jacques C. de Graaf, Jules L. L. M. Coenen, and Jacobus R. B. J. Brouwers. Management of Chemotherapy-Induced Adverse Effects in the Treatment of Colorectal Cancer. *Drug Safety*, 24(5):353–367, 2001.

[121] Jerome E. Groopman and Loretta M. Itri. Chemotherapy-induced anemia in adults: incidence and treatment. *Journal of the National Cancer Institute*, 91(19):1616–1634, 1999.

[122] Klaus Strebhardt and Axel Ullrich. Paul Ehrlich's magic bullet concept: 100 years of progress. *Nature Reviews Cancer*, 8(6):473–480, 2008.

[123] Ignacio I. Wistuba, Juri G. Gelovani, Jörg J. Jacoby, Suzanne E. Davis, and Roy S. Herbst. Methodological and practical challenges for personalized cancer therapies. *Nature Reviews Clinical Oncology*, 8(3):135–141, 2011.

[124] Quin F. Wills and Adam J. Mead. Application of single-cell genomics in cancer: promise and challenges. *Human Molecular Genetics*, 24(R1):R74–R84, 2015.

[125] P. C. Nowell. The clonal evolution of tumor cell populations. *Science*, 194(4260):23–28, 1976.

[126] Piyush B. Gupta, Christine M. Fillmore, Guozhi Jiang, et al. Stochastic state transitions give rise to phenotypic equilibrium in populations of cancer cells. *Cell*, 146(4):633–644, 2011.

[127] Maria M. Ho, Alvin V. Ng, Stephen Lam, and Jaclyn Y. Hung. Side population in human lung cancer cell lines and tumors is enriched with stem-like cancer cells. *Cancer Research*, 67(10):4827–4833, 2007.

[128] Nicholas C. Turner and Jorge S. Reis-Filho. Genetic heterogeneity and cancer drug resistance. *The Lancet Oncology*, 13(4):e178–e185, 2012.

[129] Jue Shi, James D. Orth, and Tim Mitchison. Cell type variation in responses to antimitotic drugs that target microtubules and kinesin-5. *Cancer Research*, 68(9):3269–3276, 2008.

[130] Ricky W. Johnstone, Astrid A. Ruefli, and Scott W. Lowe. Apoptosis: a link between cancer genetics and chemotherapy. *Cell*, 108(2):153–164, 2002.

[131] Sandra Gottschling, Philipp A. Schnabel, Felix J. F. Herth, and Esther Herpel. Are we Missing the Target ? – Cancer Stem Cells and Drug Resistance in Non-small Cell Lung Cancer. *Cancer Genomics & Proteomics*, 9(5):275–286, 2012.

[132] Michael Dean, Tito Fojo, and Susan Bates. Tumour stem cells and drug resistance. *Nature Reviews Cancer*, 5(4):275–284, 2005.

[133] Michael M. Gottesman. Mechanisms of cancer drug resistance. *Annual Review of Medicine*, 53:615–627, 2002.

[134] S. Jain, D. G. Hirst, and J. M. O'Sullivan. Gold nanoparticles as novel agents for cancer therapy. *British Journal of Radiology*, 85(1010):101–113, 2012.

[135] A. Marabelle, H. Kohrt, C. Caux, and R. Levy. Intratumoral immunization: a new paradigm for cancer therapy. *Clinical Cancer Research*, 20(7):1747–1756, 2014.

[136] Emanual Maverakis, LLynn A. Cornelius, Glen M. Bowen, et al. Metastatic Melanoma – A Review of Current and Future Treatment Options. *Acta Dermato-Venereologica*, 95(5):516–524, 2015.

[137] Laura A. Johnson, Richard A. Morgan, Mark E. Dudley, et al. Gene therapy with human and mouse T-cell receptors mediates cancer regression and targets normal tissues expressing cognate antigen. *Blood*, 114(3):535–546, 2009.

[138] E. M. Toloza, S. Swisher, W. McBride, et al. In vivo cancer gene therapy with a recombinant interleukin-2 adenovirus vector. *Cancer Gene Therapy*, 3(1):11–17, 1996.

[139] G. Sithanandam and L. M. Anderson. The ERBB3 receptor in cancer and cancer gene therapy. *Cancer Gene Therapy*, 15:413–448, 2008.

[140] D. D. Lasic and N. S. Templeton. Liposomes in Gene Therapy. *Advanced Drug Delivery Reviews*, 20(2-3):221–266, 1996.

[141] Andrew D. Miller. Cationic Liposomes for Gene Therapy. *Angewandte Chemie International Edition*, 37(13-14):1768–1785, 1998.

[142] L. L. Nielsen and D. C. Manevl. P53 tumor suppressor gene therapy for cancer. *Cancer Gene Therapy*, 5(1):52–63, 1998.

[143] Wei-Wei Zhang. Development and application of adenoviral vectors for gene therapy of cancer. *Cancer Gene Therapy*, 6(2):113–138, 1999.

[144] Graça Raposo and Willem Stoorvogel. Extracellular vesicles: exosomes, microvesicles, and friends. *The Journal of Cell Biology*, 200(4):373–383, 2013.

[145] Jason Webber, Robert Steadman, Malcolm D. Mason, Zsuzsanna Tabi, and Aled Clayton. Cancer exosomes trigger fibroblast to myofibroblast differentiation. *Cancer Research*, 70(23):9621–9630, 2010.

[146] J. L. Qu, X. J. Qu, M. F. Zhao, et al. Gastric cancer exosomes promote tumour cell proliferation through PI3K/Akt and MAPK/ERK activation. *Digestive and Liver Disease*, 41(12):875–880, 2009.

[147] Sonia A. Melo, Hikaru Sugimoto, Joyce T. O'Connell, et al. Cancer Exosomes Perform Cell-Independent MicroRNA Biogenesis and Promote Tumorigenesis. *Cancer Cell*, 26(5):707–721, 2014.

[148] Samir El Andaloussi, Imre Mäger, Xandra O. Breakefield, and Matthew J. A. Wood. Extracellular vesicles: biology and emerging therapeutic opportunities. *Nature Reviews Drug discovery*, 12(5):347–57, 2013.

[149] Yi Lee, Samir El Andaloussi, and Matthew J. A. Wood. Exosomes and microvesicles: Extracellular vesicles for genetic information transfer and gene therapy. *Human Molecular Genetics*, 21(R1):125–134, 2012.

[150] J. M. Mitchison and M. M. Swann. The Mechanical Properties of the Cell Surface II. The Unfertilized Sea-Urchin Egg. *The Journal of Experimental Biology*, 31:461–472, 1954.

[151] Frits M. Flesch and Barend M. Gadella. Dynamics of the mammalian sperm plasma membrane in the process of fertilization. *Biochimica et Biophysica Acta - Reviews on Biomembranes*, 1469(3):197–235, 2000.

[152] H. Teixeira, M. G. Gonçalves, N. Rozès, A. Ramos, and M. V. San Romão. Lactobacillic acid accumulation in the plasma membrane of Oenococcus oeni: A response to ethanol stress? *Microbial Ecology*, 43(1):146–153, 2002.

[153] Harvey T. McMahon and Jennifer L. Gallop. Membrane curvature and mechanisms of dynamic cell membrane remodelling. *Nature*, 438(7068):590–596, 2005.

[154] Tomasz Ochalek, Frank J. Nordt, Kjell Tullberg, and Max M. Burger. Correlation between cell deformability and metastatic potential in B16-F1 melanoma cell variants. *Cancer Research*, 48(18):5124–5128, 1988.

[155] T. W. Remmerbach, F. Wottawah, J. Dietrich, et al. Oral Cancer Diagnosis by Mechanical Phenotyping. *Cancer Research*, 69(5):1728–1732, 2009.

[156] V. Swaminathan, K. Mythreye, E. T. O'Brien, et al. Mechanical Stiffness Grades Metastatic Potential in Patient Tumor Cells and in Cancer Cell Lines. *Cancer Research*, 71(15):5075–5080, 2011.

[157] L. M. Rebelo, J. S. de Sousa, J. Mendes Filho, and M. Radmacher. Comparison of the viscoelastic properties of cells from different kidney cancer phenotypes measured with atomic force microscopy. *Nanotechnology*, 24(5):055102, 2013.

[158] Tom Bongiorno, Jacob Kazlow, Roman Mezencev, et al. Mechanical stiffness as an improved single-cell indicator of osteoblastic human mesenchymal stem cell differentiation. *Journal of Biomechanics*, 47(9):2197–2204, 2014.

[159] Arlo J. Miller and Martin C. Jr. Mihm. Melanoma. *The New England Journal of Medicine*, 355(1):51–65, 2006.

[160] Robert B. Gennis. *Biomembranes: molecular structure and function*. Springer Science+Business Media, New York, 1st edition, 1989.

[161] Gerrit van Meer, Dennis R. Voelker, and Gerald W. Feigenson. Membrane lipids: where they are and how they behave. *Nature Reviews Molecular Cell Biology*, 9(2):112–124, 2008.

[162] Kai Simons and Mathias J. Gerl. Revitalizing membrane rafts: new tools and insights. *Nature Reviews Molecular Cell Biology*, 11(10):688–699, 2010.

[163] Markus R. Wenk. Lipidomics: New tools and applications. *Cell*, 143(6):888–895, 2010.

[164] Richard G. W. Anderson. The Caveolae Membrane System. *Annual Review of Biochemistry*, 67:199–225, 1998.

[165] Daniel Lingwood and Kai Simons. Lipid rafts as a membrane-organizing principle. *Science*, 327(5961):46–50, 2010.

[166] Patrick J. Casey. Protein lipidation in cell signaling. *Science*, 268(5208):221–225, 1995.

[167] Thomas Harder and Kai Simonst. Caveolae , DIGS , and the dynamics of sphingolipid-cholesterol microdomains. *Current Opinion in Cell Biology*, 9(4):534–542, 1997.

[168] Katja Roper, Denis Corbeil, and Wieland B. Huttner. Retention of prominin in microvilli reveals distinct cholesterol-based lipid micro-domains in the apical plasma membrane. *Nature Cell Biology*, 2(9):582–592, 2000.

[169] Kai Simons and Winchil C. L. Vaz. Model systems, lipid rafts, and cell membranes. *Annual Review of Biophysics and Biomolecular Structure*, 33:269–295, 2004.

[170] Akihiro Kusumi, Chieko Nakada, Ken Ritchie, et al. Paradigm shift of the plasma membrane concept from the two-dimensional continuum fluid to the partitioned fluid: high-speed single-molecule tracking of membrane molecules. *Annual Review of Biophysics and Biomolecular Structure*, 34:351–378, 2005.

[171] Ken Jacobson, Ole G. Mouritsen, and Richard G. W. Anderson. Lipid rafts: at a crossroad between cell biology and physics. *Nature Cell Biology*, 9(1):7–14, 2007.

[172] S. J. Singer and Garth L. Nicolson. The fluid mosaic model of the structure of cell membranes. *Science*, 175(4023):720–731, 1972.

[173] Ken Jacobson, Erin D. Sheets, and Rudolf Simson. Revisiting the fluid mosaic model of membranes. *Science*, 268(5):1441–1442, 1995.

[174] James G. White, Steven M. Burris, David Tukey, Clark Smith, and C. Carlyle Clawson. Micropipette aspiration of human platelets: influence of microtubules and actin filaments on deformability. *Blood*, 64(1):210–214, 1984.

[175] Thomas Lecuit and Pierre-François Lenne. Cell surface mechanics and the control of cell shape, tissue patterns and morphogenesis. *Nature Reviews Molecular Cell Biology*, 8(8):633–644, 2007.

[176] Peter N. Brawn. The dedifferentiation of metastatic prostate carcinoma. *Cancer*, 52(2):246–251, 1983.

[177] Amin Rustom, Rainer Saffrich, Ivanka Markovic, Paul Walther, and Hans-Hermann Gerdes. Nanotubular highways for intercellular organelle transport. *Science*, 303(5660):1007–1010, 2004.

[178] Hans-Hermann Gerdes, Nickolay V. Bukoreshtliev, and João F. V. Barroso. Tunneling nanotubes: A new route for the exchange of components between animal cells. *FEBS Letters*, 581(11):2194–2201, 2007.

[179] Bruno Pontes, Nathan B. Viana, Loraine Campanati, et al. Structure and elastic properties of tunneling nanotubes. *European Biophysics Journal*, 37(2):121–129, 2008.

[180] Daniel M. Davis and Stefanie Sowinski. Membrane nanotubes: dynamic long-distance connections between animal cells. *Nature Reviews Molecular Cell Biology*, 9(6):431–436, 2008.

[181] Nathan M. Sherer and Walther Mothes. Cytonemes and tunneling nanotubules in cell-cell communication and viral pathogenesis. *Trends in Cell Biology*, 18(9):414–420, 2008.

[182] Pieta K. Mattila and Pekka Lappalainen. Filopodia: molecular architecture and cellular functions. *Nature Reviews Molecular Cell Biology*, 9(6):446–454, 2008.

[183] Anne Chauveau, Anne Aucher, Philipp Eissmann, Eric Vivier, and Daniel M. Davis. Membrane nanotubes facilitate long-distance interactions between natural killer cells and target cells. *Proceedings of the National Academy of Sciences of the United States of America*, 107(12):5545–5550, 2010.

[184] Rob Philips, Jane Kondev, Julie Theriot, and Herman G. Garcia. *Physical Biology of the Cell*. Garland Science, New York, 2nd edition, 2013.

[185] Viola Vogel and Michael Sheetz. Local force and geometry sensing regulate cell functions. *Nature Reviews Molecular Cell Biology*, 7(4):265–275, 2006.

[186] Evan A. Evans and R. Skalak. *Mechanics and Thermodynamics of Biomembranes*. CRC Press, Boca Raaton, FL, 1980.

[187] Derek Marsh. Elastic curvature constants of lipid monolayers and bilayers. *Chemistry and Physics of Lipids*, 144(2):146–159, 2006.

[188] Rumiana Dimova. Recent developments in the field of bending rigidity measurements on membranes. *Advances in Colloid and Interface Science*, 208:225–234, 2014.

[189] W. Rawicz, K. C. Olbrich, T. McIntosh, D. Needham, and E. Evans. Effect of chain length and unsaturation on elasticity of lipid bilayers. *Biophysical Journal*, 79(1):328–339, 2000.

[190] Basarab G. Hosu, Mingzhai Sun, Françoise Marga, Michel Grandbois, and Gabor Forgacs. Eukaryotic membrane tethers revisited using magnetic tweezers. *Physical Biology*, 4(2):67–78, 2007.

[191] Pedro Pascoal, Davor Kosanic, Marinela Gjoni, and Horst Vogel. Membrane nanotubes drawn by optical tweezers transmit electrical signals between mammalian cells over long distances. *Lab on a Chip*, 10(17):2235–2241, 2010.

[192] Jianwu Dai and Michael P. Sheetz. Mechanical properties of neuronal growth cone membranes studied by tether formation with laser optical tweezers. *Biophysical Journal*, 68(3):988–996, 1995.

[193] Robert M. Hochmuth, Jin-Yu Shao, Jianwu Dai, and Michael P. Sheetz. Deformation and flow of membrane into tethers extracted from neuronal growth cones. *Biophysical Journal*, 70(1):358–369, 1996.

[194] Michael Werner, Raghavendra Palankar, Loïc Arm, Ruud Hovius, and Horst Vogel. Microfluidic Single-Cell Analysis with Affinity Beads. *Small*, 11(22):2607–2613, 2015.

[195] J. Cooper McDonald, David C. Duffy, Janelle R Anderson, et al. Fabrication of microfluidic systems in poly(dimethylsiloxane). *Electrophoresis*, 21(1):27–40, 2000.

[196] Mei-Yu Hsu, Daw-Tsun Shih, Friedegund E. Meier, et al. Adenoviral Gene Transfer of β3 Integrin Subunit Induces Conversion from Radial to Vertical Growth Phase in Primary Human Melanoma. *The American Journal of Pathology*, 153(5):1435–1442, 1998.

[197] DuPont Guerry IV, Marie Synnestvedt, David E. Elder, and Delray Schultz. Lessons from tumor progression: the invasive radial growth phase of melanoma is common, incapable of metastasis, and indolent. *The Journal of Investigative Dermatology*, 100(3):342S–345S, 1993.

[198] Bengt Westermark, Ann Johnsson, Ylva Paulsson, et al. Human melanoma cell lines of primary and metastatic origin express the genes encoding the chains of platelet-derived growth factor (PDGF) and produce a PDGF-like growth factor. *Proceedings of the National Academy of Sciences of the United States of America*, 83(19):7197–7200, 1986.

[199] Takashi Chishima, Yohei Miyagi, Xiaoen Wang, et al. Cancer Invasion and Micrometastasis Visualized in Live Tissue by Green Fluorescent Protein Expression. *Cancer Research*, 57:2042–2047, 1997.

[200] Ian R. Hart and Asha Saini. Biology of tumour metastasis. *The Lancet*, 339(8807):1453–1457, 1992.

[201] Horst Pick, Evelyne L. Schmid, Ana-Paula Tairi, et al. Investigating cellular signaling reactions in single attoliter vesicles. *Journal of the American Chemical Society*, 127(9):2908–2912, 2005.

[202] Luigino Grasso. *Transmembrane Signaling Analysis in Model Membrane Systems*. PhD thesis, EPFL, 2012.

[203] Ronald A. Fisher. *Statistical Methods for Research Workers*. Oliver and Boyd, Edinburgh, 1st edition, 1925.

[204] John W. Tukey. Comparing Individual Means in the Analysis of Variance. *Biometrics*, 5(2):99–114, 1949.

[205] Gilles Weder, Mariëlle C. Hendriks-Balk, Rita Smajda, et al. Increased plasticity of the stiffness of melanoma cells correlates with their acquisition of metastatic properties. *Nanomedicine: Nanotechnology, Biology and Medicine*, 10(1):141–148, 2014.

[206] A. R. Bausch and K. Kroy. A bottom-up approach to cell mechanics. *Nature Physics*, 2(4):231–238, 2006.

[207] Erich Sackmann and Rudolf Merkel. *Lehrbuch der Biophysik*. Wiley, Weinheim, 2010.

[208] Evan A. Evans and Anthony Kwok-Cheung Yeung. Hidden dynamics in rapid changes of bilayer shape. *Chemistry and Physics of Lipids*, 73(1-2):39–56, 1994.

[209] Anthony Kwok-Cheung Yeung. *Mechanics of inter-monolayer coupling in fluid surfactant bilayers*. PhD thesis, University of British Columbia, 1994.

[210] Robert M. Hochmuth, P. R. Worthy, and Evan A. Evans. Red cell extensional recovery and determination of membrane viscosity. *Biophysical Journal*, 26(1):101–114, 1979.

[211] Evan A. Evans. Structure and Deformation Properties of red Blood Cells: Concepts and Quantitative Methods. *Methods in Enzymology*, 173:3–35, 1989.

[212] Sylvie Hénon, Guillaume Lenormand, Aalain Richert, and François Gallet. A new determination of the shear modulus of the human erythrocyte membrane using optical tweezers. *Biophysical Journal*, 76(2):1145–51, 1999.

[213] Xiao Liu, Zhi-yu Tang, Zhu Zeng, et al. The measurement of shear modulus and membrane surface viscosity of RBC membrane with Ektacytometry: A new technique. *Mathematical Biosciences*, 209(1):190–204, 2007.

[214] Tatsuro Watanabe, Hiromi Kuramochi, Atsushi Takahashi, et al. Higher cell stiffness indicating lower metastatic potential in B16 melanoma cell variants and in (2)-epigallocatechin gallate-treated cells. *Journal of Cancer Research and Clinical Oncology*, 138(5):859–866, 2012.

[215] Sanjay Kumar and Valerie M. Weaver. Mechanics, malignancy, and metastasis: The force journey of a tumor cell. *Cancer and Metastasis Reviews*, 28(1):113–127, 2009.

[216] Gang Cheng, Janet Tse, Rakesh K. Jain, and Lance L. Munn. Micro-Environmental Mechanical Stress Controls Tumor Spheroid Size and Morphology by Suppressing Proliferation and Inducing Apoptosis in Cancer Cells. *PLoS ONE*, 4(2):e4632, 2009.

[217] Ismail Emre Araci and Stephen R. Quake. Microfluidic very large scale integration (mVLSI) with integrated micromechanical valves. *Lab on a Chip*, 12(16):2803–2806, 2012.

[218] Anthony K. Au, Wilson Huynh, Lisa F. Horowitz, and Albert Folch. 3D-Printed Microfluidics. *Angewandte Chemie International Edition*, 55:2–22, 2016.

[219] Joshua S. Marcus, W. French Anderson, and Stephen R. Quake. Microfluidic single-cell mRNA isolation and analysis. *Analytical Chemistry*, 78(9):3084–3089, 2006.

[220] Mehmet Toner and Daniel Irimia. Blood-on-a-chip. *Annual Review of Biomedical Engineering*, 7(1):77–103, 2005.

[221] Christopher E. Sims and Nancy L. Allbritton. Analysis of single mammalian cells on-chip. *Lab on a Chip*, 7(4):423–440, 2007.

[222] Tzu-Chiao Chao and Alexandra Ros. Microfluidic single-cell analysis of intracellular compounds. *Journal of the Royal Society Interface*, 5(Suppl 2):S139–S150, 2008.

[223] Bruce S. Edwards, Tudor Oprea, Eric R. Prossnitz, and Larry A. Sklar. Flow cytometry for high-throughput, high-content screening. *Current Opinion in Chemical Biology*, 8(4):392–398, 2004.

[224] Stephen P. Perfetto, Pratip K. Chattopadhyay, and Mario Roederer. Seventeen-colour flow cytometry: unravelling the immune system. *Nature Reviews Immunology*, 4(8):648–655, 2004.

[225] I. Vermes, C. Haanen, and C. Reutelingsperger. Flow cytometry of apoptotic cell death. *Journal of Immunological Methods*, 243(1-2):167–190, 2000.

[226] Daniella Cohen, Jane A. Dickerson, Colin D. Whitmore, et al. Chemical cytometry: fluorescence-based single-cell analysis. *Annual Review of Analytical Chemistry*, 1:165–190, 2008.

[227] Norman J. Dovichi and Shen Hu. Chemical cytometry. *Current Opinion in Chemical Biology*, 7(5):603–608, 2003.

[228] Theodore T. Puck, Philip I. Marcus, and Steven J. Cieciura. Clonal growth of mammalian cells in vitro; growth characteristics of colonies from single HeLa cells with and without a feeder layer. *The Journal of Experimental Medicine*, 103(2):273–283, 1956.

[229] Harvey Lodish, Arnold Berk, Chris A. Kaiser, and Monty Krieger. *Molecular Cell Biology*. W. H. Freeman, 6th edition, 2006.

[230] Elias Metchnikoff. Über die intracelluläre Verdauung bei Coelenteraten. *Zoologischer Anzeiger*, 3:261–263, 1880.

[231] Elias Metchnikoff. Über eine Sprosspilzkrankheit der Daphnien. Beitrag zur Lehre über den Kampf der Phagocyten gegen Krankheitserreger. *Archiv für pathologische Anatomie und Physiologie und für klinische Medicin*, 96(2):177–195, 1884.

[232] Stephanie E. A. Gratton, Patricia A. Ropp, Patrick D. Pohlhaus, et al. The effect of particle design on cellular internalization pathways. *Proceedings of the National Academy of Sciences of the United States of America*, 105(33):11613–11618, 2008.

[233] Julie A. Champion, Amanda Walker, and Samir Mitragotri. Role of particle size in phagocytosis of polymeric microspheres. *Pharmaceutical Research*, 25(8):1815–1821, 2008.

[234] Torunn Elisabeth Tjelle, Torunn Løvdal, and Trond Berg. Phagosome dynamics and function. *BioEssays*, 22(3):255–263, 2000.

[235] Kristian Berg, Pål Kristian Selbo, Lina Prasmickaite, et al. Photochemical internalization: A novel technology for delivery of macromolecules into cytosol. *Cancer Research*, 59(6):1180–1183, 1999.

[236] Pål Kristian Selbo, Anette Weyergang, Anders Høgset, et al. Photochemical internalization provides time- and space-controlled endolysosomal escape of therapeutic molecules. *Journal of Controlled Release*, 148(1):2–12, 2010.

[237] Christophe Laloi and Michel Havaux. Key players of singlet oxygen-induced cell death in plants. *Frontiers in Plant Science*, 6:39, 2015.

[238] Gary J. Kelloff and Caroline C. Sigman. Cancer biomarkers: selecting the right drug for the right patient. *Nature Reviews Drug Discovery*, 11(3):201–214, 2012.

[239] I. H. Malitson. Interspecimen Comparison of the Refractive Index of Fused Silica. *Journal of the Optical Society of America*, 55(10):1205–1209, 1965.

[240] YongKeun Park, Monica Diez-Silva, Gabriel Popescu, et al. Refractive index maps and membrane dynamics of human red blood cells parasitized by Plasmodium falciparum. *Proceedings of the National Academy of Sciences of the United States of America*, 105(37):13730–13735, 2008.

[241] L. Diéguez, N. Darwish, M. Mir, et al. Effect of the Refractive Index of Buffer Solutions in Evanescent Optical Biosensors. *Sensor Letters*, 7:851–855, 2009.

[242] Lester Kobzik. Lung macrophage uptake of unopsonized environmental particulates. Role of scavenger-type receptors. *Journal of immunology*, 155(1):367–376, 1995.

[243] Brendan P. Cormack, Rahpael H. Valdivia, and Stanley Falkow. FACS-optimized mutants of the green fluorescent protein (GFP). *Gene*, 173:33–38, 1996.

[244] Nathan C. Shaner, Robert E. Campbell, Paul A. Steinbach, et al. Improved monomeric red, orange and yellow fluorescent proteins derived from Discosoma sp. red fluorescent protein. *Nature Biotechnology*, 22(12):1567–1572, 2004.

[245] E. Hochuli, W. Bannwarth, H. Döbeli, R. Gentz, and D. Stüber. Genetic Approach to Facilitate Purification of Recombinant Proteins with a Novel Metal Chelate Adsorbent. *Nature Biotechnology*, 6(11):1321–1325, 1988.

[246] Norman C. Li, Li Chu Ting, Charles T. Fujii, and James M. White. Association of Imidazole with Nickel(II) and Alkaline Earth Ions. *Journal of the American Chemical Society*, 77(4):859–861, 1955.

[247] G. Schwarzenbach. Der Chelateffekt. *Helvetica Chimica Acta*, 35(7):2344–2359, 1952.

[248] Jacky Schmitt, Heike Hess, and Hendrick G. Stunnenberg. Affinity Purification of Histidine-Tagged Proteins. *Molecular Biology Reports*, 18(3):223–230, 1993.

[249] Jeffrey R. Whiteaker, Lei Zhao, Heidi Y. Zhang, et al. Antibody-based enrichment of peptides on magnetic beads for mass-spectrometry-based quantification of serum biomarkers. *Analytical Biochemistry*, 362(1):44–54, 2007.

[250] Dmitry R. Bandura, Vladimir I. Baranov, Olga I. Ornatsky, et al. Mass cytometry: Technique for real time single cell multitarget immunoassay based on inductively coupled plasma time-of-flight mass spectrometry. *Analytical Chemistry*, 81(16):6813–6822, 2009.

[251] Serena Di Palma and Bernd Bodenmiller. Unraveling cell populations in tumors by single-cell mass cytometry. *Current Opinion in Biotechnology*, 31:122–129, 2015.

[252] Javier Atencia and David J. Beebe. Controlled microfluidic interfaces. *Nature*, 437(7059):648–655, 2005.

[253] Keith J. Morton, Kevin Loutherback, David W. Inglis, et al. Crossing microfluidic streamlines to lyse, label and wash cells. *Lab on a Chip*, 8(9):1448–1453, 2008.

[254] Mark M. Wang, Eugene Tu, Daniel E. Raymond, et al. Microfluidic sorting of mammalian cells by optical force switching. *Nature Biotechnology*, 23(1):83–87, 2005.

[255] Ivan R. Perch-Nielsen, Peter John Rodrigo, Carlo Amadeo Alonzo, and Jesper Glückstad. Autonomous and 3D real-time multi-beam manipulation in a microfluidic environment. *Optics Express*, 14(25):12199–12205, 2006.

[256] Mingyan He, J. Scott Edgar, Gavin D. M. Jeffries, et al. Selective encapsulation of single cells and subcellular organelles into picoliter- and femtoliter-volume droplets. *Analytical Chemistry*, 77(6):1539–1544, 2005.

[257] Futian Han, Yan Wang, Christopher E. Sims, et al. Fast electrical lysis of cells for capillary electrophoresis. *Analytical Chemistry*, 75(15):3688–3696, 2003.

[258] Theodore S. Lawrence, William H. Beers, and Norton B. Gilula. Transmission of hormonal stimulation by cell-to-cell communication. *Nature*, 272(5653):501–506, 1978.

[259] Jean-Claude Hervé and Mickaël Derangeon. Gap-junction-mediated cell-to-cell communication. *Cell and Tissue Research*, 352(1):21–31, 2013.

[260] Iraj Laffafian and Maurice B. Hallett. Lipid-protein cargo transfer: A mode of direct cell-to-cell communication for lipids and their associated proteins. *Journal of Cellular Physiology*, 210(2):336–342, 2007.

[261] T. M. Jessell and E. R. Kandel. Synaptic transmission: a bidirectional and self-modifiable form of cell-cell communication. *Cell*, 72 Suppl:1–30, 1993.

[262] Zdena Palková, Blanka Janderová, Jiri Gabriel, et al. Ammonia mediates communication between yeast colonies. *Nature*, 390(6659):532–536, 1997.

[263] Aldebaran M. Hofer, Silvana Curci, Marc A. Doble, Edward M. Brown, and David I. Soybel. Intercellular communication mediated by the extracellular calcium-sensing receptor. *Nature Cell Biology*, 2(7):392–398, 2000.

[264] Peter B. Guthrie, Joshua Knappenberger, Menahem Segal, et al. ATP released from astrocytes mediates glial calcium waves. *The Journal of Neuroscience*, 19(2):520–528, 1999.

[265] Julian M. Davidson and Seymour Levine. Endocrine Regulation of Behavior. *Annual Review of Physiology*, 34:375–408, 1972.

[266] Kaitlyn E. Ryan and Chin Chiang. Hedgehog secretion and signal transduction in vertebrates. *The Journal of Biological Chemistry*, 287(22):17905–17913, 2012.

[267] Dana Gancz and Lilach Gilboa. Hormonal control of stem cell systems. *Annual Review of Cell and Developmental Biology*, 29:137–62, 2013.

[268] Don S. Schlach and Seymour Reichlin. Plasma Growth Hormone Concentration in the Rat Determined by Radioimmunoassay: Influence of Sex, Pregnancy, Lactation, Anesthesia, Hypophysectomy and Extrasellar Pituitary Transplants. *Endocrinology*, 79(2):275–280, 1966.

[269] K. Albertsson-Wikland, S. Rosberg, J. Karlberg, and T. Groth. Analysis of 24-hour growth hormone profiles in healthy boys and girls of normal stature: relation to puberty. *The Journal of Clinical Endocrinology & Metabolism*, 78(5):1195–1201, 1994.

[270] Hadi Valadi, Karin Ekström, Apostolos Bossios, et al. Exosome-mediated transfer of mRNAs and microRNAs is a novel mechanism of genetic exchange between cells. *Nature Cell Biology*, 9(6):654–659, 2007.

[271] Vandhana Muralidharan-Chari, James W. Clancy, Alanna Sedgwick, and Crislyn D'Souza-Schorey. Microvesicles: mediators of extracellular communication during cancer progression. *Journal of Cell Science*, 123(10):1603–1611, 2010.

[272] Graça Raposo, Hans W. Nijman, Willem Stoorvogel, et al. B Lymphocytes Secrete Antigen-presenting Vesicles. *The Journal of Experimental Medicine*, 183(3):1161–1172, 1996.

[273] Mihail Hristov, Wolfgang Erl, Stefan Linder, and Peter C. Weber. Apoptotic bodies from endothelial cells enhance the number and initiate the differentiation of human endothelial progenitor cells in vitro. *Blood*, 104(9):2761–2766, 2004.

[274] Jean Michel Escola, Monique J. Kleijmeer, Willem Stoorvogel, et al. Selective enrichment of tetraspan proteins on the internal vesicles of multivesicular endosomes and on exosomes secreted by human B-lymphocytes. *Journal of Biological Chemistry*, 273(32):20121–20127, 1998.

[275] Wiebke Möbius, Yoshiko Ohno-Iwashita, Elly G. van Donselaar, et al. Immunoelectron microscopic localization of cholesterol using biotinylated and non-cytolytic perfringolysin O. *The Journal of Histochemistry and Cytochemistry*, 50(1):43–55, 2002.

[276] Kristin Denzer, Marco van Eijk, Monique J. Kleijmeer, et al. Follicular dendritic cells carry MHC class II-expressing microvesicles at their surface. *The Journal of Immunology*, 165(3):1259–1265, 2000.

[277] Julia Mallegol, Guillaume Van Niel, Corinne Lebreton, et al. T84-intestinal epithelial exosomes bear MHC class II/peptide complexes potentiating antigen presentation by dendritic cells. *Gastroenterology*, 132(5):1866–1876, 2007.

[278] Angela Montecalvo, Adriana T. Larregina, William J. Shufesky, et al. Mechanism of transfer of functional microRNAs between mouse dendritic cells via exosomes. *Blood*, 119(3):756–766, 2012.

[279] J. Ratajczak, K. Miekus, M. Kucia, et al. Embryonic stem cell-derived microvesicles reprogram hematopoietic progenitors: evidence for horizontal transfer of mRNA and protein delivery. *Leukemia*, 20(5):847–856, 2006.

[280] S. Gatti, S. Bruno, M. C. Deregibus, et al. Microvesicles derived from human adult mesenchymal stem cells protect against ischaemia-reperfusion-induced acute and chronic kidney injury. *Nephrology Dialysis Transplantation*, 26(5):1474–1483, 2011.

[281] Ian Del Conde, Corie N. Shrimpton, Perumal Thiagarajan, and José A. López. Tissue-factor-bearing microvesicles arise from lipid rafts and fuse with activated platelets to initiate coagulation. *Blood*, 106(5):1604–1611, 2005.

[282] Janusz Rak and Abhijit Guha. Extracellular vesicles - vehicles that spread cancer genes. *Bioessays*, 34(6):489–497, 2012.

[283] Khalid Al-Nedawi, Brian Meehan, Johann Micallef, et al. Intercellular transfer of the oncogenic receptor EGFRvIII by microvesicles derived from tumour cells. *Nature Cell Biology*, 10(5):619–624, 2008.

[284] Johan Skog, Tom Würdinger, Sjoerd van Rijn, et al. Glioblastoma microvesicles transport RNA and proteins that promote tumour growth and provide diagnostic biomarkers. *Nature Cell Biology*, 10(12):1470–1476, 2008.

[285] Giovanni Camussi, Maria Chiara Deregibus, Stefania Bruno, Cristina Grange, and Valentina Fonsato. Exosomes/microvesicle-mediated epigenetic reprogramming of cells. *Cancer Research*, 1(1):98–110, 2011.

[286] Khalid Al-Nedawi, Brian Meehan, Robert S. Kerbel, Anthony C. Allison, and Janusz Rak. Endothelial expression of autocrine VEGF upon the uptake of tumor-derived microvesicles containing oncogenic EGFR. *Proceedings of the National Academy of Sciences of the United States of America*, 106(10):3794–3799, 2009.

[287] Guillaume Van Niel, Graça Raposo, Céline Candalh, et al. Intestinal epithelial cells secrete exosome–like vesicles. *Gastroenterology*, 121(2):337–349, 2001.

[288] Romain Wyss, Luigino Grasso, Camille Wolf, et al. Molecular and Dimensional Profiling of Highly Purified Extracellular Vesicles by Fluorescence Fluctuation Spectroscopy. *Analytical Chemistry*, 86:7229–7233, 2014.

[289] C. Anthony Hunt. Liposomes disposition in vivo V. Liposome stability in plasma and implications for drug carrier function. *Biochimica et Biophysica Acta*, 719(3):450–463, 1982.

[290] Marcel B. Bally, Rajiv Nayar, Dana Masin, et al. Liposomes with entrapped doxorubicin exhibit extended blood residence times. *Biochimica et Biophysica Acta*, 1023(1):133–139, 1990.

[291] Gregory Gregoriadis and Christine Davis. Stability of liposomes invivo and invitro is promoted by their cholesterol content and the presence of blood cells. *Biochemical and Biophysical Research Communications*, 89(4):1287–1293, 1979.

[292] T. M. Allen, C. Hansen, F. Martin, C. Redemann, and A. Yau-Young. Liposomes containing synthetic lipid derivatives of poly(ethylene glycol) show prolonged circulation half-lives in vivo. *Biochemica & Biophysica Acta - Biomembranes*, 1066(1):29–36, 1991.

[293] Hiroshi Yoshioka. Surface modification of haemoglobin-containing liposomes with polyethylene glycol prevents liposome aggregation in blood plasma. *Biomaterials*, 12(9):861–864, 1991.

[294] Guangya Xiang, Jun Wu, Yanhui Lu, Zhilan Liu, and Robert J. Lee. Synthesis and evaluation of a novel ligand for folate-mediated targeting liposomes. *International Journal of Pharmaceutics*, 356(1-2):29–36, 2008.

[295] T. D. Heath, R. T. Fraley, and D. Papahdjopoulos. Antibody targeting of liposomes: cell specificity obtained by conjugation of F(ab')2 to vesicle surface. *Science*, 210(4469):539–541, 1980.

[296] Chuan Hu, Mahiuddin Ahmed, Thomas J. Melia, et al. Fusion of Cells by Flipped SNAREs. *Science*, 300(5626):1745–1749, 2003.

[297] J. B. Bock and Richard H. Scheller. SNARE proteins mediate lipid bilayer fusion. *Proceedings of the National Academy of Sciences of the United States of America*, 96(22):12227–12229, 1999.

[298] Yu A. Chen and Richard H. Scheller. Snare-Mediated Membrane Fusion. *Nature Reviews Molecular Cell Biology*, 2(2):98–106, 2001.

[299] N. Zhu, Denny Liggitt, and Robert Debs. Systemic Gene Expression after Intravenous DNA Delivery into Adult Mice. *Science*, 261(5118):209–211, 1993.

[300] Ramila Philip, Denny Liggitt, Mohan Philip, Paul Dazin, and Robert Debs. In vivo gene delivery: Efficient transfection of T lymphocytes in adult mice. *Journal of Biological Chemistry*, 268(22):16087–16090, 1993.

[301] S. Chesnoy and L. Huang. Structure and Function of Lipid-DNA Complexes for Gene Delivery. *Annual Review of Biophysics and Biomolecular Structure*, 29:27–47, 2000.

[302] D. Liu, T. Ren, and X. Gao. Cationic Transfection Lipids. *Current Medicinal Chemistry*, 10(14):1307–1315, 2003.

[303] Pieter Vader, Xandra O. Breakefield, and Matthew J. A. Wood. Extracellular vesicles: emerging targets for cancer therapy. *Trends in Molecular Medicine*, 20(7):385–393, 2014.

[304] Miglena I. Angelova and Dimiter S. Dimitrov. Liposome Electroformation. *Faraday Discussion of the Chemical Society*, 81:303–311, 1986.

[305] L.-Ruth Montes, Alicia Alonso, Felix M. Goñi, and Luis A. Bagatolli. Giant unilamellar vesicles electroformed from native membranes and organic lipid mixtures under physiological conditions. *Biophysical Journal*, 93(10):3548–3554, 2007.

[306] Loïc Arm. *Photoactivatable Chelating Peptide to Cluster Membrane Receptors on Artificial Cells*. Master thesis, EPFL, 2011.

[307] Carmen Alvarez-Lorenzo, Lev Bromberg, and Angel Concheiro. Light-sensitive Intelligent Drug Delivery Systems. *Photochemistry and Photobiology*, 85(4):848–860, 2009.

[308] Martti Louhivuori, H. Jelger Risselada, Erik van der Giessen, and Siewert J. Marrink. Release of content through mechano-sensitive gates in pressurized liposomes. *Proceedings of the National Academy of Sciences of the United States of America*, 107(46):19856–19860, 2010.

[309] Guohui Wu, Alexander Mikhailovsky, Htet A. Khant, et al. Remotely Triggered Liposome Release by Near-Infrared Light Absorption via Hollow Gold Nanoshells. *Journal of the American Chemical Society*, 130(26):8175–8177, 2008.

[310] Shao-Ling Huang and Robert C. MacDonald. Acoustically active liposomes for drug encapsulation and ultrasound-triggered release. *Biochimica et Biophysica Acta - Biomembranes*, 1665(1-2):134–141, 2004.

[311] Pierre-Yves Bolinger. *Integrated nanoreactor system: triggering (bio-)chemical reactions in single vesicles*. PhD thesis, EPFL, 2006.

[312] M. B. Yatvin, W. Kreutz, B. A. Horwitz, and M. Shinitzky. pH-sensitive liposomes: possible clinical implications. *Science*, 210(4475):1253–1255, 1980.

[313] Justin R. Griffiths. Are cancer cells acidic? *British Journal of Cancer*, 64(3):425–427, 1991.

[314] Oleg V. Gerasimov, Jeremy A. Boomer, Marquita M. Qualls, and David H. Thompson. Cytosolic drug delivery using pH- and light-sensitive liposomes. *Advanced Drug Delivery Reviews*, 38(3):317–338, 1999.

[315] Amichai Yavlovich, Alok Singh, Sergey Tarasov, et al. Design of Liposomes Containing Photopolymerizable Phospholipids for Triggered Release of Contents. *Journal of Thermal Analysis and Calorimetry*, 98(1):97–104, 2009.

[316] Amichai Yavlovich, Alok Singh, Robert Blumenthal, and Anu Puri. A Novel class of Phototriggerable liposomes containing DPPC:DC 8,9 PC as Vehicle for delivery of Doxorubicin to Cells. *Biochimica et Biophysica Acta*, 1808(1):117–126, 2011.

[317] Senji Sakanaka, Mujo Kim, Makoto Taniguchi, and Takehiko Yamamoto. Antibacterial Substances in Japanese Green Tea Extract against Streptococcus mutans , a Cariogenic Bacterium. *Agricultural and Biological Chemistry*, 53(9):2307–2311, 1989.

[318] Yukihiro Tamba, Shinya Ohba, Masayo Kubota, et al. Single GUV method reveals interaction of tea catechin (-)-epigallocatechin gallate with lipid membranes. *Biophysical Journal*, 92(May):3178–3194, 2007.

[319] Marianne Lilletvedt, H. H. Tønnesen, A. Høgset, L. Nardo, and S. Kristensen. Physicochemical characterization of the photosensitizers TPCS2a and TPPS2a 1. Spectroscopic evaluation of drug - Solvent interactions. *Pharmazie*, 65(8):588–595, 2010.

[320] Marshal Mandelkern, John G. Elias, Don Eden, and Donald M. Crothers. The dimensions of DNA in solution. *Journal of Molecular Biology*, 152(1):153–161, 1981.

[321] Kim S. Horger, Daniel J. Estes, Ricardo Capone, and Michael Mayer. Films of Agarose Enable Rapid Formation of Giant Liposomes in Solutions of Physiologic Ionic Strength. *Journal of the American Chemical Society*, 131(5):1810–1819, 2009.

[322] Margaret N. Holme, Illya A. Fedotenko, Daniel Abegg, et al. Shear-stress sensitive lenticular vesicles for targeted drug delivery. *Nature Nanotechnology*, 7(8):536–543, 2012.

[323] Yung Chieh Tan, Kanaka Hettiarachchi, Maria Siu, Yen Ru Pan, and Abraham Phillip Lee. Controlled microfluidic encapsulation of cells, proteins, and microbeads in lipid vesicles. *Journal of the American Chemical Society*, 128(17):5656–5658, 2006.

[324] Jeanne C. Stachowiak, David L. Richmond, Thomas H. Li, et al. Unilamellar vesicle formation and encapsulation by microfluidic jetting. *Proceedings of the National Academy of Sciences of the United States of America*, 105(12):4697–702, 2008.

Acknowledgements - Remerciements

Ces cinq dernières années ont été très riches en émotions, avec des hauts et des bas de très grande amplitude. Passer au travers d'une telle expérience seul, c'est certainement quelque chose d'impossible pour le commun des mortels. Aussi voudrais-je prendre le temps de quelques lignes pour remercier toutes les personnes qui m'ont aidé, soutenu, supporté ou qui ont contribué au fait que je ne laisse pas tout tomber pour ouvrir une fromagerie dans la région d'Im Fang, pas loin du col du Jaun.

Le LCPPM et autour

Je commencerai tout d'abord par saluer les membres du LCPPM, l'équipe que j'ai eu le plaisir d'intégrer le lundi 2 mai 2011. Le Professeur **Horst Vogel**, directeur du laboratoire, m'a ouvert les portes de son sanctuaire de la recherche qui allait devenir ma seconde maison pour les années à venir. Grâce à lui, j'ai pu explorer des sujets extrêmement intéressants et utiliser des méthodes d'analyses variées particuliprement excitantes, le tout sans avoir à me préoccuper de devoir mobiliser des fonds pour y parvenir. Son soutien à travers cette période m'a été très précieux et je le remercie du fond du coeur de m'avoir supporté pendant des longues années, de m'avoir soutenu dans les moments difficiles et d'avoir fait du mieux qu'il a pu pour que j'en arrive ici aujourd'hui. Mention spéciale pour les soirées de Noël particulièrement mémorables!!

J'adresse également de profonds remerciements à **Michael Werner** et **Luigino Grasso**, qui ont été pour moi de véritables mentors. Michael Werner m'a guidé durant mes premiers contacts avec certains instruments qu'il avait lui-même construits et qui deviendront rapidement capitaux pour les projets sur lesquels j'ai travaillé. Luigino Grasso m'a montré la passion de la science et a toujours su se placer dans le rôle de la personne qui amenait la motivation lorsqu'elle manquait, tant au labo qu'en soirées.

Je remercie également chaleureusement mes collègues de bureau, avec qui j'ai cohabité durant les dernières années au 3ème étage du CH B:

Ruud Hovius, le plus ancien du bureau et mon mentor de l'école doctorale. Merci pour avoir partagé tes connaissances avec moi et de m'avoir débloqué de nombreuses situations compliquées, notamment vis-à-vis du projet du chapitre 3. Merci d'avoir été un super camarade et un référant de talent.

Luc Veya, qui a vécu avec moi cinq années et demie l'expérience de la thèse doctorale. Merci d'avoir été un fantastique collègue et un très bon ami, avec qui partagé une bière ou faire un tour à la salle de sport est toujours une option. Tes coneseils sont toujours très précieux, ce fut un honneur de clore avec toi la grande liste des docteurs du LCPPM.

Wolfgang Grosse, dit Dr. Gang, l'ado métalleux du bureau, pour avoir su garder une ambiance bon enfant permanente dans le bureau. Une bière par-ci, un schnapps par-là et c'est la bonne humeur qui prend vite le dessus sur le travail. Merci de m'avoir convaincu de continuer au moment où j'étais au plus bas.

Horst Pick pour ses nombreux conseils et pour m'avoir soutenu sur le projet Nano Tera. La vie est dure, mais il faut continuer à avancer: no pain, no gain!!

Les autres membres du LCPPM ont aussi eu une place importante au cours de ces années d'EPFL. Merci beaucoup à eux tous: **Verena Tabet**, sans qui le labo serait perdu. Merci de prendre en charge toutes ces petites choses pour lesquelles un doctorat n'est décidément pas suffisant, comme la paperasse administrative ou l'allumage de bougies. **Romain Wyss** pour les échanges enrichissants sur des sujets divers et variés, de la science au sport en passant par la littérature. **Marc Brugarolas** pour le partage d'un grand nombre de connaissances annexes très utiles au quotidien et pour les sessions de grimpe; la chasse continue!! **Samuel Terretaz** pour ses encouragements constants et son attitude toujours positive. **Joachim Piguet**, grâce à qui j'ai appris qu'on pouvait partager beaucoup avec quelqu'un qui vient d'un endroit où le brouillard est parfois plus dense qu'à Payerne. **Catarina Alves** avec qui j'ai pu partager des moments très amusants et riches en amitié. **Thamani Dahoun** pour ses leçons de vie. **Cédric Deluz** pour m'avoir introduit à l'équipe EPI et au volley-ball et pour ses enseignements sur la vie en laboratoire. **Olivia Baud** pour les nombreuses discussion très sympathiques au café ou autour d'une bonne bière. **Sophie Roizard** pour la danse et les discussion alimentairement non-pertinentes. **Enrico Condemi** pour les encouragements à toujours aller de l'avant, quelles que soient les épreuves qui se dressent sur le chemin. **Menno Tol** pour la chaise de bureau la plus confortable de l'étage que je t'ai subtilisée. **Davor Kosanic** et **Hugues Nury** pour l'*epicness*

apportée au labo. **Ghérici Hassaïne** pour les discussions fructifiantes sur des thèmes variés que nous avons eues et pour l'humour incroyable doont tu as toujours fait preuve. Prof. **Michaer Mayer** pour avoir joué le rôle d'expert durant mon examen, mais aussi pour avoir participé au grand concours de consommation d'alcool entre deux générations de LCPPM avec son camarade Dimitrios Stamou durant une summer school au Portugal. **Virginia Crivelli** pour avoir été une super étudiante et qui a notamment collaboré sur les expériences de la section 3.3.4 et 3.3.5. **Matthias Urfer** pour la session de pêche dans le lac gelé.

Petit coucou aux conjoints que j'ai eu le plaisir de rencontrer.

D'autres personnes qui n'ont pas passé par le LCPPM, mais qui entretiennent des relations suivies avec, ont généreusement accepté de participer à mon examen oral: Prof. **Mathias Winterhalter** pour avoir pris le rôle du doyen du jury de mon examen et pour les nombreuses discussions constructives que nous avons eues durant vos nombreuses visites. Prof. **Kai Johnsson**, mon co-directeur de thèse, dont le cours de 1ère année de chimie biologique de 2007 avait accueilli le groupe Diels-Alder pour chanter la glycolise. Prof. **Hatice Altug** pour avoir participé en tant que membre du jury à mon examen oral.

La famille

Tout cela n'aurait pas été possible sans une famille apportant un soutien sans faille, toujours derrière moi, malgré les coups durs.
Marcia, Maman, je t'aime. Merci d'être là. Merci pour tout, pour être la personne accueillante et souriante chez qui il fait toujours bon de revenir. **Caroline**, ma petite soeur chérie, On en aura bavé, mais les jours radieux arrivent. Mon cousin **Christophe** et ma marraine **Elisabeth** ont été des soutiens très précieux tout au long de l'aventure et je les en remercie infiniment. Et merci à tous les autres membres de ma famille de Suisse ou du Brésil, dont les encouragements ne cessaient d'affluer tout au long de ces dernières années.

Helvétia

Je tiens ici à saluer les membres de ma société d'étudiants Helvétia, avec qui j'ai passé des moments inoubliables depuis 2007. J'adresse un merci tout particulier à **Nicolò Tartini** pour son aide apportée pour l'analyse statistique. Merci également à **Arnaud de Charrière de Sévery** pour avoir pris le relais à Helvétia et continué à porter la flamme. Et un très grand merci à **Jean-Denis Briod**, **Olivier Meuwly**, **Quentin Vergères**, **Philippe Gitz** et tous les autres

pour leur soutien, leurs conseils et leur appui durant le temps de cette thèse. L'Helvétia m'aura permis de faire de grandes choses et d'évoluer sur le plan humain comme jamais auparavant, de faire des voyages et de connaître des gens incroyables à travers toutes l'Europe. Un grand merci à tous les membres des autres sociétés (et associations assimilées) pour les moments de détente légèrement éthylique. 10 ans que ça dure quand même!! Et c'est pas fini!!

Tous les autres

Merci enfin à toutes les personnes qui m'ont accompagné durant ces 6 dernières années d'une autre manière et qui m'ont permis d'arriver jusqu'au bout. Les autres doctorants avec qui j'ai pu faire route: **Valentin Manzanares, Véronique Amstutz, Aurore Delachat, Jonas Milani, Louise Bryan, Virginie Uhlmann, Denis Sallin, Lucas-Alexandre Stern, Lucie Rivier, Marcel Schreier, Olivier Sallin, Bastien Vuichoud, Charles Guinand, Nadia Baati** et tous les autres avec qui j'ai passé des moments inoubliables. Restons en contact!!

Un grand merci à **Gilles Weder** et au secteur 745 de la division T du CSEM pour leur précieux avis et conseils qui m'ont aidé à préparer la présentation orale de mon examen.

Enfin un grand merci à tous ceux dont je n'ai pas parlé jusque là et qui ont été présents pendant ces cinq années et des poussières. Une expérience comme une thèse doctorale ne peux se faire qu'entouré par ses amis, ses proches. C'est à vous tous que je dois d'être arrivé jusque là et j'attends avec impatience les nombreuses aventures que nous allons encore partager durant les années avenir.

Curriculum vitæ

Loïc Arvind Roger Arm

Born on February 6, 1988 in Neuchâtel, Switzerland

2011 - 2016	PhD thesis under the supervision of Prof. Horst Vogel and Prof. Kai Johnsson at the Institute of Chemical Sciences and Engineering, EPFL
2009 - 2011	Master of Science in Molecular and Biological Chemistry, EPFL
2006 - 2009	Bachelor of Science in Chemistry, EPFL
2003 - 2006	Maturité cantonale, option spécifique Latin, Gymnase d'Yverdon